DISSERTATION

ASPECTS OF WEED RESISTANCE TO AUXINIC HERBICIDES

Submitted by

Marcelo Rodrigues Alves de Figueiredo

Department of Agricultural Biology

In partial fulfillment of the requirements

For the Degree of Doctor of Philosophy

Colorado State University

Fort Collins, Colorado

Summer 2020

Doctoral Committee:

Advisor: Todd A. Gaines

Cristiana T. Argueso
Franck E. Dayan
Anireddy S.N. Reddy

ABSTRACT

ASPECTS OF WEED RESISTANCE TO AUXINIC HERBICIDES

Synthetic auxins have been widely used for selective control of broadleaf weeds since the mid-1940s. After more than 70 years using synthetic auxin herbicides, there are 41 different resistant species reported. Weed resistance to auxin herbicides is poorly understood and in most reported cases, no studies have been done to investigate the mechanistic changes that occur in resistant populations. The mechanisms of herbicide resistance in weeds are classified as 1) target-site when mutations reduce the interaction of the herbicide molecule to its binding site and/or changes of gene expression of the targeted enzyme to compensate for herbicide inhibition; and as 2) non-target-site mechanisms, which include any genetic mutations that will prevent or reduce the herbicide reaching its site of action. In this present research, two 2,4-D resistant weed species were studied, and the mechanisms of resistance were elucidated, where one species evolved metabolic non-target-site resistance to 2,4-D and the second species evolved a novel mechanism of target side modification.

In 2009, an *Amaranthus tuberculatus* (common waterhemp) population with ten-fold resistance to 2,4-D was found in Nebraska, USA. Using the same 2,4-D-resistant and a known susceptible *A. tuberculatus* population from Indiana, the mechanism of 2,4-D resistance was examined by conducting [^{14}C] 2,4-D absorption, translocation and metabolism experiments. No differences were found in 2,4-D absorption, but resistant plants translocated more of the radioactive material than susceptible *A. tuberculatus*. Resistant plants metabolized [^{14}C] 2,4-D more rapidly than susceptible plants. The main metabolites were purified and their structures

were solved by NMR and HRMS. Susceptible plants conjugate 2,4-D to 2,4-D Aspartic Acid (2,4-D-Asp). Resistant plants showed a distinct metabolic profile where 2,4-D is hydroxylated into 5-OH-2,4-D, conjugated in a sugar metabolite (5-OH-2,4-D-Glucoside) and malonylated into 5-OH-2,4-D-(6-O-Malonyl)-Glucoside. Pre-treatment with the cytochrome P450 inhibitor malathion inhibited 2,4-D hydroxylation. Toxicological studies in waterhemp and Arabidopsis confirmed that the hydroxylated metabolite lost its auxinic action and toxicity. In contrast, the 2,4-D-Asp metabolite induced auxin inhibition to the plants tested. These results demonstrate that resistant *A. tuberculatus* evolved novel detoxification reactions that rapidly metabolize 2,4-D, potentially mediated by cytochrome P450. That novel mechanism is more efficient and produces metabolites with lower toxicity compared to the innate aspartic acid conjugation. Metabolism-based herbicide resistance poses a serious challenge for weed management due to the potential for cross-resistance to other herbicides.

Sisymbrium orientale (Indian hedge mustard) is an important weed species in Australia reducing yields in crops and pastures. In 2005, a 2,4-D and MCPA resistant population was reported in the Port Broughton region in South Australia. Aux/IAAs are dynamic repressor proteins that regulate Auxin Response Factors (ARFs) to activate auxin related genes and are also co-receptors for auxins and synthetic auxin herbicides. The degradation of Aux/IAAs is done by the enzyme complex E3, called $SCF^{TIR1/AFB}$, which, in the presence of auxin, performs ubiquitination on Aux/IAA making it a target of proteasome 26S, an enzyme responsible for proteolysis in eukaryotes. An RNAseq study showed that a 27 bp deletion in Aux/IAA2 (IAA2) degron tail was correlated to the resistant phenotype. The mutant allele was functionally validated to confer 2,4-D resistance by transforming *Arabidopsis thaliana* with the wild type *So*IAA2 and *So*$IAA2_{\Delta 27}$ alleles. Performing binding analysis by surface plasmon resonance, the

association of TIR1 in the presence of auxin (IAA, 2,4-D and dicamba) showed slower association and faster dissociation to the resistant IAA2 peptide compared to the susceptible IAA2 peptide. Our results suggest that the loss of 9 amino acids located in the degron tail may reduce the capacity of IAA2 to “embrace” TIR1 in the presence of auxin, reducing ubiquitination rate, resulting in higher stability to repress auxin response factors and ultimately conferring resistance to 2,4-D.

ACKNOWLEDGEMENTS

I would like to acknowledge:

- God, for all the good that He has done in my life, although I do not deserve it;

- My wife Ana Beatriz, the love of my life, that gave up a successful career in law to come to the USA with me, always being at my side during the challenges and comforting during the moments of struggling. For believing in me and my capacities even when I was losing hope. Also, for her help, being an excellent lab technician, which without her help I would not be able to get this work done;

- My children, Cecilia and the new baby that we are expecting, for giving meaning to my life and strength to accomplish this work;

- My parents Suzana and Mario Augusto for giving their life to me and for the efforts in paying for my education since I was a child;

- Patrick and Melinda Slade for the help and support, being my “American family”;

- Dr. Todd Gaines that accepted me as his PhD student despite my difficulties with the English language and my inexperience in molecular biology. For the trust and for always listening to what I was trying to say. Also, for be open to new projects and techniques that I proposed, even if they were hard to perform, expensive or crazy;

- Dr. Cris Argueso for her guidance and advice that taught me so much. Cris was always available to talk to me, giving me encouragement, corrections and pushing me towards

excellence. She also opened her lab for me to do some experiments and kindly shared her Arabidopsis lines;

- Dr. Franck Dayan that helped me with his experience in mass spectrometry and biochemistry;

- Dr. Anireddy Reddy for the advising and partnership with the Aux/IAA2 project. For opening his lab for me to perform Arabidopsis transformation and kindly sharing plasmids and bacteria strains;

- Dr. Anita Küpper that started the first experiments on those projects. For the teaching, the exciting moments that we had in the lab and for the philosophical conversations;

- Dr. Kasavajhala Prasad for helping with Arabidopsis transformation;

- Dr. Claudia Boot on NMR and HRMS analysis;

- Dr. Karl Ravet for the scientific discussions, advising and experiment planning;

- Drs. Olve Peersen and Grace Campagnola on the protein extraction, size exclusion chromatography and CD analysis on Aux/IAA2;

- Mr. Hamlin Barnes on metabolite synthesis;

- Dr. Christopher Preston on providing ***Sisymbrium orientale*** **seeds;**

- Dr. Richard Napier for the SPR analysis;

- Drs. Mithila Jugulam, Patrick Tranell and Darci Giaccomini for helping on *Amarathus tuberculatus* project;

- Rachel Chayer for helping me review the grammar and English in this work;

- Weed Lab team, specially Dr. Phil Westra and Scott Nissen for their advice. My other grad student colleagues for the exciting scientific discussions and a special thanks for all the hourly students that helped me with the endless manual work in the experiments.

- Brazilian governmental scholarship from the National Council for Scientific and Technological Development (CNPq - 207387/2014-1) that paid for the first four years of my PhD;

- Corteva Agriscience financial support for the experiments that were performed in this work;

- To all who contributed directly or indirectly to this work.

Thank you very much!

TABLE OF CONTENTS

LIST OF TABLES

LIST OF FIGURES

CHAPTER I – INTRODUCTION

AUXINIC HERBICIDES

Chemical structure and its properties

Auxinic herbicides are generally characterized as low molecular weight small molecules that structure consists of an aromatic group and a carboxylic group, similar to the natural auxin, indole acetic acid (IAA). The auxinic herbicides are divided in four different classes according to their chemical structures: Phenoxy-carboxylic acids, Benzoic acids, Pyridine-carboxylic acids and Quinoline-carboxylic acids. Structural variations of each molecule changes its binding capacity to receptor proteins and its stability through metabolization into the plant cell (Tan et al., 2007; Lee et al., 2014), conferring the phytotoxic properties characteristic to this herbicide class.

Auxin mechanism of action

Auxins can induce rapid changes in gene expression through a ubiquitin-proteasome system in the plant cell nucleus. The ubiquitin-proteasome system consists of a post translational protein modification called ubiquitination, where ubiquitin moieties are covalently attached to a targeted protein. Ubiquitinated proteins are recognized by proteasomes, enzymatic complexes that degrade proteins (Smalle and Vierstra, 2004). The process of protein ubiquitination is facilitated by an auxin specialized E3 ligase complex, SKP1-CULLIN1-F-BOX PROTEIN (SCF), that has a vast F-Box interacting domain. F-Box proteins are substrate specific targeting subunits, specialized to facilitate the ubiquitination in the SCF complex. TRANSPORT INHIBITOR RESPONSE 1 (TIR1) and the homologs AUXIN SIGNALING F-BOX 1-5 (AFB1-

5) are auxin dependent receptors that contain on their C-terminal an 18 leucine-rich repeat domain (LRR). The LRR domain contains an auxin binding pocket, where the hormone acts as a "molecular glue," targeting the AUXIN/INDOLE-3-ACETIC ACID INDUCIBLE (Aux/IAA) transcriptional repressor for ubiquitination and proteasome degradation. Aux/IAA proteins are short lived transcriptional repressors of AUXIN RESPONSE FACTORS (ARF), transcription factors of auxin responsive genes. When Aux/IAA proteins are degraded via ubiquitination, ARF proteins are depressed and auxin related genes are activated, leading to early auxin related responses (Figure 1.1 – Reviewed at Calderon-Villalobos et al., 2010; Dinesh et al., 2016).

Post translational inductions of auxin herbicides

Auxin herbicide action in plants is characterized by three distinct responsive phases: stimulation, inhibition and decay (Figures 1.2 and 1.3 – reviewed at Grossmann, 2010b). The first phase is characterized by the activation of metabolic process related to abnormal growth (3-4 hours after treatment) producing the first symptoms of leaf epinasty, tissue swelling and stem curling. Plant epinasty occurs due to the disturbance of cell growth through cytoskeleton reorganization and osmotic conditions, inducing abaxial leaf cells to grow more rapidly than adaxial cells. Post translational responses of auxinic herbicides induce mitochondria and peroxisome mediated production of reactive oxygen species and nitric oxide accumulation, trigging epinasty by disturbing actin architecture in the plant cell. In that process, actin suffers carbonylation and S-nitrosylation, which reduces the size of its filaments, leading to reorganization of microtubules. Peroxisomal enzymes XDH and ACX1 catalyze reactions that produce high amounts of ROS as sub-products, which seem to be related to auxin related epinasty symptoms. Arabidopsis defective lines for those enzymes showed reduced leaf and stem curling after 2,4-D treatment (Pazmiño et al., 2014; Rodríguez-Serrano et al., 2014; Sandalio et

al., 2016). Activation of those genes is probably correlated to $SCF^{TIR/AFB}$ transcriptional activation since mutants on those auxin receptors prevent early epinasty symptoms when plants are treated with auxin herbicides (See sections at CANONICAL AUXIN ROUTE). Symptoms of tissue swelling are also characteristic from the first phase, where auxin induces the transcription of ATPases that pump H^+ to the plasmatic membrane, acidifying the cell apoplast (Takahashi et al., 2012) and activating expansins that break the covalent bonds of cellulose and cellulase, increasing cell wall fluidity (Cosgrove, 2000). Acidification of the protoplast also activates potassium channels that will reduce osmotic potential at the symplast and aquaporins will facilitate water influx, leading to cell turgidity (Claussen et al., 1997; Philippar et al., 2006). The process of apoplast acidification involves the $SCF^{TIR/AFB}$ canonic route by the transcription of SMALL AUXIN UP-REGULATED RNA (SAUR) that directly interacts with and stop the inhibitory action of 2C protein phosphatase D (PP2C-D) of H^+ ATPases at the plasmatic membrane (Spartz et al., 2014; Sun et al., 2016).

In the second phase, there is a stress response due the accumulation of abscisic acid (ABA) and ethylene by the overexpression of genes coding for the proteins 9-cis-epoxycarotenoid dioxygenase (NCED) and 1-aminocyclopropane-1-carboxylic acid (ACC) synthase, respectively involved in the biosynthesis of those hormones. ACC synthase multigene family encodes for proteins that convert S-adenosyl-L-methionine into l-amino-cyclopropene-carboxylase that will be turned into ethylene catalyzed by ACC oxidase in a reaction that will release toxic cyanide as one of the sub-products (Grossmann et al., 2001; Kraft et al., 2007). Ethylene is a gaseous hormone that will lead to leaf senescence and inhibition of auxin transport. NCED acts at the chloroplast, catalyzing the conversion of terpenoid xanthins into xanthoxin, which is released into the cytoplasm. Under stress conditions, acidification in the cytoplasm

activates enzymes that will turn xanthoxin into ABA. Accumulation of ABA induces stomatal closure, leading to tissue drought stress, accumulation of reactive oxygen species due to decline of photosynthetic activity, and induction of NADPH oxidase in the plasmatic membrane (Grossmann et al., 2001; Grossmann, 2010b).

In the final phase, the accumulation of reactive oxygen species will interact with the plasma membrane, reacting with phospholipids, promoting lipid unsaturation, cytosol leakage, and cell death. At the plant tissue level, the leaves wilt, turning to a yellow chlorotic state. Stem swelling and curling cause destruction of the vascular system, culminating in tissue necrosis and decay (Reviewed at Grossmann, 2010b; Wang et al., 2017).

HERBICIDE RESISTANCE

The occurrence of herbicide resistance in weed populations consists of a lower injury response to an applied herbicide dose that would be lethal to a natural population (Hance, 1983; Penner, 1994). Resistance is governed by naturally occurring genetic variations during the process of DNA repair and replication. In the process of adaptation, the accumulation of specific or several polymorphisms will change protein functions, causing changes in biochemical, physiological and/or morphological aspects of the living organism that will confer successful adaptation to environment induced stresses. In weeds, the pressure caused by herbicide application can select individuals containing genetic traits that will induce herbicide resistant phenotypes. This selective advantage will increase the number of adapted herbicide resistance individuals, causing a shift in the population to mostly resistant individuals (reviewed by Délye et al., 2013).

Weed resistance can occur through several mechanisms that are usually divided into two categories, target site and non-target site mechanisms (Reviewed by Délye et al., 2013; Ghanizadeh and Harrington, 2017). Target site resistance refers to changes in the DNA sequence of the herbicide target protein , leading to structural changes that will reduce the capacity of the herbicide to reach or interact with the enzyme binding site (Devine and Shukla, 2000). Another mechanism related to target site is gene amplification and overexpression of the herbicide target enzyme, where the overproduction of the herbicide target protein compensates for herbicide inhibition (Gaines et al., 2010). Non-target-site resistance consists of genetic modifications leading to mechanisms that will prevent or reduce the quantity of herbicide reaching its site of action. Non-target-site can happen due to changes in herbicide absorption, exudation or compartmentalization into the vacuole. Additionally, xenobiotic-metabolizing enzymes can metabolize herbicides, changing the chemical structure to reduce its capacity to interact at the target site (Ghanizadeh and Harrington, 2017).

Auxin herbicides have been used in weed control since 1945 and the first two cases of resistance were reported in 1957 in wild carrot (*Daucus carota*) in Canada and spreading dayflower (*Commelina diffusa*) in Hawaii. After that, new cases were not reported until 22 years later in Canada thistle (*Cirsium arvense*) in Sweden, with still only three species resistant to 2,4-D at that time. Until now, after more than 70 years using synthetic auxin herbicides, there are just 41 different resistant species reported. However, herbicide resistance to auxinic herbicides in weeds remains poorly understood and in most reported cases, no studies have been done to investigate the molecular mechanisms that would govern those resistant phenotypes. The following section will present the main findings in plant auxin biology related to main genes

involved in auxin perception, movement and metabolism, in which mutations could lead to auxin resistance.

CANONICAL AUXIN ROUTE

TIR/AFBs

The protein complex Skp1-Cullin-TIR/AFB ($SCF^{TIR/AFBs}$) is responsible for the degradation of auxin transcriptional repressor proteins called Aux/IAA. Auxin is a "molecular glue" that binds both proteins. Then, the SCF complex ubiquitinates the Aux/IAA, leading to its degradation via 26S proteasome and activation of auxin response factors (ARF), those transcription factors will activate genes in early auxin responses (Tan et al., 2007). The assembly of $SCF^{TIR/AFB}$ (Figure 1.4) involves several regulators that mutations and changes of expression leads to auxin resistance. Ubiquitin E1 enzymes (AXR1 and ECR1) transfer the ubiquitin-like proteins RUB/NEDD8 to a E2 enzyme (RCE1) that will neddylate a lysine residue on CUL1 to activate the ubiquitin ligase activity of the SFC protein complex (Pozo et al., 1998; Zhang et al., 2008). The fine control of RUB/NEDD8 association on SCF is done by COP9 signalosome (CSN), an eight-subunit protein that removes RUB/NEDD8 (deneddylation) from CUL1, disassembling the SCF complex, pulling apart the substrate adaptor (ASK/TIR1) from CUL1/ASK1 (Schwechheimer et al., 2001; Huang et al., 2013). The deneddylated CUL1/ASK1 binds to CAND1 and remains inactive until it becomes neddylated again for SCF complex reassembly. In Arabidopsis, CAND1 mutants (*eta2-1*) increased the abundance of SCF^{TIR1} and were sensitive to auxins (Zhang et al., 2008). In all the proteins described above, mutations lead to IAA and 2,4-D resistance (AXR1 and ECR1 (Estelle and Somerville, 1987; del Pozo et al., 2002); RUB/NEDD8 (Bostick et al., 2004) ; CSN (Schwechheimer et al., 2001; Huang et al.,

2013); CUL1 (Hellmann et al., 2003; Yu et al., 2015). AXR1 mutants were highly resistant to picloram and florpyrauxifen-benzyl (Walsh et al., 2006).

Mutations of molecular chaperones can also lead to auxin resistance. HEAT SHOCK FACTOR 90 (HSP90) and its co-chaperone SUPPRESSOR OF G2 ALLELE SKP1 (SGT1) act together as $SCF^{TIR/AFB}$ conformation modulators, probably to maintain the proper folding of the protein complex (Gray et al., 2003; Wang et al., 2016; Watanabe et al., 2016). Mutations of SGT1 (*eta3* and sgt1b-1) confer resistance to IAA and 2,4-D. Another mutant, sgt1b-4, was highly resistant to picloram and florpyrauxifen-benzyl (Walsh et al., 2006). Overexpression of a negative mutant of HSP90 induced normal Arabidopsis root growth under 2,4-D exposure, which suggests that the unfolding of SCF^{TIR1} leads to auxin resistance (Watanabe et al., 2016).

In the auxin binding site, a structural study on TIR1-ASK1 crystallography showed that single amino acid substitutions at G146D (*tir1-1*), G441D (*tir1-2*), P409S (*tir1-6*) and L112Q (*tir1-7*) can induce the loss of auxin binding capacity of TIR1 (Tan et al., 2007; Dinesh et al., 2016). Loss-of-function mutations of TIR1 and AFB5 in Arabidopsis caused resistance to dicamba (*ti1-1* and *afb5*) and 2,4-D (just *tir1-1*) (Gleason et al., 2011). The affinity of different auxin herbicides in their capacity of assembling TIR1 and AFB5 on IAA7 degron peptides was studied using Surface Plasmon Resonance (SPR) (Lee et al., 2014) on the synthetic auxin families. Phenoxyacetic acids have high binding properties on TIR1; quinclorac on AFB5 and Pyridine derivates on both coreceptors. Picloram, fluroxypyr and florpyrauxifen-benzyl had higher affinity to AFB5. Similar results were found on *afb5-1* and *afb5-4* resistance to picloram and florpyrauxifen-benzyl. *Kochia scoparia* was the only weed species for which TIR1/AFB binding capacity was tested on a yeast two hybrid assay (Y2H), *Ks*TIR1 interacted with 2,4-D and triclopyr, while the *Ks*AFB6 homolog ligated to 2,4-D, quinclorac and triclopyr (LeClere et

al., 2018). Based on the past results found in Arabidopsis, it is possible that mutations on TIR/AFBs or its reduction of expression can lead to auxin herbicide resistance in weeds (Table 1.1 shows the binding specificity of different synthetic auxin chemical families to interact to TIR/AFB proteins).

Aux/IAA

Aux/IAA proteins are repressor proteins that dimerize Auxin Response Factors (ARF) inhibiting transcription of auxin responsive genes. Aux/IAA proteins are structured in four different domains. Domain I is required for transcription repression; domain II is the auxin binding site, having the degron motif required for protein degradation; domains III and IV are heterodimers that interact with ARF for transcription repression. Aux/IAA proteins are very dynamic regulators, having a half-life of 6 to 8 minutes (Abel et al., 1994; Abel et al., 1995).

Mutations of Aux/IAA proteins in the degron region lead to an auxin resistant phenotype with serious changes in plant morphology (Table 1.2). Mutations in IAA7 (AXR2) degron showed reduced effect on root growth under 2,4-D, florpyrauxifen-benzyl, and picloram (Walsh et al., 2006). In a resistant population of *Kochia scoparia,* a *Ks*IAA16 single amino acid non-synonymous mutation in the degron was reported reducing dicamba and 2,4-D binding capacity to *Ks*TIR1 and *Ks*AFB6 (LeClere et al., 2018).

Auxin insensitivity is not limited to only changes in the degron, as other mutations in Aux/IAA proteins can induce the loss of ubiquitination sites (lysines, cysteines, serines and threonines), reducing its rate of proteolysis. The correlation of ubiquitination residues (especially lysines) and protein stability is observed among Aux/IAA homologs, where variation of those residues in number and position along the protein can alter its ubiquitination (Winkler et al.,

2017). Beyond the ubiquitination sites, Aux/IAA proteins have flexible disordered regions at the degron vicinity playing non-auxin dependent interactions with TIR/AFB proteins. Those interactions may work as guides to the Aux/IAA degron in order to achieve its binding at the TIR/AFB protein site in the presence of auxin. Amino acid changes or deletions that would reduce the length or folding of those flexible disordered regions can reduce auxin co-receptor interaction, depleting ubiquitination (Niemeyer et al., 2020).

Changes in Aux/IAA protein expression may also induce herbicide resistance. In rice (*Oryza sativa*), overexpression of *Os*IAA1 increased auxin resistance. On the other hand, the overexpression of *Si*IAA15 in tomato caused herbicide related symptoms on leaves, reduced root development and seed sterility, while gene silencing transformants of *Si*IAA15 were resistant to ABA and NAA. In that case, *Si*IAA15 repression may function in a herbicide related phenotype inducing ABA responses (Xu et al., 2015).

Overall, Aux/IAA transcription repression regulates auxin homeostasis in plant cells and there are several changes in protein structure that can increase its stability. Due to the simple structure and dynamic function of its degradation and synthesis, changes to Aux/IAA proteins structure or expression may be the most likely mechanism of auxinic herbicide resistance to occur in weeds (Table 1.2 shows several Aux/IAA proteins among plant species that mutations or changes of expression potentially would lead to synthetic auxin resistance).

ARF TRANSCRIPTION FACTORS

Auxin Response Factors are transcription factors repressed by Aux/IAA proteins that bind to auxin response elements (AuxREs – TGTCTC or TGTCGG) on the promoter regions of auxin related genes (Ulmasov et al., 1997a). They are composed of four main domains. N-

terminal Domain I is responsible for DNA binding; Domain II corresponds to a long glutamine-rich region that characterizes ARF as a transcription activator or a repressor (Ulmasov et al., 1999a). C-terminal PB1 domain (domains III/IV) oligomerize with Aux/IAA PB1 domain, conferring physical repression (Nanao et al., 2014). In Arabidopsis, there are 23 different ARF proteins, 18 negative and 5 positive transcriptional regulators. Due to gene functional redundancy, most of the ARF proteins mutants show modest changes in phenotype. In the literature, just ARF7 and ARF19 presented strong changes related to auxin responses (Okushima et al., 2005). ARF7 (*msg1* and *nph4*) and ARF19 (*arf19*-1) mutations showed resistant to 2,4-D and IAA (Watahiki and Yamamoto, 1997). Overexpression of ARF19 leads auxin-like symptoms as drastic reduction in plant size, epinastic leaves and small numbers of siliques. Double mutants carrying nph4-1(ARF7) and *arf19-1* presented increased resistance to auxins as 2,4-D and IAA (Li et al., 2006). Increments of Aux/IAA repression or changes on ARF proteins target gene regulation may lead to herbicide resistance in weeds.

NON-CANONICAL AUXIN ROUTE

Plant receptor like kinases govern cellular responses by activating their substrate by catalyzing phosphorylation. Located at the plasmatic membrane, Transmembrane Kinases (TMKs – Xu et al., 2014a) are associated with auxin signaling, where, in the presence of the hormone, the C-terminal on TMK is cleaved. This $TMK1_{C\text{-}terminus}$ moves to the nucleus and stabilizes Aux/IAA proteins. This regulates auxin response factors that will induce transcriptional responses of auxin (Cao et al., 2019). TMK gene family is composed of four functional overlapping members, due to gene redundancy, just double null mutants (*tmk1; tmk4)* induce auxin insensitivity and triple mutations on *tmk1;tmk3;tmk4* lead to complete insensitive phenotypes. The mutants showed insensitivity to IAA, 2,4-D and NAA. Double and triple

mutants showed severe auxin like phenotypes as reduced size, low root development, underdeveloped siliques and low seed production. Quadruple mutants were sterile (Dai et al., 2013).

TRANSPORTERS

The mechanism of auxin transport in plants started to be investigated in the 1970s, where the first models of chemiosmotic movement were proposed. Auxins are weak acids and can move passively through the plasma membrane in their protonated form, taking advantage of the pH differences between symplast and apoplast generated by H^+-ATPase. The active injection of protons to the apoplast makes its pH more acidic, leading to partial protonation of auxin molecules, and supporting their spontaneous diffusion to the symplast (reviewed at Robert and Friml, 2009). The hypothesis that influx and efflux transporters would be additionally involved in auxin movement in plants was postulated already when the chemiosmotic model was proposed. With the advent of Arabidopsis as a model species, molecular genetic studies identified three different classes of auxin transporters.

Auxin polar transport is governed by the PIN-formed (PIN) efflux carriers, that are important for determining the direction of auxin flow. Synthetic auxins are a poor substrate for PIN transporters (Delbarre et al., 1996), however, the overexpression of PIN7 increased the efflux of 2,4-D, which suggests that these transporters may have some importance in herbicide movement in plants (Petrášek et al., 2006).

AUX/LAX are influx carriers first identified in Arabidopsis mutants (*aux1*), defective in auxin uptake and resistant to IAA and 2,4-D. AUX1 is analogous to amino acid permeases and is located on the plasma membrane in plant cells (reviewed at Robert and Friml, 2009). AUX/LAX

proteins carriers have specific affinity to the natural auxin and phenoxyacetic acids, but low specificity to other classes of auxinic herbicides (Hoyerova et al., 2018).

Major facilitator superfamily (MFS) transporters are also involved in auxin transport. In an Arabidopsis mutant for a member of MSF family, TRANSPORTER OF IBA1 (TOB1), located on plasma and vacuole membranes, showed resistance to the auxin precursor Indole 3-butyric acid (IBA) and its synthetic analog 4-(2,4-dichlorophenoxy)butyric acid (2,4-DB).

ATP-binding cassette transporters (ABC) are active transporters that work against the auxin gradients by hydrolyzing ATP. The application of ABC transporter inhibitors reduced 2,4-D translocation in the weed *Raphanus raphanistrum* (Goggin et al., 2016). In Arabidopsis, several genes of ABC subfamilies "B" and "G" were identified as auxin transports. ABCG37 is an active plasma membrane efflux auxin transporter of IBA, 2,4-D and 2,4-DB and mutants show resistance to the herbicide. The analog ABCG36 showed resistance just for 2,4-DB (Růžička et al., 2010). In Arabidopsis ABCB4 and rice OsABCB14 is involved in 2,4-D uptake and mutants show insensitivity to the auxin (Kubeš et al., 2012; Xu et al., 2014b). Overexpression of ABC transporters is associated with antibiotic and fungicide resistance in microorganisms, inducing rapid efflux of toxic compounds. This mechanism of resistance is more common than transporter loss of function (Dermauw and Van Leeuwen, 2014). In weeds, there are to date no confirmed cases of auxin herbicide resistance involving transporters.

DETOXIFICATION AND CONJUGATION ENZYMES

In terms of metabolism, auxinic herbicides can undergo two main kinds of reactions. Reactions of detoxification are performed by monoxygenase and dioxygenase enzymes that hydroxylate active regions of the herbicide molecule, making it unable to bind to its receptor.

Those reactions are usually irreversible, so the product is not converted back to the original parent compound. Studies on 2,4-D metabolism in agronomic species show that both dicot and monocot species were able to hydroxylate the phenoxy group of the herbicide and the products of the reaction did not show auxinic effects, except for 3-OH-2,4-D which was more active than the parent 2,4-D (Wightman and Setterfield, 1968; Ercegovich et al., 1971; Witham et al., 1971; Feung et al., 1975a; Feung et al., 1978; Hamburg et al., 2001).

The other kind of reaction that auxinic herbicides can undergo is conjugation with sugars or amino acid. In those, the herbicide molecule reacts with amino acids or sugars that inactivate its activity. Those reactions are usually transient, since the conjugates can be hydrolyzed, turning back to the herbicide active form. Herbicide glucosylation is performed by O-glucosyltransferase (OGT) enzymes using UDP-glucose as the sugar donor molecule to hydroxyl nucleophilic acids at the herbicide molecule. 2,4-D is converted to 2,4-D glucose ester in both resistant and susceptible populations of wild radish (*Raphanus raphanistrum*). Bioassays showed that those conjugates retained auxin activity, probably being converted back to 2,4-D parent by glucosidase enzymes (Goggin et al., 2018). GRETCHEN HAGEN3 (GH3) is a diverse family of genes responsible for performing amino acid conjugation in endogenous IAA. The main products generated in the enzyme reaction are IAA aspartic acid and IAA glutamic acid. Those conjugates can be hydrolyzed by aminohydrolases and be converted back to IAA active auxin. GH3s also conjugate 2,4-D and dicamba to Aspartyl and glutamic acid conjugates. In a broad study on the different families of GH3s from several plant species, it was found that the soybean GmGH3.26 was the most efficient for conjugating 2,4-D (Chiu et al., 2018). The aminohydrolases AtILL5- and AtIAR3-like were able to convert the amino-acid conjugates back to 2,4-D active form. For dicamba, the *Brassica rapa* BrGH3.15 showed very low activity for conjugating the herbicide.

No aminohydrolases were able to convert dicamba conjugates back to the herbicide original active form. GH3s are good candidates for metabolic weed resistance for synthetic herbicides due to the enormous diversity of that gene family among plant species.

Auxin herbicide selectivity between monocot and dicot species may be in part explained by the metabolic pathways that synthetic auxins undergo. In monocot species such as wheat and barley, reactions of hydroxylation may be predominant (Feung et al., 1975a; Scheel and Sandermann, 1981a; Scheel and Sandermann, 1981b), while in susceptible dicot species, such as soybean and Arabidopsis, amino acid conjugation is the main metabolic pathway. Dicot species, such as soybean, can produce hydroxylated metabolites, but in smaller amounts compared to amino acid conjugates (Eyer et al., 2016; Scheel and Sandermann, 1981a; Scheel and Sandermann, 1981b). Changes in expression and binding capacity of the herbicide at those enzymes that perform hydroxylation reactions may lead to herbicide resistance in dicot species. In soybean lines resistant to 2,4-D, there is higher accumulation of hydroxylated glycoside comparing to nonresistant control lines (Feung et al., 1978). Some weed resistant populations for auxinic herbicides showed rapid herbicide metabolism comparing to non-resistant populations including MCPA resistant hemp nettle (*Galeopsis tetrahit* L. – Weinberg et al., 2006), and chickweed (*Stellaria media*) resistant to mecoprop (Coupland et al., 1990), however further metabolite characterization was not done to identify the reaction performed on the parent herbicide compound.

STUDYING AUXIN WEED RESISTANCE

The study of the genetic changes that induce resistance to auxinic herbicide in weeds is still a challenge. Several proteins are involved in hormonal signaling and regulation. The

activation of auxin transcriptional responses triggers a complex network of responses involving other hormones and several metabolic reactions that are difficult to be isolated for scientific experimentation (Figure 1.3). To make this situation even more complex, many of the genes that may govern the reactions related to resistant phenotypes have little or no activity in heterologous model species. The complexity of weed genome architecture is an aggravation to this difficulty and the lack of homozygous weed strains as standardized genetic material for the proper use in genetics, molecular biology and bioinformatics needs to be better developed for the proper study and validation of weed genetic functions.

HYPOTHESIS AND OBJECTIVES

The study of auxin resistance in weed species shows off as a field of new possibilities to understand how genetic diversity occurs under herbicide selective pressure in agronomic systems. Moreover, characterization of the mechanisms of weed resistance may help to answer eventual aspects of auxin metabolism and signaling that remain unknown or may not happen in model plant species. To have a better understanding of adaptation to hormone responses in auxin resistant dicot invasive plants, the objective of this work is to characterize the two distinct mechanisms of 2,4-D resistance that occurred in populations from two different species, one from the USA and other from Australia.

The first case is a population of *Amaranthus tuberculatus* resistant to 2,4-D from the state of Nebraska in the USA. Preliminary studies on herbicide metabolism raised the hypothesis that the resistance was governed by non-target-site mechanisms. Considering that, experiments performed in this study focusing on answering the following questions:

- Which mechanism of resistance is involved?

- What are the differences in herbicide physiology (absorption, translocation and metabolism) between resistant and susceptible plants?
- What are the quantitative and qualitative differences in herbicide metabolism between resistant and susceptible plants?
- Are those metabolites produced in a specific organ in the plant?
- How toxic are those metabolites? Do they induce auxinic responses?
- Which enzymes would be governing the metabolic processes?

The second study comprehends the identification and characterization of an auxin target site resistance in *Sisymbrium orientale* from the region of Adelaide, South Australia. In this population, a 27 base pair deletion was found at the degron tail of an Aux/IAA2 protein. During the discovery process, the following questions were raised:

- How many and which genes are responsible for the resistant trait?
- What are the genetic polymorphisms that differentiate Aux/IAA2 between susceptible and resistant phenotypes?
- Does the Aux/IAA2 resistant allele truly lead to auxin resistance?
- Would it cause resistance if cloned into a heterologous plant system?
- What are differences of Aux/IAA2 transcriptional induction between resistant and susceptible plants?
- Where do these changes occur in the protein structure and what are the consequences for its function, stability, oligomerization and binding to auxin molecules?

This work will broaden the current understanding of the mechanisms of auxin resistance in weed species.

REFERENCES

Abel S, Nguyen MD, Theologis A (1995) ThePS-IAA4/5-like Family of Early Auxin-inducible mRNAs inArabidopsis thaliana. Journal of Molecular Biology 251:533-549

Abel S, Oeller PW, Theologis A (1994) Early auxin-induced genes encode short-lived nuclear proteins. Proceedings of the National Academy of Sciences 91:326-330

Bostick M, Lochhead SR, Honda A, Palmer S, Callis J (2004) Related to Ubiquitin 1 and 2 Are Redundant and Essential and Regulate Vegetative Growth, Auxin Signaling, and Ethylene Production in Arabidopsis. The Plant Cell 16:2418-2432

Calderon-Villalobos LI, Tan X, Zheng N, Estelle M (2010) Auxin perception--structural insights. Cold Spring Harb Perspect Biol 2:a005546-a005546

Calderón Villalobos LIA, Lee S, De Oliveira C, Ivetac A, Brandt W, Armitage L, Sheard LB, Tan X, Parry G, Mao H, Zheng N, Napier R, Kepinski S, Estelle M (2012) A combinatorial TIR1/AFB–Aux/IAA co-receptor system for differential sensing of auxin. Nature Chemical Biology 8:477-485

Cao M, Chen R, Li P, Yu Y, Zheng R, Ge D, Zheng W, Wang X, Gu Y, Gelová Z, Friml J, Zhang H, Liu R, He J, Xu T (2019) TMK1-mediated auxin signalling regulates differential growth of the apical hook. Nature 568:240-243

Chiu L-W, Heckert MJ, You Y, Albanese N, Fenwick T, Siehl DL, Castle LA, Tao Y (2018) Members of the GH3 Family of Proteins Conjugate 2,4-D and Dicamba with Aspartate and Glutamate. Plant and Cell Physiology 59:2366-2380

Claussen M, Lüthe H, Blatt M, Böttger M (1997) Auxin-induced growth and its linkage to potassium channels. Planta 201:227-234

Cosgrove DJ (2000) Loosening of plant cell walls by expansins. Nature 407:321-326

Coupland D, Lutman PJ, Heath C (1990) Uptake, translocation, and metabolism of mecoprop in a sensitive and a resistant biotype of *Stellaria media*. Pest. Biochem. Physiol. 36:61-67

Dai N, Wang W, Patterson SE, Bleecker AB (2013) The TMK subfamily of receptor-like kinases in Arabidopsis display an essential role in growth and a reduced sensitivity to auxin. PloS one 8:e60990-e60990

del Pozo JC, Dharmasiri S, Hellmann H, Walker L, Gray WM, Estelle M (2002) AXR1-ECR1-dependent conjugation of RUB1 to the Arabidopsis Cullin AtCUL1 is required for auxin response. The Plant cell 14:421-433

Delbarre A, Muller P, Imhoff V, Guern J (1996) Comparison of mechanisms controlling uptake and accumulation of 2,4-dichlorophenoxy acetic acid, naphthalene-1-acetic acid, and indole-3-acetic acid in suspension-cultured tobacco cells. Planta 198:532-541

Délye C, Jasieniuk M, Le Corre V (2013) Deciphering the evolution of herbicide resistance in weeds. Trends in Genetics 29:649-658

Dermauw W, Van Leeuwen T (2014) The ABC gene family in arthropods: Comparative genomics and role in insecticide transport and resistance. Insect Biochemistry and Molecular Biology 45:89-110

Devine MD, Shukla A (2000) Altered target sites as a mechanism of herbicide resistance. Crop Protection 19:881-889

Dinesh DC, Villalobos LIAC, Abel S (2016) Structural Biology of Nuclear Auxin Action. Trends in Plant Science 21:302-316

Ercegovich CD, Hamilton RH, Hurter J, Hall JK (1971) Metabolism of phenoxyacetic acids. Metabolism of 2,4-dichlorophenoxyacetic acid and 2,4,5-trichlorophenoxyacetic acid by bean plants. Journal of Agricultural and Food Chemistry 19:480-483

Estelle MA, Somerville C (1987) Auxin-resistant mutants of Arabidopsis thaliana with an altered morphology. Molecular and General Genetics MGG 206:200-206

Eyer L, Vain T, Pařízková B, Oklestkova J, Barbez E, Kozubíková H, Pospíšil T, Wierzbicka R, Kleine-Vehn J, Fránek M, Strnad M, Robert S, Novak O (2016) 2,4-D and IAA Amino Acid Conjugates Show Distinct Metabolism in Arabidopsis. PLOS ONE 11:e0159269

Feung C-S, Hamilton RH, Mumma RO (1975) Metabolism of 2,4-dichlorophenoxyacetic acid. VII. Comparison of metabolites from five species of plant callus tissue cultures. Journal of Agricultural and Food Chemistry 23:373-376

Feung CS, Loerch SL, Hamilton RH, Mumma RO (1978) Comparative metabolic fate of 2,4-dichlorophenoxyacetic acid in plants and plant tissue culture. Journal of Agricultural and Food Chemistry 26:1064-1067

Fukaki H, Tameda S, Masuda H, Tasaka M (2002) Lateral root formation is blocked by a gain-of-function mutation in the SOLITARY-ROOT/IAA14 gene of Arabidopsis. The Plant Journal 29:153-168

Gaines TA, Zhang W, Wang D, Bukun B, Chisholm ST, Shaner DL, Nissen SJ, Patzoldt WL, Tranel PJ, Culpepper AS, Grey TL, Webster TM, Vencill WK, Sammons RD, Jiang J, Preston C, Leach JE, Westra P (2010) Gene amplification confers glyphosate resistance in Amaranthus palmeri. Proceedings of the National Academy of Sciences 107:1029-1034

Ghanizadeh H, Harrington KC (2017) Non-target Site Mechanisms of Resistance to Herbicides. Critical Reviews in Plant Sciences 36:24-34

Gleason C, Foley RC, Singh KB (2011) Mutant Analysis in Arabidopsis Provides Insight into the Molecular Mode of Action of the Auxinic Herbicide Dicamba. PLOS ONE 6:e17245

Goggin DE, Cawthray GR, Powles SB (2016) 2,4-D resistance in wild radish: reduced herbicide translocation via inhibition of cellular transport. Journal of Experimental Botany 67:3223-3235

Goggin DE, Nealon GL, Cawthray GR, Scaffidi A, Howard MJ, Powles SB, Flematti GR (2018) Identity and Activity of 2,4-Dichlorophenoxyacetic Acid Metabolites in Wild Radish (Raphanus raphanistrum). Journal of Agricultural and Food Chemistry 66:13378-13385

Gray WM, Muskett PR, Chuang H-w, Parker JE (2003) Arabidopsis SGT1b is required for SCF(TIR1)-mediated auxin response. The Plant cell 15:1310-1319

Grossmann K (2010) Auxin herbicides: current status of mechanism and mode of action. Pest Management Science 66:113-120

Grossmann K, Kwiatkowski J, Tresch S (2001) Auxin herbicides induce H2O2 overproduction and tissue damage in cleavers (Galium aparine L.). Journal of Experimental Botany 52:1811-1816

Hamann T, Benkova E, Bäurle I, Kientz M, Jürgens G (2002) The Arabidopsis BODENLOS gene encodes an auxin response protein inhibiting MONOPTEROS-mediated embryo patterning. Genes & Development 16:1610-1615

Hamann T, Mayer U, Jurgens G (1999) The auxin-insensitive bodenlos mutation affects primary root formation and apical-basal patterning in the Arabidopsis embryo. Development 126:1387-1395

Hamburg A, Puvanesarajah V, Burnett TJ, Barnekow DE, Premkumar ND, Smith GA (2001) Comparative Degradation of [14C]-2,4-Dichlorophenoxyacetic Acid in Wheat and Potato after Foliar Application and in Wheat, Radish, Lettuce, and Apple after Soil Application. Journal of Agricultural and Food Chemistry 49:146-155

Hance RJ (1983) Herbicide Resistance in Plants. Edited by H. M. Le Baron and J. Gressel. Chichester, England: Wiley-Interscience (1982), pp. 401, £37.00. Experimental Agriculture 19:361-361

Hellmann H, Hobbie L, Chapman A, Dharmasiri S, Dharmasiri N, del Pozo C, Reinhardt D, Estelle M (2003) Arabidopsis AXR6 encodes CUL1 implicating SCF E3 ligases in auxin regulation of embryogenesis. EMBO J 22:3314-3325

Hoyerova K, Hosek P, Quareshy M, Li J, Klima P, Kubes M, Yemm AA, Neve P, Tripathi A, Bennett MJ, Napier RM (2018) Auxin molecular field maps define AUX1 selectivity: many auxin herbicides are not substrates. New Phytologist 217:1625-1639

Hua Z, Vierstra RD (2011) The Cullin-RING Ubiquitin-Protein Ligases. Annual Review of Plant Biology 62:299-334

Huang H, Quint M, Gray WM (2013) The eta7/csn3-3 Auxin Response Mutant of Arabidopsis Defines a Novel Function for the CSN3 Subunit of the COP9 Signalosome. PLOS ONE 8:e66578

Kraft M, Kuglitsch R, Kwiatkowski J, Frank M, Grossmann K (2007) Indole-3-acetic acid and auxin herbicides up-regulate 9-cis-epoxycarotenoid dioxygenase gene expression and abscisic acid accumulation in cleavers (Galium aparine): interaction with ethylene. Journal of Experimental Botany 58:1497-1503

Kubeš M, Yang H, Richter GL, Cheng Y, Młodzińska E, Wang X, Blakeslee JJ, Carraro N, Petrášek J, Zažímalová E, Hoyerová K, Peer WA, Murphy AS (2012) The Arabidopsis concentration-dependent influx/efflux transporter ABCB4 regulates cellular auxin levels in the root epidermis. The Plant Journal 69:640-654

LeClere S, Wu C, Westra P, Sammons RD (2018) Cross-resistance to dicamba, 2,4-D, and fluroxypyr in Kochia scoparia is endowed by a mutation in an AUX/IAA gene. Proceedings of the National Academy of Sciences 115:E2911-E2920

Lee S, Sundaram S, Armitage L, Evans JP, Hawkes T, Kepinski S, Ferro N, Napier RM (2014) Defining Binding Efficiency and Specificity of Auxins for SCFTIR1/AFB-Aux/IAA Co-receptor Complex Formation. ACS Chemical Biology 9:673-682

Li J, Dai X, Zhao Y (2006) A role for auxin response factor 19 in auxin and ethylene signaling in Arabidopsis. Plant physiology 140:899-908

Nagpal P, Walker LM, Young JC, Sonawala A, Timpte C, Estelle M, Reed JW (2000) AXR2 Encodes a Member of the Aux/IAA Protein Family. Plant Physiology 123:563-574

Nakamura A, Umemura I, Gomi K, Hasegawa Y, Kitano H, Sazuka T, Matsuoka M (2006) Production and characterization of auxin-insensitive rice by overexpression of a mutagenized rice IAA protein. The Plant Journal 46:297-306

Nanao MH, Vinos-Poyo T, Brunoud G, Thévenon E, Mazzoleni M, Mast D, Lainé S, Wang S, Hagen G, Li H, Guilfoyle TJ, Parcy F, Vernoux T, Dumas R (2014) Structural basis for oligomerization of auxin transcriptional regulators. Nature Communications 5:3617

Niemeyer M, Moreno Castillo E, Ihling CH, Iacobucci C, Wilde V, Hellmuth A, Hoehenwarter W, Samodelov SL, Zurbriggen MD, Kastritis PL, Sinz A, Calderón Villalobos

LIA (2020) Flexibility of intrinsically disordered degrons in AUX/IAA proteins reinforces auxin co-receptor assemblies. Nature Communications 11:2277

Okushima Y, Overvoorde PJ, Arima K, Alonso JM, Chan A, Chang C, Ecker JR, Hughes B, Lui A, Nguyen D, Onodera C, Quach H, Smith A, Yu G, Theologis A (2005) Functional Genomic Analysis of the AUXIN RESPONSE FACTOR Gene Family Members in Arabidopsis thaliana: Unique and Overlapping Functions of ARF7 and ARF19. The Plant Cell 17:444-463

Ouellet F, Overvoorde PJ, Theologis A (2001) IAA17/AXR3: Biochemical Insight into an Auxin Mutant Phenotype. The Plant Cell 13:829-841

Pazmiño DM, Rodríguez-Serrano M, Sanz M, Romero-Puertas MC, Sandalio LM (2014) Regulation of epinasty induced by 2,4-dichlorophenoxyacetic acid in pea and Arabidopsis plants. Plant Biology 16:809-818

Penner D (1994) Herbicide action and metabolism. Turf Weeds and Their Control:37-70

Petrášek J, Mravec J, Bouchard R, Blakeslee JJ, Abas M, Seifertová D, Wiśniewska J, Tadele Z, Kubeš M, Čovanová M, Dhonukshe P, Skůpa P, Benková E, Perry L, Křeček P, Lee OR, Fink GR, Geisler M, Murphy AS, Luschnig C, Zažímalová E, Friml J (2006) PIN Proteins Perform a Rate-Limiting Function in Cellular Auxin Efflux. Science 312:914-918

Philippar K, Büchsenschütz K, Edwards D, Löffler J, Lüthen H, Kranz E, Edwards KJ, Hedrich R (2006) The auxin-induced K+ channel gene Zmk1 in maize functions in coleoptile growth and is required for embryo development. Plant Molecular Biology 61:757-768

Pozo JCd, Timpte C, Tan S, Callis J, Estelle M (1998) The Ubiquitin-Related Protein RUB1 and Auxin Response in Arabidopsis. Science 280:1760-1763

Prigge MJ, Greenham K, Zhang Y, Santner A, Castillejo C, Mutka AM, O'Malley RC, Ecker JR, Kunkel BN, Estelle M (2016) The Arabidopsis Auxin Receptor F-Box Proteins AFB4 and AFB5 Are Required for Response to the Synthetic Auxin Picloram. G3: Genes|Genomes|Genetics 6:1383-1390

Rinaldi MA, Liu J, Enders TA, Bartel B, Strader LC (2012) A gain-of-function mutation in IAA16 confers reduced responses to auxin and abscisic acid and impedes plant growth and fertility. Plant Molecular Biology 79:359-373

Robert HS, Friml J (2009) Auxin and other signals on the move in plants. Nature Chemical Biology 5:325-332

Rodríguez-Serrano M, Pazmiño DM, Sparkes I, Rochetti A, Hawes C, Romero-Puertas MC, Sandalio LM (2014) 2,4-Dichlorophenoxyacetic acid promotes S-nitrosylation and oxidation of actin affecting cytoskeleton and peroxisomal dynamics. Journal of Experimental Botany 65:4783-4793

Rogg LE, Lasswell J, Bartel B (2001) A Gain-of-Function Mutation in IAA28 Suppresses Lateral Root Development. The Plant Cell 13:465-480

Růžička K, Strader LC, Bailly A, Yang H, Blakeslee J, Łangowski Ł, Nejedlá E, Fujita H, Itoh H, Syōno K, Hejátko J, Gray WM, Martinoia E, Geisler M, Bartel B, Murphy AS, Friml J (2010) Arabidopsis PIS1 encodes the ABCG37 transporter of auxinic compounds including the auxin precursor indole-3-butyric acid. Proceedings of the National Academy of Sciences 107:10749-10753

Sandalio LM, Rodríguez-Serrano M, Romero-Puertas MC (2016) Leaf epinasty and auxin: A biochemical and molecular overview. Plant Science 253:187-193

Santner A, Calderon-Villalobos LIA, Estelle M (2009) Plant hormones are versatile chemical regulators of plant growth. Nature Chemical Biology 5:301-307

Scheel D, Sandermann H (1981a) Metabolism of 2,4-dichlorophenoxyacetic acid in cell suspension cultures of soybean (Glycine max L.) and wheat (Triticum aestivum L.). Planta 152:253-258

Scheel D, Sandermann H (1981b) Metabolism of 2,4-dichlorophenoxyacetic acid in cell suspension cultures of soybean (Glycine max L.) and wheat (Triticum aestivum L.): I. General results. Planta 152:248-252

Schwechheimer C, Serino G, Callis J, Crosby WL, Lyapina S, Deshaies RJ, Gray WM, Estelle M, Deng X-W (2001) Interactions of the COP9 Signalosome with the E3 Ubiquitin Ligase SCF^{TIR1} in Mediating Auxin Response. Science 292:1379-1382

Smalle J, Vierstra RD (2004) THE UBIQUITIN 26S PROTEASOME PROTEOLYTIC PATHWAY. Annual Review of Plant Biology 55:555-590

Song Y, You J, Xiong L (2009) Characterization of OsIAA1 gene, a member of rice Aux/IAA family involved in auxin and brassinosteroid hormone responses and plant morphogenesis. Plant Molecular Biology 70:297-309

Spartz AK, Ren H, Park MY, Grandt KN, Lee SH, Murphy AS, Sussman MR, Overvoorde PJ, Gray WM (2014) SAUR Inhibition of PP2C-D Phosphatases Activates Plasma Membrane H⁺-ATPases to Promote Cell Expansion in Arabidopsis. The Plant Cell 26:2129-2142

Sun N, Wang J, Gao Z, Dong J, He H, Terzaghi W, Wei N, Deng XW, Chen H (2016) Arabidopsis SAURs are critical for differential light regulation of the development of various organs. Proceedings of the National Academy of Sciences 113:6071-6076

Takahashi K, Hayashi K-i, Kinoshita T (2012) Auxin Activates the Plasma Membrane H⁺-ATPase by Phosphorylation during Hypocotyl Elongation in Arabidopsis. Plant Physiology 159:632-641

Tan X, Calderon-Villalobos LIA, Sharon M, Zheng C, Robinson CV, Estelle M, Zheng N (2007) Mechanism of auxin perception by the TIR1 ubiquitin ligase. Nature 446:640-645

Tatematsu K, Kumagai S, Muto H, Sato A, Watahiki MK, Harper RM, Liscum E, Yamamoto KT (2004) MASSUGU2 Encodes Aux/IAA19, an Auxin-Regulated Protein That Functions Together with the Transcriptional Activator NPH4/ARF7 to Regulate Differential Growth Responses of Hypocotyl and Formation of Lateral Roots in Arabidopsis thaliana. The Plant Cell 16:379-393

Tian Q, Reed JW (1999) Control of auxin-regulated root development by the Arabidopsis thaliana SHY2/IAA3 gene. Development 126:711-721

Ulmasov T, Hagen G, Guilfoyle TJ (1997) ARF1, a Transcription Factor That Binds to Auxin Response Elements. Science 276:1865-1868

Ulmasov T, Hagen G, Guilfoyle TJ (1999) Activation and repression of transcription by auxin-response factors. Proc Natl Acad Sci U S A 96:5844-9

Walsh TA, Neal R, Merlo AO, Honma M, Hicks GR, Wolff K, Matsumura W, Davies JP (2006) Mutations in an Auxin Receptor Homolog AFB5 and in SGT1b Confer Resistance to Synthetic Picolinate Auxins and Not to 2,4-Dichlorophenoxyacetic Acid or Indole-3-Acetic Acid in Arabidopsis. Plant Physiology 142:542-552

Wang R, Zhang Y, Kieffer M, Yu H, Kepinski S, Estelle M (2016) HSP90 regulates temperature-dependent seedling growth in Arabidopsis by stabilizing the auxin co-receptor F-box protein TIR1. Nature Communications 7:10269

Wang T-Y, Libardo MDJ, Angeles-Boza AM, Pellois J-P (2017) Membrane Oxidation in Cell Delivery and Cell Killing Applications. ACS chemical biology 12:1170-1182

Watahiki MK, Yamamoto KT (1997) The massugu1 Mutation of Arabidopsis Identified with Failure of Auxin-Induced Growth Curvature of Hypocotyl Confers Auxin Insensitivity to Hypocotyl and Leaf. Plant Physiology 115:419-426

Watanabe E, Mano S, Nomoto M, Tada Y, Hara-Nishimura I, Nishimura M, Yamada K (2016) HSP90 Stabilizes Auxin-Responsive Phenotypes by Masking a Mutation in the Auxin Receptor TIR1. Plant and Cell Physiology 57:2245-2254

Weinberg T, Stephenson GR, McLean MD, Hall JC (2006) MCPA (4-chloro-2-ethylphenoxyacetate) resistance in hemp-nettle (*Galeopsis tetrahit* L.). J. Agric. Food Chem. 54:9126-9134

Wightman F, Setterfield G (1968) Biochemistry and physiology of plant growth substances: proceedings: The Runge

Winkler M, Niemeyer M, Hellmuth A, Janitza P, Christ G, Samodelov SL, Wilde V, Majovsky P, Trujillo M, Zurbriggen MD, Hoehenwarter W, Quint M, Calderón Villalobos LIA (2017) Variation in auxin sensing guides AUX/IAA transcriptional repressor ubiquitylation and destruction. Nature Communications 8:15706

Witham FH, Feung C-S, Hamilton RH (1971) Metabolism of 2,4-dichlorophenoxyacetic acid by soybean cotyledon callus tissue cultures. Journal of Agricultural and Food Chemistry 19:475-479

Xu T, Dai N, Chen J, Nagawa S, Cao M, Li H, Zhou Z, Chen X, De Rycke R, Rakusová H, Wang W, Jones AM, Friml J, Patterson SE, Bleecker AB, Yang Z (2014a) Cell Surface ABP1-TMK Auxin-Sensing Complex Activates ROP GTPase Signaling. Science 343:1025-1028

Xu T, Wang Y, Liu X, Gao S, Qi M, Li T (2015) Solanum lycopersicum IAA15 functions in the 2,4-dichlorophenoxyacetic acid herbicide mechanism of action by mediating abscisic acid signalling. Journal of Experimental Botany 66:3977-3990

Xu Y, Zhang S, Guo H, Wang S, Xu L, Li C, Qian Q, Chen F, Geisler M, Qi Y, Jiang DA (2014b) OsABCB14 functions in auxin transport and iron homeostasis in rice (Oryza sativa L.). The Plant Journal 79:106-117

Yang X, Lee S, So J-h, Dharmasiri S, Dharmasiri N, Ge L, Jensen C, Hangarter R, Hobbie L, Estelle M (2004) The IAA1 protein is encoded by AXR5 and is a substrate of SCFTIR1. The Plant Journal 40:772-782

Yu H, Zhang Y, Moss BL, Bargmann BOR, Wang R, Prigge M, Nemhauser JL, Estelle M (2015) Untethering the TIR1 auxin receptor from the SCF complex increases its stability and inhibits auxin response. Nature Plants 1:14030

Zhang W, Ito H, Quint M, Huang H, Noël LD, Gray WM (2008) Genetic analysis of CAND1–CUL1 interactions in Arabidopsis supports a role for CAND1-mediated cycling of the SCF^{TIR1} complex. Proceedings of the National Academy of Sciences 105:8470-8475

Table 1.1: Characterized co-receptor ligand specificity among different synthetic auxin classes.

Auxin Class		TIR1	AFB4	AFB5	AFB6	Species	Method	Reference
Phenoxyacetic acids	2,4-D	X			X	*Arabidopsis thaliana; Kochia scoparia*	*In planta (tir1-1*, *afb5-1)*; Y2H; SPR	(Gleason et al., 2011; LeClere et al., 2018; Lee et al., 2014; Walsh et al., 2006)
	Dichlorprop	X				*Arabidopsis thaliana*	SPR	(Lee et al., 2014)
Quinolinones	Quinclorac			X		*Arabidopsis thaliana*	SPR	(Lee et al., 2014)
Picolinates	Clopyralid	X			X	*Kochia scoparia*	Y2H	(LeClere et al., 2018)
	Picloram	X	X	X		*Arabidopsis thaliana*	*In planta (tir1-1, afb4-8, afb5-5);* SPR	(Lee et al., 2014; Prigge et al., 2016; Walsh et al., 2006)
	Triclopyr	X		X		*Arabidopsis thaliana*	SPR	(Lee et al., 2014)
	Fluroxypyr	X		X		*Arabidopsis thaliana*	SPR	(Lee et al., 2014)
	Florpyrauxifen-benzyl	X		X		*Arabidopsis thaliana*	*In planta (tir1-1, afb5);* SPR	(Lee et al., 2014; Walsh et al., 2006)
Benzoic acids	Dicamba	X		X	X	*Arabidopsis thaliana; Kochia scoparia*	*In planta (tir1-1, afb5-1)*; Y2H; SPR	(Gleason et al., 2011; LeClere et al., 2018; Lee et al., 2014)

Table 1.2: Characterized mutants in Arabidopsis Aux/IAA genes that lead to auxin insensitivity.

Species	AUX/IAA	Genetic/expression changes	Auxin insensitivity	Phenotype	Method	Reference
Arabidopsis thaliana	*IAA1*	Degron AA change (P61S)	2,4-D, 1-NAA, IAA	Changes on leaf morphology, agravitropism	*axr5-1 ;* EMS mutation	(Nagpal et al., 2000; Yang et al., 2004)
	IAA3	Degron AA change (G67E; P69S)	2,4-D, IAA	Short roots, curled leaves	*shy2-2, shy2-3*	(Tian and Reed, 1999)
	IAA7	Domain I AA change (L15F) Degron AA change (P87S)	Picloram, Florpyrauxifen-benzyl, 2,4-D	Short hypocotyl, agravitropism, no root hairs	*axr2-1-r4, axr2-1, axr2-1-r3,* EMS mutation, Y2H	(Calderón Villalobos et al., 2012; Nagpal et al., 2000; Walsh et al., 2006)
	IAA12	Degron AA change (P74S)	2,4-D, IAA	No root meristem growth	*Bdli*, EMS mutation	(Hamann et al., 2002; Hamann et al., 1999)
	IAA14	Degron AA change (P81S, P82A, P82S)	2,4-D, IAA, NAA	No lateral roots, root hairs, agravitropism	*slr, EMS* mutation	(Fukaki et al., 2002)
	IAA16	Degron AA change (P65L)	2,4-D (high resistance), IAA	Drastic reduction on plant size and leaf morphology, short root hairs	*Iaa16-1,* EMS mutation	(Rinaldi et al., 2012)
	IAA17	Degron AA change (P88L)	IAA	Insensitive to Ethylene	*axr3*, EMS mutation	(Ouellet et al., 2001)
	IAA19	Degron AA change (G73R, P75L, P76L, P76S)	2,4-D (Just shoots, not roots), IAA	Changes on hypocotyl and lateral root formation	*msg2,* EMS mutation	(Tatematsu et al., 2004)
	IAA28	Degron AA change (P53L)	IAA	Changes on leaf morphology, infertile dwarfs	*iaa28-1,* EMS mutation	(Rogg et al., 2001)

Solanum lycopersicum	*SiIAA15*	Downregulation	NAA	Silencing leads to auxin tolerance	Antisense construct; 35S:: *SiIAA15*	(Xu et al., 2015)
Oryza sativa	*OsIAA1*	Over expression	Increased 2,4-D tolerance, IAA	Changes on plant size and reduced root elongation	*Ubi-1::OsIAA1*; Transgenic transformation	(Song et al., 2009)
	OsIAA3	Degron AA change (P58L)	Increased 2,4-D tolerance	Agraviotropic, abnormal and reduced leaves, reduced root formation	Overexpression of mOsIAA3-GR, Transgenic transformation	(Nakamura et al., 2006)
Kochia scoparia	*KsIAA16*	Degron AA change (G to N)	Dicamba; 2,4-D	Reduced plant size, biomass and seed production	Y2H, heterologous expression in *Arabidopsis*	(LeClere et al., 2018)

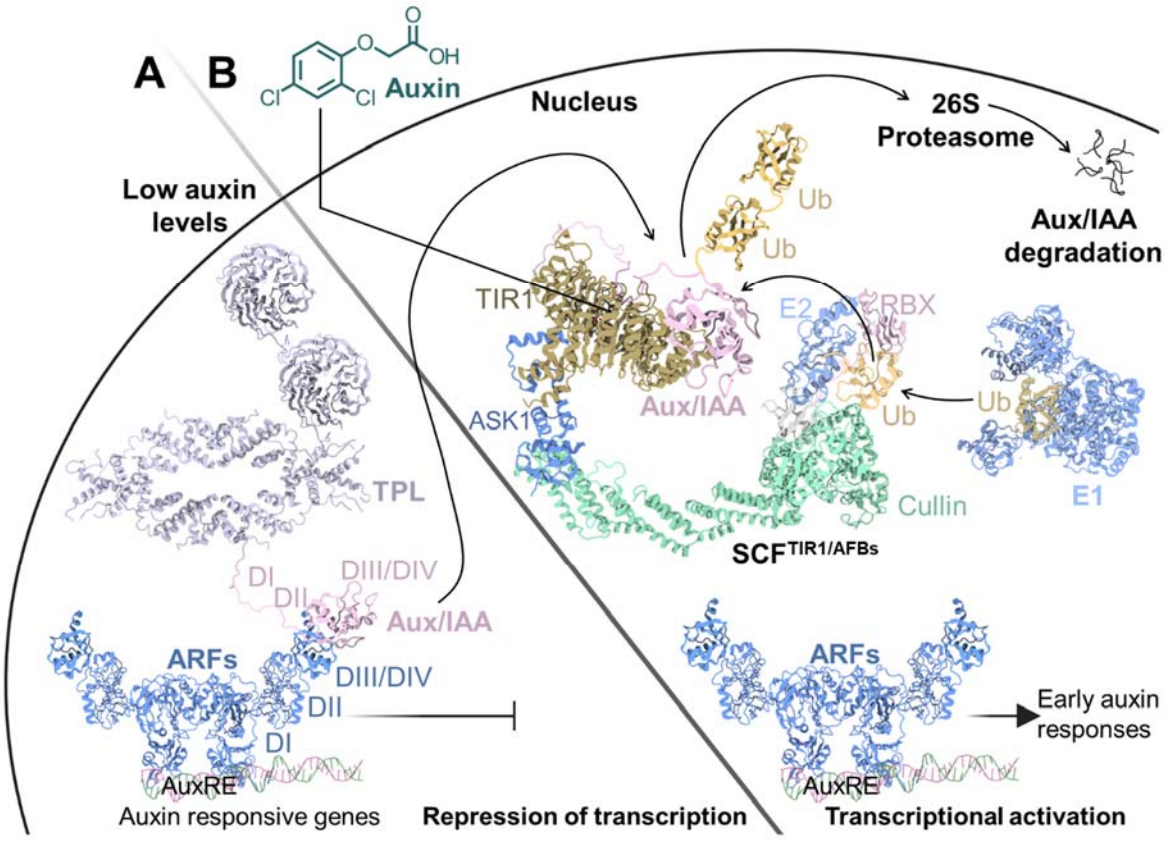

Figure 1.1: Model of the canonical auxin signaling pathway. Auxin binds to the F-Box protein TIR1, targeting auxin/indole acetic acid proteins (Aux/IAAs) for degradation. A) In the plant cell nucleus, under low levels of auxin, Aux/IAA proteins and the corepressor TPL interact with Auxin Response Factors (ARFs) to induce gene transcription repression in auxin responsive genes. B) Under high auxin concentrations, the complex TIR1-auxin-Aux/IAA is formed, leading to the ubiquitination of the repressor protein that will be subsequently degraded by 26S proteasome. The transcriptional activation in genes mediated by ARFs leads to auxin responses, ARFs transcription targets DNA promoter regions that contain the auxin response elements (AuxRE). Adapted from (Santner et al., 2009).

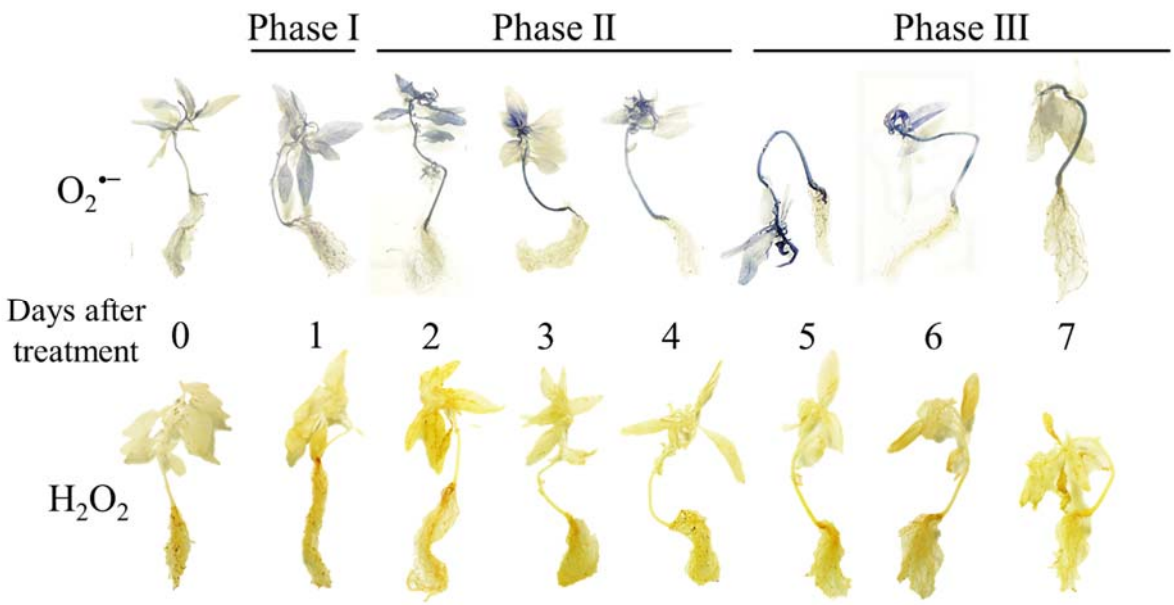

Figure 1.2: Reactive oxygen species (ROS) production in *Amaranthus tuberculatus*. Histological analysis showing the production of $O_2^{\cdot-}$ and H_2O_2 in different days after 2,4-D application. In phase I of herbicide action, old leaves and stems start to present traces of ROS, which may lead to the first epinastic effects. Phase II may occur at days 2, 3 and 4, when the $O_2^{\cdot-}$ production increases in response of the accumulation of the hormones, abscisic acid and ethylene. In days 5, 6, and 7, the production of ROS increases at meristems and stems, culminating in tissue death on the seventh day, where most of the ROS staining signals disappear (Phase III).

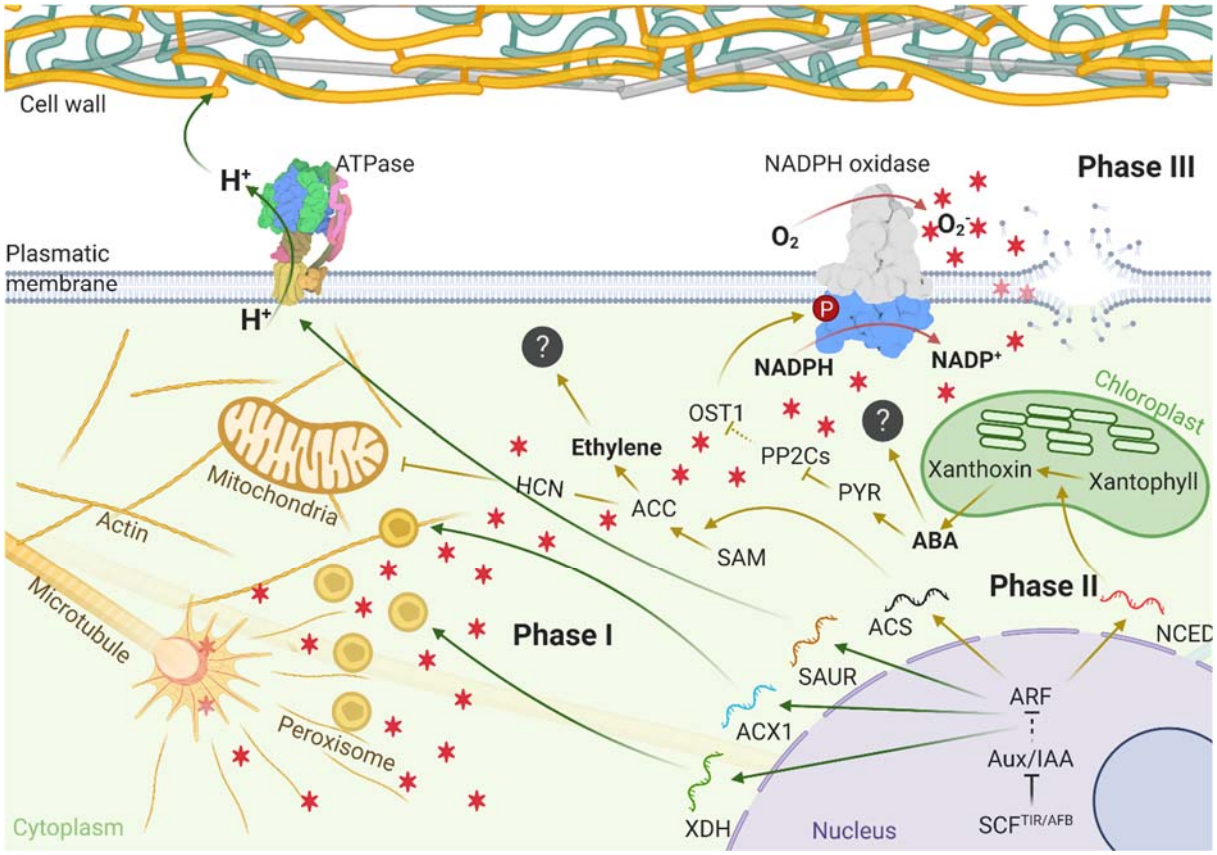

Figure 1.3: Proposed mechanism of auxinic herbicide action in plant cells.
After herbicide application, the synthetic auxin induces Aux/IAA degradation via $SCF^{TIR/AFB}$ ubiquitination pathway. In the first phase on auxin herbicide action (stimulation phase green arrows), auxin response factors (ARFs) transcribe genes like xanthine dehydrogenase (XDH) and acyl CoA oxidase (ACX1) leading to enzymatic reactions that will generate high amounts of reactive oxygen species (ROS) and nitric-oxide (symbolized by red stars). The accumulation of those reaction-sub-products will induce carbonylation and S-nitrosylation in actin, reducing the size of its filaments and it will lead to a broad reorganization of cell microtubules. Additionally, in this first phase ARFs will transcribe the SMALL AUXIN UP-REGULATED RNA (SAUR) gene family that will induce the activation of plasmatic membrane ATPases. The active injection of protons to the symplast will reduce its pH, causing the activation of expansins that act at the cell walls, reducing its stiffness to facilitate cell expansion. In the phase II, called inhibition (yellow arrows), there is an accumulation of abscisic acid (ABA) mediated by the 9-cis-epoxycarotenoid dioxygenase (NCED) upregulation. ABA then finds its receptor, PYR, that will inhibit the phosphatase PP2Cs repressor of enzyme kinases. With the inactivation of the repressor, OST1 kinases will activate NADPH oxidase that will catalyze $O_2^{\cdot-}$ production, increasing oxidative stress. Auxin additionally induces the accumulation of ethylene by the transcription of genes encoding 1-aminocyclopropane-1-carboxylic acid synthase (ACS), catalyzing the conversion of convert S-adenosyl-L-methionine (SAM) into l-amino-cyclopropene-carboxylase (ACC) that will be turned into ethylene, releasing cyanide (HCN) as a sub-product. HCN will inhibit the mitochondria membrane electron transport chain, depleting aerobic ATP production. The accumulation of ethylene and ABA will additionally induce hormonal responses that may contribute for the process of cell death, however the specific

responses between those hormones and auxin herbicide action were not deeply investigated yet. In the final phase III, called decay, the accumulation of ROS will disrupt the plasmatic membrane integrity, leading to cytosol leak and cell death.

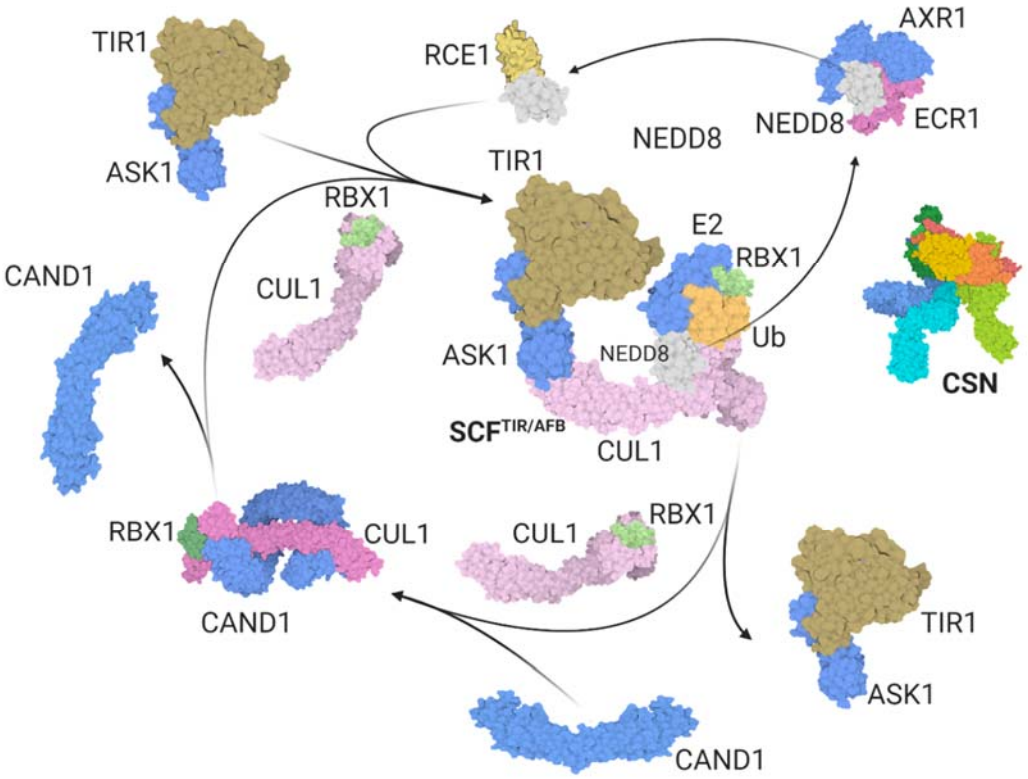

Figure 1.4: $SCF^{TIR/AFB}$ regulatory cycle involving CAND1 and CSN-mediated neddylation/deneddylation of the cullin (CUL1) subunit.
The disassembling of the $SCF^{TIR/SCF}$ protein complex can happen before or after Aux/IAA ubiquitination. The process starts with the association between $SCF^{TIR/AFB}$ and COP9/signalosome (CSN), where the CSN5 subunit (yellow protein subunit of CSN) deneddylates (removes NEDD8) from the cullin (CUL1) at the SCF. NEDD8 will then be transferred to an E1 ubiquitin-conjugating enzyme (AXR1/ECR1) and subsequently passed to an E2 (RCE1) to finally neddylate the CUL1 again for proper SCF assembling. De-neddylated CUL1 can transiently associate to a U-shaped protein called CAND1, preventing the formation of the SCF complex. Eventual dissociation of CUL1 from CAND1 allows its re-association with ASK1-TIR1 F-box and to be re-neddylated for proper re-assemblance of the $SCF^{TIR/AFB}$ complex. Adapted from (Hua and Vierstra, 2011).

CHAPTER II – Metabolism of 2,4-dichlorophenoxyacetic acid contributes to resistance in a common waterhemp (*Amaranthus tuberculatus*) population

INTRODUCTION

The synthetic auxin herbicide 2,4-D was introduced for weed control in agriculture in the mid-1940s (Burnside, 1996) and has since become one of the most widely used herbicides in the world. This and other auxinic herbicides are popular among growers, in part because of their ability to selectively control broadleaf weeds. In 2005, the United States Environmental Protection Agency estimated annual 2,4-D use in agriculture and non-agriculture settings at 20.9 million kg (2005). Even after the introduction of newer herbicides, such as glyphosate, triazines, and acetolactate synthase (ALS) inhibitors, auxinic herbicide use has remained high, primarily because of their selectivity, efficacy, broad-spectrum, and low cost (Burnside, 1996). More recently, the widespread and increasing evolution of resistance in weed species to various other herbicides has resulted in an increase in auxinic herbicide use. The development and commercialization of 2,4-D-resistant cotton (*Gossypium hirsutum*) and soybean (*Glycine max*) crop varieties (Wright et al., 2010) will likely increase 2,4-D use for in-crop selective weed control.

Synthetic auxin herbicides are known to mimic several physiological and biochemical responses induced by the natural plant hormone, indole acetic acid (IAA – Grossmann, 2010a). Despite their extensive use in agriculture for several decades, the precise mechanism of synthetic auxin herbicide action is not completely understood. Upon discovery of IAA receptors Transport Inhibitor Response 1 (TIR1) and Auxin F-Box (AFB) proteins (Dharmasiri et al., 2005; Kepinski and Leyser, 2005), the role of these proteins in auxinic herbicide-mediated responses has also been examined (Walsh et al., 2006; Gleason et al., 2011). One hypothesis is that functional

redundancy in auxin receptors (i.e., TIR1 and AFBs 1-5) might contribute to multiple sites of action for auxinic herbicides. The precise role of these proteins in auxinic herbicide-mediated responses is still elusive. Previous research also suggests that auxinic herbicides activate metabolic processes that initiate ethylene accumulation, resulting in epinasty (Grossmann, 2010a). Other factors potentially leading to plant death include abscisic acid (ABA) accumulation resulting in 1) photosynthesis inhibition, 2) H_2O_2 production, and 3) increase in reactive oxygen species (ROS) (Grossmann et al., 2001; Grossmann, 2010a).

The selectivity of auxinic herbicides in controlling broadleaf species is primarily due to auxinic herbicide metabolism by tolerant species (Coupland, 1994). Metabolism also plays a key role in conferring resistance to these herbicides in dicot species as well (Hatzios and Penner, 1982). In most cases, auxinic herbicides undergo oxidation, hydrolysis, or conjugation resulting in reduced biological activity (Ashton and Crafts, 1981; Hatzios and Penner, 1982; Kreuz et al., 1996). In tolerant monocots, metabolic reactions typically occur through ring hydroxylation followed by irreversible glucose conjugation (Devine et al., 1992). In sensitive dicots, auxinic herbicides may be conjugated to amino acids, which are reversible to active forms and may still have partial herbicidal activity themselves (Scheel and Sandermann, 1981c).

Amaranthus tuberculatus (Moq.) Sauer var. *rudis* (Sauer) Costea and Tardif (common waterhemp) is a major troublesome weed of cropping systems in North America (Trucco and Tranel, 2011). Especially in agricultural fields of the Midwestern United States, this weed poses a serious problem causing significant yield losses in maize (*Zea mays*) and soybean (Hager et al., 2002; Steckel and Sprague, 2004; Costea et al., 2005; Steckel, 2007). *A. tuberculatus* is dioecious and a prolific seed producer, which enables rapid spread (Costea et al., 2005). High genetic variability coupled with intense herbicide selection pressure has resulted in evolution of

resistance to several commonly used herbicides in *A. tuberculatus* (Bell et al., 2013; Nandula et al., 2013; Lorentz et al., 2014). US Midwestern populations of *A. tuberculatus* have various combinations of herbicide resistance spanning six modes of action including photosystem II (PSII)-inhibitors, ALS-inhibitors, protoporphyrinogen oxidase (PPO) inhibitors, 4-hydroxyphenylpyruvate dioxygenase (HPPD) inhibitors, 5-enolpyruvylshikimate-3-phosphate synthase (*EPSPS*) inhibitors, and 2,4-D (Heap, 2020).

Herbicide resistance has become a major global issue and numerous agriculturally important weeds have confirmed resistance to multiple herbicide modes of action (Heap, 2020). Even after several decades of continuous auxinic herbicide use, the rate of resistance evolution to auxinic herbicides is comparatively low (Jugulam et al., 2011). There are currently 34 weed species known to have evolved resistance to auxinic herbicides (Heap, 2020), including *A. tuberculatus*. In 2009, the first failure to control *A. tuberculatus* with 2,4-D was reported in Nebraska, USA. This population was confirmed to have evolved resistance to 2,4-D with a resistance ratio of 10 relative to a susceptible population (Bernards et al., 2012). The resistance mechanism in this *A. tuberculatus* population has not been determined. The objective of this research was to examine [^{14}C] 2,4-D uptake, translocation, and metabolism in an effort to identify the resistance mechanism.

MATERIALS AND METHODS

The 2,4-D-resistant *A. tuberculatus* from southeast Nebraska was used in this research (Bernards et al., 2012). This population was found in a seed production field of little bluestem (*Schizachyrium scoparia* Michx. Nash) that had been in no-till management with annual application of 2,4-D for over 10 years. The 2,4-D resistant *A. tuberculatus* seed was collected

from the field followed by one generation of 2,4-D selection in the greenhouse to produce the seed used in these studies. An *A. tuberculatus* population from Nebraska known to be susceptible to 2,4-D was also used for comparison.

[^{14}C] 2,4-D Absorption and Translocation

Resistant and susceptible *A. tuberculatus* seeds were planted on potting soil**,** kept in a 4ºC room for one week and then transferred to a greenhouse with controlled conditions at 25 ºC and 75% RH until reaching 8 cm or 4 true leaves. Plants were then transplanted to fine washed silica, irrigated with fertilizer (0.05% Miracle-Gro solution, Scotts Miracle-Gro Company, Marysville, OH), and transferred to a growth chamber under the same conditions as the greenhouse except for the lighting which was supplied with fluorescent and incandescent light.

Plants were treated at the stage of 4-6 true leaves (1 week after transplanting). The fourth true leaf was marked and covered with aluminum foil. Plants were then sprayed in a single nozzle overhead track sprayer (DeVries Generation III Research Sprayer, Hollandale, MN, USA) with 500 g ha^{-1} 2,4-D (2,4-D amine, 455 g L^{-1}, DuPont) in a water volume of 224 L ha^{-1} containing 1% COC. The aluminum foil was then removed and a solution of [^{14}C]-2,4-D mixed with formulated 2,4-D and COC was applied using 10 droplets of 1 µl each, so that the treated leaf received the same amount of herbicide as the rest of the plant (5 µg cm^{-2} and 3 µl cm^{-2}). Total radioactivity applied per plant was 3.33 KBq (200,000 dpm). Three replications per time point were used, and the experiment was repeated.

Evaluation time points were at 12, 24, 48, 96, and 192 HAT. The treated leaves were cut and washed with 5 ml of 10% methanol and 1% NIS washing solution. The leaf rinse solution was mixed with 10 ml of scintillation cocktail (Ecoscint^{TM} XR) and measured for radioactivity

using LSS (Packard Tri-carb 2300TR). Roots were washed with 10 ml water, and 3 ml of the wash solution was measured with LSS. Plants including treated leaves were pressed in newspaper and dried in a 60 ºC oven for 72 h before exposure to Phosphor Screen film for 3 d followed by imaging with a Typhoon Trio Imager (GE Healthcare). The dried tissue was separated into treated leaf, untreated leaves, stem, and roots, and then oxidized in a Biological oxidizer (OX500) followed by radioactivity measurement with LSS. The proportion of absorbed herbicide was calculated using the following equation:

$$\%H_{abs} = [(^{14}C\ ot) / (^{14}C\ ot + {}^{14}C\ wl)] \times 100$$

where "$\%H_{abs}$" is the proportion of absorbed herbicide, "^{14}C ot" is the amount of ^{14}C measured in oxidized tissue, and "^{14}C wl" is the amount of ^{14}C detected in the treated leaf. For herbicide translocation studies the following equation was used:

$$\%H_{tr} = 100 - [(^{14}C\ al) / (^{14}C\ al + {}^{14}C\ ot) \times 100]$$

where "$\%H_{tr}$" is the proportion of translocated herbicide, "^{14}C al" is the amount of ^{14}C measured in the treated leaf, and "^{14}C ot" is the amount of ^{14}C detected in other untreated tissues of the plant.

[^{14}C] Metabolism

Plants were treated with the same procedures and conditions as the absorption and translocation studies. They were harvested at 12, 24, 48, 96, 192, and 264 HAT and at each time point, treated leaf and sand were washed and the plant tissue was rapidly frozen in liquid nitrogen and stored at -80 ºC. Metabolite extraction was performed by grinding the entire plant with a mortar and pestle, then digesting tissue with a 10 ml solution of 1% acetic acid in 50 ml

plastic tubes on a table shaker for 10 min. Extracts were put in 50 ml centrifuge filters with 25 ml microfiltration membranes (pore size of 0.45 µm), then the tissue digestion step was repeated two more times. Filters and tissue were dried and kept for oxidation to quantify the non-extracted metabolites. Final extracted volume of 30 ml was applied to a solid phase extraction C18 cartridge, and 5 ml of digestion solution that passed through the cartridge was quantified by LSS. About 95% of radioactivity interacted with the silica matrix and was recovered with 4 ml of acetonitrile and dried in an evaporation system under vacuum at 40 ^{o}C. Entire extracts were suspended in 225 µl of HPLC A solvent and filtered in 1.5 ml centrifuge tubes with 0.4 µm microfiltration membranes at 12,000×g. Filtered solution (200 µl) was used for HPLC (Hitachi Instruments, Inc., San Jose, CA) using a C18 4.6 mm by 150 mm column (C18 Column, Zorbax Eclipse XDB-C18, Agilent Technologies, Santa Clara, CA, USA), attached to a radio-detector (FlowStar LB 513, Berthold Technologies GmbH & Co.) with a flow cell YG-150-U5D solid cell YG-Scintillator (150 µl). Mobile Phase A contained 89.9% water, 10% acetonitrile, and 0.1% formic acid and phase B contained 99.9% acetonitrile and 0.1% formic acid. A calibration curve for radioactivity detection was constructed using a series of different counts of [^{14}C]-2,4-D (8.3 Bq, 16.7 Bq, 83.3 Bq, 166.7 Bq, 1666.7 Bq, and 3333.3 Bq). The proportion of 2,4-D metabolism was calculated using the equation:

$\%2,4\text{-}D_{Parent}$ = [(HPLC detected 2,4-D) / (HPLC detected 2,4-D + HPLC detected metabolites + counts in oxidized filters + counts in digestion solution after C18 cartridge separation + counts in washed sand)] ×100

where "$\%2,4\text{-}D_{Parent}$" is the proportion of non-metabolized herbicide. The experiment had 3 replications and it was repeated.

Malathion Effects on 2,4-D Resistance and Metabolism

Resistant and susceptible *A. tuberculatus* plants were grown in a greenhouse under controlled conditions as described above, except that plants were grown in potting soil. Half of the resistant and susceptible plants were treated with malathion (Spectracide, United Industries Corporation, St. Louis, MO) at 2,000 g ha^{-1}, 24 h before 2,4-D treatment. Plants were treated with 2,4-D (2,4-D amine, 455 g L^{-1}, DuPont) at the developmental stage of 4-5 true leaves and treatments were 0, 15, 30, 63, 125, 250, 500, 1,000, 2,000, and 6,000 g ha^{-1}. Plants were harvested 28 d after treatment and dried in a 60 ºC oven before weighing.

Another study to analyze malathion effects on 2,4-D metabolism was conducted as described above. Half of the plants transplanted to fine silica were sprayed with malathion at 2,000 g ha^{-1}, and at 24 HAT all resistant and susceptible plants were treated with [^{14}C] 2,4-D as described above. After 264 h, [^{14}C] 2,4-D treated leaves and roots were washed and the tissue was frozen with liquid nitrogen for metabolite extraction as described above. The amount of 2,4-D recovered was calculated using the equation "$\%2,4\text{-}D_{Parent}$" described above. Each treatment had 3 replications and the experiment was repeated.

Data Analysis

The experiments were analyzed using the software R (R, 2015). Absorption and translocation over time were analyzed using a rectangular hyperbolic model (Kniss et al., 2011). 2,4-D metabolism and 2,4-D dose response with malathion were analyzed using a three-parameter log-logistic model (Knezevic et al., 2007). Malathion effect on 2,4-D metabolism was analyzed using a factorial ANOVA in R and contrast comparisons were adjusted by the Tukey method.

RESULTS

[^{14}C] 2,4-D Absorption and Translocation

To investigate the 2,4-D resistance mechanisms in *A. tuberculatus*, we first determined if reduced absorption or translocation of [^{14}C] 2,4-D contributed to resistance. There were no differences in the amount of [^{14}C] 2,4-D absorbed between 2,4-D-resistant or -susceptible plants at all harvest times (Figure 2.1A, Supplementary Tables 2.1 and 2.2). No difference was found in A_{max} (maximum absorption) between populations (S: 73% ±4 and R: 73% ±4) (Figure 2.1A), or in t_{90} (time in h for 90% of maximum absorption) between populations (S: 43 h ±4 and R: 33 h ±7).

2,4-D is a systemic herbicide which translocates via xylem and phloem to other parts of the plant following absorption. Translocation was similar between resistant and susceptible plants through 96 HAT (Figure 2.1B, Supplementary Tables 2.1 and 2.2). Although the experiment was conducted over a reasonable time course of 192 h, 2,4-D translocation in resistant plants did not reach an asymptote by the last time point. The T_{192} value (translocation at 192 HAT) was higher in resistant plants (42 h ±9) than in susceptible plants (23 h ±6). This suggests 2,4-D translocation in susceptible plants is self-limiting beyond 96 HAT when plant death occurs, while 2,4-D translocation continues in resistant plants. Phosphor images confirmed no differences in translocation between the two populations through 96 HAT (Figure 2.1C). Therefore, differences in 2,4-D absorption or translocation do not contribute substantially to 2,4-D resistance in this *A. tuberculatus* population.

[^{14}C] 2,4-D Metabolism

To determine if 2,4-D metabolism was a factor in the resistance mechanism of this *A. tuberculatus* population, we measured how much [^{14}C] 2,4-D was metabolized over time. The parent compound of [^{14}C] 2,4-D resolved at peak retention time (RT) of about 12.5 min by reverse-phase HPLC with no other peaks observed (data not shown). This indicates that peaks at other retention times observed in plant lysates are products derived from 2,4-D metabolism (Figures 2.2A, B). At 264 HAT, a large amount of 2,4-D was detected and just one main metabolite was produced in susceptible plants (metabolite 1), at RT of 10.40 min (Figure 2.2A). In resistant plants, a small 2,4-D peak was detected and another main metabolite was produced at RT of 8 min (metabolite 4, Figure 2.2B). Additional metabolites were also detected, including metabolite 1 also found in susceptible plants, metabolite 2 (RT = 9.5 min), metabolite 3 (RT = 8.7 min), metabolite 5 (RT = 7 min), and metabolite 6 (RT = 2 min) (Figure 2.2B). Analyzing metabolism over time using a log-logistic model (Figure 2.2C, Supplementary Table 2.1) showed that resistant plants had a 2,4-D half-life (time to reach 50% 2,4-D metabolism) of 22 h ±4, five times faster than susceptible plants (105 h ±7). The time to reach 70% 2,4-D metabolism in resistant plants was 54 h ±4, and 307 h ±36 for susceptible plants. From these results, it is evident that the resistant *A. tuberculatus* plants rapidly metabolize 2,4-D (Supplementary Table 2.3).

Malathion Effects on 2,4-D Resistance and Metabolism

To test the hypothesis that enhanced 2,4-D metabolism was conferred by cytochrome P450, the known cytochrome P450-inhibitor malathion was tested. The dose required to reduce growth by 50% (GR_{50}) in resistant plants in the absence of malathion was 176 g ha^{-1} ±37, eight times higher than the GR_{50} for susceptible plants (22 g ha^{-1} ±5). Pre-treatment with malathion followed by 2,4-D dose response resulted in the resistant population having a 7-fold reduction in

GR_{50} compared to no pre-treatment and a similar 2,4-D response as the susceptible population (Figure 2.3A, Supplementary Table 2.1). With malathion pre-treatment, the GR_{50} for resistant plants was 27 g ha^{-1} ±10, similar to the GR_{50} for susceptible plants following malathion pre-treatment (22 g ha^{-1} ±3).

To investigate whether malathion affected 2,4-D metabolism, malathion treated and untreated plants were treated with [^{14}C] 2,4-D and harvested 264 HAT. Malathion reduced 2,4-D metabolism in both resistant and susceptible populations (Figure 2.3B). With 2,4-D treatment only, susceptible plants had 25% of the parent 2,4-D remaining at 264 HAT while resistant plants had 7% parent 2,4-D remaining. Following malathion treatment, the resistant and susceptible populations had similar amounts (73% and 74%, respectively) of parent 2,4-D remaining at 264 HAT (Figure 2.3B, Supplementary Table 2.1).

DISCUSSION

Metabolism of 2,4-D primarily contributes to 2,4-D resistance in *A. tuberculatus*

Auxinic herbicides were the first chemical family of selective herbicides to be discovered and are the most widely used selective herbicides. The phenoxy herbicide 2,4-D is effective in controlling a number of broadleaf weeds including *A. tuberculatus*. Herbicide resistance mechanisms have been categorized into two types, a) non-target-site, involving decreased absorption, translocation and/or enhanced herbicide metabolism, and b) target-site, resulting from mutations in the target gene or increased levels of the target protein by gene amplification or transcriptional upregulation (Powles and Yu, 2010). Previous research found that auxinic herbicide resistance in wild mustard (*Sinapis arvensis*) (Peniuk et al., 1993), false cleavers (*Galium spurium*) (Van Eerd et al., 2005), kochia (*Kochia scoparia* – Cranston et al., 2001) and

yellow starthistle (*Centaurea solstitialis*) (Fuerst et al., 1996; Valenzuela-Valenzuela et al., 2001) was not due to differences in herbicide absorption, translocation and/or metabolism and, by deduction, might be due to other mechanisms, such as altered target site. A different dicamba-resistant *K. scoparia* population was found to have reduced dicamba translocation (Pettinga et al., 2017).

In this research, 2,4-D resistance was investigated by determining [^{14}C] 2,4-D uptake, translocation, and metabolism in resistant and susceptible *A. tuberculatus* populations from NE. Our results indicate that 2,4-D absorption and translocation were similar between resistant and susceptible *A. tuberculatus*, and therefore do not appear to contribute to resistance. Previously, a similar amount of total 2,4-D absorption and translocation was reported in leafy spurge (*Euphorbia esula*) and cucumber (*Cucumis sativus* –Slife et al., 1962; Lym and Moxness, 1989). However, in 2,4-D susceptible ground ivy (*Glechoma hederacea*), 37% more 2,4-D was absorbed than in resistant plants (Kohler et al., 2004). In a Jimsonweed (*Datura stramonium*) population susceptible to 2,4-D, about 70% of the absorbed 2,4-D was translocated within the plant (Fites et al., 1964). Reduced MCPA (phenoxy herbicide) translocation was found in resistant hemp-nettle (*Galeopsis tetrahit*) compared to susceptible (Weinberg et al., 2006). Reduced 2,4-D translocation conferred resistance in a wild radish (*Raphanus raphanistrum*) population (Goggin et al., 2016). However, in another wild radish population resistant to MCPA, it was found that the resistant plants translocated MCPA more rapidly to roots than did susceptible plants, and also less [^{14}C] MCPA (as % applied) was recovered in resistant plants than in susceptible plants at 48 and 72 HAT (Jugulam et al., 2013). In that study, [^{14}C] MCPA was translocated to the roots, but in *A. tuberculatus*, most of the translocated radioactivity was found in the foliage and stems, but very little in the roots. The higher translocation observed in

resistant *A. tuberculatus* at 264 HAT may be related to the possible greater mobility of 2,4-D metabolites than parent 2,4-D, as well as the possibility of self-limiting translocation in susceptible plants once plant death occurs.

Our results show that enhanced 2,4-D metabolism contributes to resistance in the *A. tuberculatus* population from NE. The susceptible plants had higher parent [^{14}C] 2,4-D remaining at all time points. The model of 2,4-D metabolism over time showed that resistant plants metabolized 2,4-D seven times faster than did susceptible plants. Previously, 2,4-D-susceptible hemp dogbane (*Apocynum cannabinum*) was found to metabolize only 48% of the herbicide at 12 d after application (Schultz and Burnside, 1980). *Euphorbia esula* plants susceptible to 2,4-D contained 85% of the parent [^{14}C] 2,4-D at 72 HAT (Lym and Moxness, 1989). One study reported elevated 2,4-D metabolism in less-susceptible wild cucumber when compared to more-susceptible cultivated cucumber (Slife et al., 1962). An MCPA-resistant *G. tetrahit* population had increased MCPA metabolism compared to a susceptible population (Weinberg et al., 2006). The bacterial aryloxyalkanoate dioxygenase transformed in 2,4-D resistant crops show that rapid 2,4-D metabolism can confer robust 2,4-D resistance (Wright et al., 2010). Collectively these results suggest that if enough 2,4-D is metabolized in *A. tuberculatus* from 24-48 HAT, the enhanced metabolism will enable the resistant plant to survive short-term 2,4-D induced toxicity and continue to grow.

Auxinic herbicide selectivity in crops is primarily dependent on plant metabolism of these herbicides. Metabolic detoxification of 2,4-D typically occurs through side-chain cleavage, or ring hydroxylation followed by glucose conjugation. Tolerant plants can convert the parent biologically active molecule to more polar and insoluble residues (Hock and Elstner, 2004). Sensitive species can sometimes metabolize 2,4-D faster than tolerant species, however, the main

metabolites formed in sensitive species are reversible conjugates that can rapidly convert back to the biologically active, parent compound (Peterson et al., 2016). The metabolites produced by tolerant species are generally more stable and irreversible (Peterson et al., 2016). In auxinic herbicide-tolerant monocots, the formation of stable metabolites via phenyl and heterocyclic ring hydroxylation followed by subsequent sequestration of the non-biologically active compounds has been reported (Feung et al., 1975b).

The specific reactions involved in 2,4-D detoxification in our resistant population need to be investigated. One main metabolite was produced in susceptible plants while resistant plants produced the same metabolite with several additional metabolites. The structures of these metabolites have not yet been identified, but this information would help determine the biochemical steps involved in the enhanced 2,4-D metabolism in resistant plants. In our malathion experiments, we showed that this cytochrome P450 inhibitor reduced 2,4-D metabolism at 264 HAT in resistant plants and reversed 2,4-D resistance in a whole-plant dose response. Cytochrome P450s are versatile enzymes involved in phase I of herbicide metabolism including ring hydroxylation and plants have a high diversity of cytochrome P450 gene families that are able to metabolize natural and xenobiotic compounds (Werck-Reichhart et al., 2000; Siminszky, 2006a). Many weed species have been reported with enhanced metabolic resistance mediated by cytochrome P450s to various herbicide modes of action including ALS, acetyl Co-A carboxylase (ACCase), photosystem II, and HPPD (Yuan et al., 2007; Yu and Powles, 2014). Metabolic resistance in *A. tuberculatus* has been previously reported for ALS (Guo et al., 2015), photosystem II (Ma et al., 2013) and HPPD herbicides (Ma et al., 2013; Kaundun et al., 2017), with different cytochrome P450 genes likely conferring HPPD resistance in different populations (Ma et al., 2013; Oliveira et al., 2017). 2,4-D has been reported as an inducer of cytochrome

P450 activity in plants both *in vitro* (Adele et al., 1981; Yamada et al., 2000) and *in vivo* (Han et al., 2013), including inducing demethylation and ring-methyl hydroxylation of chlortoluron in tobacco (*Nicotiana tabacum*) cells (Yamada et al., 2000). More recent studies showed that ACCase susceptible *Lolium* plants pre-treated with 2,4-D had induction of cytochrome P450 transcripts (Gaines et al., 2014b) and higher rates of diclofop-methyl metabolism, which was reversed after malathion treatment (Han et al., 2013).

In conclusion, these results clearly demonstrate 2,4-D metabolism as a contributing factor for 2,4-D resistance in *A. tuberculatus*. Reversal of resistance and reduced 2,4-D metabolism following treatment with the cytochrome P450 inhibitor malathion indicate that one or more cytochrome P450 genes mediate this enhanced 2,4-D metabolism. Metabolism-based herbicide resistance is a particular challenge as it may confer complex and sometimes unpredictable cross-resistance to current as well as yet-to-be-discovered herbicides (Délye, 2013; Yu and Powles, 2014).

REFERENCES

(2005) US EPA, 2,4-D RED Facts, EPA-738-F-05-002. Available: https://www3.epa.gov/pesticides/chem_search/reg_actions/reregistration/fs_PC-030001_30-Jun-05.pdf.

Adele P, Reichhart D, Salaün J-P, Benveniste I, Durst F (1981) Induction of cytochrome P-450 and monooxygenase activity by 2, 4-dichlorophenoxyacetic acid in higher plant tissue. Plant Science Letters 22:39-46

Ashton FM, Crafts AS (1981) Mode of Action of Herbicides. Wiley.

Bell MS, Hager AG, Tranel PJ (2013) Multiple resistance to herbicides from four site-of-action groups in waterhemp (*Amaranthus tuberculatus*). Weed Sci. 61:460-468

Bernards ML, Crespo RJ, Kruger GR, Gaussoin R, Tranel PJ (2012) A Waterhemp (Amaranthus tuberculatus) Population Resistant to 2,4-D. Weed Science 60:379-384

Burnside OC (1996) The history of 2,4-D and its impact on development of the discipline of weed science in the United States. Pages 5-16 *in* Burnside OC, ed. Biologic and economic assessment of benefits from use of phenoxy herbicides in the United States: Washington, DC: U.S. Department of Agriculture NAPIAP Rep. 1-PA-96

Costea M, Weaver SE, Tardif FJ (2005) The biology of invasive alien plants in Canada. 3. *Amaranthus tuberculatus* (Moq.) Sauer var. *rudis* (Sauer) Costea & Tardif. Can. J. Plant Sci. 85:507-522

Coupland D (1994) Resistance to the auxin analog herbicides. Pages 171-214 *in* Powles SB, Holtum JAM, eds. Herbicide Resistance in Plants: Biology and Biochemistry

Cranston HJ, Kern AJ, Hackett JL, Miller EK, Maxwell BD, Dyer WE (2001) Dicamba resistance in kochia. Weed Sci. 49:164-170

Délye C (2013) Unravelling the genetic bases of non-target-site-based resistance (NTSR) to herbicides: a major challenge for weed science in the forthcoming decade. Pest Manag. Sci. 69:176-187

Devine M, Duke SO, Fedtke C (1992) Physiology of herbicide action. PTR Prentice Hall.

Dharmasiri N, Dharmasiri S, Estelle M (2005) The F-box protein TIR1 is an auxin receptor. Nature 435:441

Feung C-S, Hamilton RH, Mumma RO (1975) Metabolism of 2, 4-dichlorophenoxyacetic acid. VII. Comparison of metabolites from five species of plant callus tissue cultures. J. Agric. Food Chem. 23:373-376

Fites R, Slife F, Hanson J (1964) Translocation and metabolism of radioactive 2, 4-D in jimsonweed. Weeds 12:180-183

Fuerst E, Sterling T, Norman M, Prather T, Irzyk G, Wu Y, Lownds N, Callihan R (1996) Physiological characterization of picloram resistance in yellow starthistle. Pest. Biochem. Physiol. 56:149-161

Gaines TA, Lorentz L, Figge A, Herrmann J, Maiwald F, Ott MC, Han H, Busi R, Yu Q, Powles SB, Beffa R (2014) RNA-Seq transcriptome analysis to identify genes involved in metabolism-based diclofop resistance in *Lolium rigidum*. Plant J. 78:865-876

Gleason C, Foley RC, Singh KB (2011) Mutant analysis in Arabidopsis provides insight into the molecular mode of action of the auxinic herbicide dicamba. PLoS One 6:e17245

Godar AS, Varanasi VK, Nakka S, Prasad PV, Thompson CR, Jugulam M (2015) Physiological and molecular mechanisms of differential sensitivity of Palmer amaranth (*Amaranthus palmeri*) to mesotrione at varying growth temperatures. PLoS One 10:e0126731

Goggin DE, Cawthray GR, Powles SB (2016) 2,4-D resistance in wild radish: reduced herbicide translocation via inhibition of cellular transport. Journal of Experimental Botany 67:3223-3235

Grossmann K (2010) Auxin herbicides: current status of mechanism and mode of action. Pest Manag. Sci. 66:113-120

Grossmann K, Kwiatkowski J, Tresch S (2001) Auxin herbicides induce H2O2 overproduction and tissue damage in cleavers (Galium aparine L.). Journal of Experimental Botany 52:1811-1816

Guo J, Riggins CW, Hausman NE, Hager AG, Riechers DE, Davis AS, Tranel PJ (2015) Nontarget-site resistance to ALS inhibitors in waterhemp (*Amaranthus tuberculatus*). Weed Sci. 63:399-407

Hager AG, Wax LM, Stoller EW, Bollero GA (2002) Common waterhemp (*Amaranthus rudis*) interference in soybean. Weed Sci. 50:607-610

Han H, Yu Q, Cawthray GR, Powles SB (2013) Enhanced herbicide metabolism induced by 2,4-D in herbicide susceptible *Lolium rigidum* provides protection against diclofop-methyl. Pest Manag. Sci. 69:996-1000

Hatzios KK, Penner D (1982) Metabolism of herbicides in higher plants. Burgess Publishing Company.

Heap I The international survey of herbicide resistant weeds. Accessed May 23, 2020. Available on-line: www.weedscience.com. (2020).

Hock B, Elstner EF (2004) Plant toxicology. CRC Press.

Jugulam M, DiMeo N, Veldhuis LJ, Walsh M, Hall JC (2013) Investigation of MCPA (4-chloro-2-ethylphenoxyacetate) resistance in wild radish (*Raphanus raphanistrum* L.). J. Agric. Food Chem. 61:12516-12521

Jugulam M, Hall JC, Johnson WG, Kelley KB, Riechers DE (2011) Evolution of resistance to auxinic herbicides: historical perspectives, mechanisms of resistance, and implications for broadleaf weed management in agronomic crops. Weed Sci. 59:445-457

Kaundun SS, Hutchings S-J, Dale RP, Howell A, Morris JA, Kramer VC, Shivrain VK, Mcindoe E (2017) Mechanism of resistance to mesotrione in an *Amaranthus tuberculatus* population from Nebraska, USA. PloS One 12:e0180095

Kepinski S, Leyser O (2005) The Arabidopsis F-box protein TIR1 is an auxin receptor. Nature 435:446

Knezevic SZ, Streibig JC, Ritz C (2007) Utilizing R software package for dose-response studies: The concept and data analysis. Weed Technol. 21:840-848

Kniss AR, Vassios JD, Nissen SJ, Ritz C (2011) Nonlinear regression analysis of herbicide absorption studies. Weed Sci. 59:601-610

Kohler EA, Throssell CS, Reicher ZJ (2004) 2, 4-D rate response, absorption, and translocation of two ground ivy (*Glechoma hederacea*) populations. Weed Technol. 18:917-923

Kreuz K, Tommasini R, Martinoia E (1996) Old enzymes for a new job (herbicide detoxification in plants). Plant Physiol. 111:349

Lorentz L, Gaines TA, Nissen SJ, Westra P, Strek H, Dehne HW, Ruiz-Santaella JP, Beffa R (2014) Characterization of glyphosate resistance in *Amaranthus tuberculatus* populations. J. Agric. Food Chem. 62:8134-8142

Lym RG, Moxness KD (1989) Absorption, translocation, and metabolism of picloram and 2, 4-D in leafy spurge (*Euphorbia esula*). Weed Sci. 37:498-502

Ma R, Kaundun SS, Tranel PJ, Riggins CW, McGinness DL, Hager AG, Hawkes T, McIndoe E, Riechers DE (2013) Distinct detoxification mechanisms confer resistance to mesotrione and atrazine in a population of waterhemp. Plant Physiol. 163:363-377

Nandula VK, Ray JD, Ribeiro DN, Pan Z, Reddy KN (2013) Glyphosate resistance in tall waterhemp (*Amaranthus tuberculatus*) from Mississippi is due to both altered target-site and nontarget-site mechanisms. Weed Sci. 61:374-383

Oliveira MC, Gaines TA, Dayan FE, Patterson EL, Jhala AJ, Knezevic SZ (2017) Reversing resistance to tembotrione in an *Amaranthus tuberculatus* (var. *rudis*) population from Nebraska, USA with cytochrome P450 inhibitors. Pest Manag. Sci.:Early View

Peniuk M, Romano M, Hall J (1993) Physiological investigations into the resistance of a wild mustard (*Sinapis arvensis* L.) biotype to auxinic herbicides. Weed Res. 33:431-440

Peterson MA, McMaster SA, Riechers DE, Skelton J, Stahlman PW (2016) 2, 4-D past, present, and future: a review. Weed Technol. 30:303-345

Powles SB, Yu Q (2010) Evolution in action: Plants resistant to herbicides. Annu. Rev. Plant Biol. 61:317-347

R (2015) R Core Team (2015). R: A language and environment for statistical computing. R Foundation for Statistical Computing, Vienna, Austria. URL http://www.R-project/org/.

Scheel D, Sandermann H (1981) Metabolism of 2, 4-dichlorophenoxyacetic acid in cell suspension cultures of soybean (*Glycine max* L.) and wheat (*Triticum aestivum* L.). Planta 152:253-258

Schultz M, Burnside O (1980) Absorption, translocation, and metabolism of 2, 4-D and glyphosate in hemp dogbane (*Apocynum cannabinum*). Weed Sci. 28:13-20

Siminszky B (2006) Plant cytochrome P450-mediated herbicide metabolism. Phytochem. Rev. 5:445-458

Slife F, Key J, Yamaguchi S, Crafts A (1962) Penetration, translocation, and metabolism of 2, 4-D and 2, 4, 5-T in wild and cultivated cucumber plants. Weeds 10:29-35

Steckel LE (2007) The dioecious *Amaranthus* spp.: here to stay. Weed Technol. 21:567-570

Steckel LE, Sprague CL (2004) Common waterhemp (*Amaranthus rudis*) interference in corn. Weed Sci. 52:359-364

Trucco F, Tranel PJ (2011) Amaranthus. Pages 11-21 Wild Crop Relatives: Genomic and Breeding Resources: Springer

Valenzuela-Valenzuela JM, Lownds NK, Sterling TM (2001) Clopyralid uptake, translocation, metabolism, and ethylene induction in picloram-resistant yellow starthistle (*Centaurea solstitialis* L.). Pest. Biochem. Physiol. 71:11-19

Van Eerd LL, Stephenson GR, Kwiatkowski J, Grossmann K, Hall JC (2005) Physiological and biochemical characterization of quinclorac resistance in a false cleavers (*Galium spurium* L.) biotype. J. Agric. Food Chem. 53:1144-1151

Walsh TA, Neal R, Merlo AO, Honma M, Hicks GR, Wolff K, Matsumura W, Davies JP (2006) Mutations in an Auxin Receptor Homolog AFB5 and in SGT1b Confer Resistance to Synthetic Picolinate Auxins and Not to 2,4-Dichlorophenoxyacetic Acid or Indole-3-Acetic Acid in Arabidopsis. Plant Physiology 142:542-552

Weinberg T, Stephenson GR, McLean MD, Hall JC (2006) MCPA (4-chloro-2-ethylphenoxyacetate) resistance in hemp-nettle (*Galeopsis tetrahit* L.). J. Agric. Food Chem. 54:9126-9134

Werck-Reichhart D, Hehn A, Didierjean L (2000) Cytochromes P450 for engineering herbicide tolerance. Trends Plant Sci. 5:116-123

Wright TR, Shan G, Walsh TA, Lira JM, Cui C, Song P, Zhuang M, Arnold NL, Lin G, Yau K (2010) Robust crop resistance to broadleaf and grass herbicides provided by aryloxyalkanoate dioxygenase transgenes. Proc. Natl. Acad. Sci. USA 107:20240-20245

Yamada T, Kambara Y, Imaishi H, Ohkawa H (2000) Molecular Cloning of Novel Cytochrome P450 Species Induced by Chemical Treatments in Cultured Tobacco Cells. Pesticide Biochemistry and Physiology 68:11-25

Yu Q, Powles S (2014) Metabolism-based herbicide resistance and cross-resistance in crop weeds: A threat to herbicide sustainability and global crop production. Plant Physiol. 166:1106-1118

Yuan JS, Tranel PJ, Stewart CN (2007) Non-target-site herbicide resistance: a family business. Trends Plant Sci. 12:6-13

.

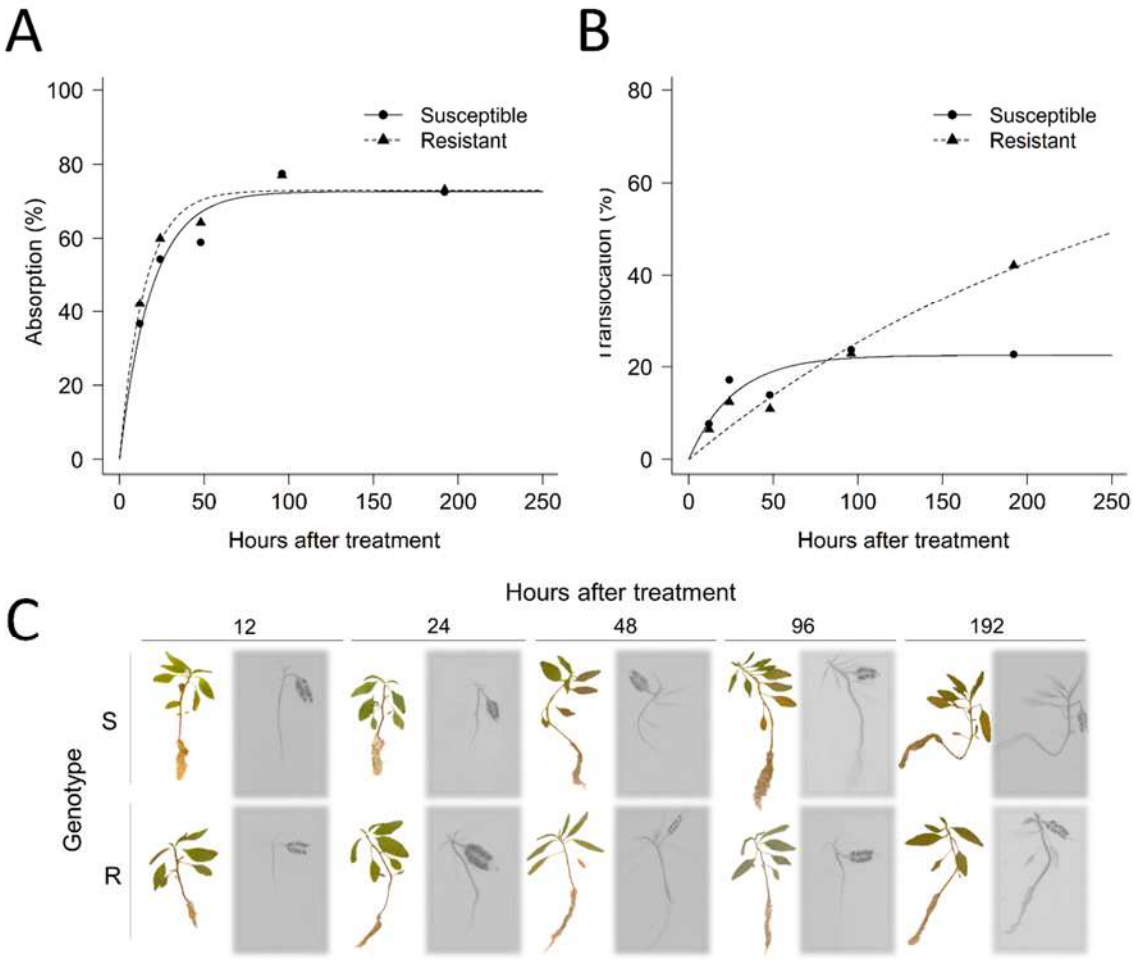

Figure 2.1. [^{14}C]-labeled 2,4-D absorption and translocation in resistant (R) and susceptible (S) *A. tuberculatus* over a 96 h time course. A) 2,4-D absorption as percentage of applied radioactivity. B) 2,4-D translocation as percentage of absorbed radioactivity. C) Phosphor images showing 2,4-D translocation over time with the corresponding plant color image to the left of the phosphor image.

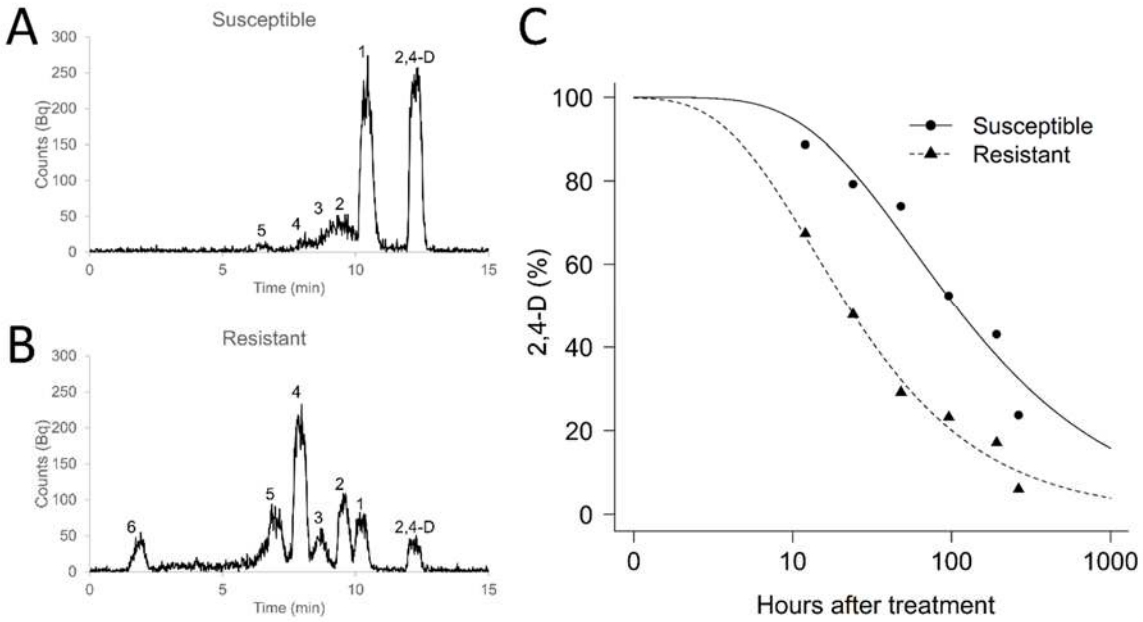

Figure 2.2. [^{14}C]-labeled 2,4-D metabolism in resistant and susceptible *A. tuberculatus*. A) Susceptible and B) resistant HPLC chromatograms of [^{14}C] 2,4-D metabolism at 264 HAT (radioactive units in Bq vs retention time in min), with different metabolites numbered in order of their respective retention times. C) Non-linear regression of 2,4-D metabolism at different time points after herbicide treatment with dashed lines indicating 2,4-D half-life.

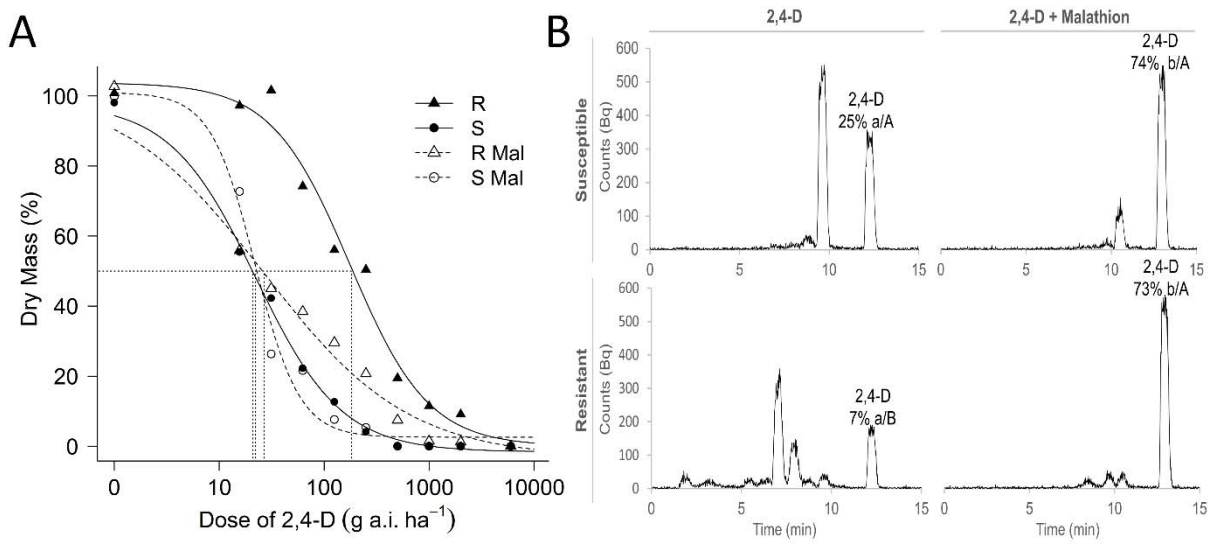

Figure 2.3. Malathion reverses 2,4-D resistance and metabolism in resistant (R) and susceptible (S) *A. tuberculatus*. A) Dry weight dose response of R and S with and without malathion pre-treatment (Mal), 28 d after 2,4-D application with dashed lines indicating GR_{50} (2,4-D dose required to reduce biomass by 50%). B) HPLC chromatograms of [^{14}C] 2,4-D metabolism (radioactive units in Bq vs retention time in min) at 264 h after 2,4-D application in R and S with and without malathion pre-treatment. Percentage indicated above 2,4-D retention time (13.4 min) represents the mean parent [^{14}C] 2,4-D measured in all replicates. Other peaks represent 2,4-D metabolites. Letters represent significant differences between R and S (upper case) or between malathion treatments (lower case) with Tukey's test (n=6; $\alpha = 0.5$).

CHAPTER III – Chemical and toxicological characterization of 2,4-Dicholorophenoxyacetic acid metabolites in a resistant population of waterhemp (*Amaranthus tuberculatus*) shows the evolution of a non-intrinsic detoxification metabolic route

INTRODUCTION

Herbicides are small molecules that are toxic to plants. With the advances of chemistry starting in the 20th century, these molecules became available for growers and due to the efficacy in weed control, herbicides became one of the most important tools in reducing crop losses to pests (Oerke, 2006; Davies, 2013). One of the first discovered herbicides was 2,4-Dichlorophenoxyactic acid, a molecule that mimics the growth regulation responses of the natural auxin Indole acetic acid in plants. As a synthetic auxin, 2,4-D acts in the plant cell nucleus as a "molecular glue" linking the E3 protein complex $SCF^{TIR1/AFB}$ and the repressor protein Aux/IAA, inducing ubiquitination of Aux/IAA and proteolysis in the 25S proteasome. The Aux/IAA proteins are transcriptional repressors for the Auxin Response Factors (ARFs) and after Aux/IAA degradation, ARFs induce the transcription of auxin related genes that results in auxin early responses (Tan et al., 2007; Dinesh et al., 2016). Due to high stability of 2,4-D in the cell environment, it induces disturbances in auxin responses leading to Ethylene and Abscisic Acid synthesis that will induce plant epinasty, stomata closure, and reactive oxygen species accumulation, culminating in tissue necrosis (Grossmann, 2010b). Despite being used for decades in extensive areas around the world, there are just 45 reported cases of 2,4-D resistance in weeds (Heap, 2020).

Weed resistance mechanisms are classified in target-site and non-target site resistance (Reviewed by Ghanizadeh and Harrington, 2017). Target-site resistance occurs due to changes in target-site proteins modifying its structure in specific sites, reducing the binding properties of the

herbicide (Devine and Shukla, 2000). Gene amplification and overexpression of the herbicide receptor are also considered a target-site resistance, in this case, the targeted enzyme is produced in high amounts that can compensate for the herbicide inhibition, maintaining the metabolic pathway that would be inhibited (Gaines et al., 2010). In non-target site resistance mechanisms, the herbicide does not reach its site of action due to changes in absorption, exudation, or compartmentalization into the vacuole. Herbicides can be metabolized by plant enzymes that change its chemical structure, reducing its binding kinetics to the target site (Ghanizadeh and Harrington, 2017). Herbicide metabolism in plants occurs in three different phases. The first phase consists of an introduction of a polar functional group catalyzed by an enzyme, those groups can be a hydroxy, amino, thiol or carboxyl. With the addition of that active group on the herbicide molecule, the subsequent phase II occurs, where the molecule will be conjugated with an exogenous or endogenous compound to facilitate detoxification and compartmentalization. Sugars, amino-acids, and glutathione are the most common endogenous substrates for herbicide conjugation. A second conjugation can happen with malonyl or acetyl groups, and subsequently, the metabolized compound is compartmentalized or incorporated into polymers at cell walls by covalent bounds, as the final phase of herbicide metabolism (Hatzios, 1997). Those reactions occur in 2,4-D metabolism in higher plants through two pathways. Pathway I is characterized by ring hydroxylation reactions that can happen in several positions of the aryl group. After hydroxylation, the metabolized herbicide can undergo sugar or amino acid conjugation at the gained hydroxyl group. Pathway II consists of reactions of amino acid or sugar conjugations that occur at the carboxyl group of 2,4-D.

Metabolizing enzymes, in some cases, can target several herbicides, within the same or different modes of action, so resistant populations can show unexpected resistance to other

herbicides that were never sprayed in the area that resistance was selected (Preston, 2004). Cytochrome P450s are heme-thiolate proteins that occur on the plant microsome membrane. They catalyze monooxygenase reactions, hydroxylating a substrate in the first phase of herbicide metabolism (Siminszky, 2006b). Plants have hundreds of P450 coding genes in their genome that act in numerous biochemical pathways (Bak et al., 2011). The application of 2,4-D can induce the expression of P450s, acting sometimes as safeners for other herbicides (Yamada et al., 2000; Gaines et al., 2014a). In weed species, the identification of different P450s involved in herbicide resistance were identified in *Echinochloa phyllopogon* (Iwakami et al., 2014; Guo et al., 2019; Iwakami et al., 2019). For dicot weed species, herbicide metabolism was primarily related to the action of P450 enzymes (Torra et al., 2017; Küpper et al., 2018; Oliveira et al., 2018; Lu et al., 2019; Obenland et al., 2019;), but to date no specific P450 genes metabolizing herbicides have been characterized from dicot weed species.

Amarathus tuberculatus (waterhemp) is a problematic dicot weed in North America. Occurring in annual crops, it grows very fast, achieving a height of over three meters, dense foliar areas, and one plant can produce high amounts of dormant seeds (Costea et al., 2005). There are 60 cases of herbicide resistance reported in the USA and Canada in this species, including a case with multiple resistance to six different herbicides mode of action (Shergill et al., 2018). In 2009, a 2,4-D resistant waterhemp population was identified in Nebraska (Bernards et al., 2012); 2016 in Illinois (Heap, 2020) and 2018 in Missouri (Shergill et al., 2018); studies show that resistant plants rapidly metabolize 2,4-D, showing distinct metabolic profile compared to susceptible populations (Figueiredo et al., 2018). Treating resistant plants with P450 inhibitors reduced 2,4-D metabolism and restored its phytotoxicity (Figueiredo et al., 2018). Interestingly, high temperatures increase 2,4-D metabolism in resistant plants (Shyam et al., 2019) indicating a

high enzymatic activity in those conditions. In order to have a better understanding of 2,4-D chemical transformations that are occurring in resistant populations of waterhemp, this study provides the structural characterization of 2,4-D metabolites produced by resistant and susceptible waterhemp populations. It also explores the toxicological effects of the main metabolites in both waterhemp populations and in Arabidopsis. This current study gives new insights on synthetic auxin metabolism in dicot plants and the role of P450s in non-target-site herbicide resistance.

MATERIAL AND METHODS

Metabolism extraction, purification, and characterization

The populations used in this research were the same used in Figueiredo et al. (2018), which were a susceptible population from Indiana and a resistant population from Nebraska. Plants were cultivated on potting soil, after planting they were kept at 4ºC for one week and transferred to greenhouse at 25ºC, 75% RT. For radiolabeled herbicide treatments, plants grew in a growth chamber under the same conditions as the greenhouse, but with different light sources, which were incandescent for greenhouse and fluorescent for growth chamber.

The extraction of 2,4-D metabolites was the same as Figueiredo et al. (2018), three hundred plants of both resistant and susceptible phenotypes were sprayed with 500 g ha^{-1} of 2,4-D (2,4-D amine; 455 g L^{-1}; DuPont, Wilmington, DE, USA) in a water volume of 224 L ha^{-1} and 1% crop oil concentrate (COC). Plants were treated at the stage of six true leaves and eight centimeters tall. Additionally, another fifteen plants were treated with 10 droplets of 1 uL of [^{14}C] 2,4-D solution having formulated 2,4-D and COC with total radioactivity of 8.333 KBq (500,000 dpm) per plant. After 264 hours, all plants were harvested. Radiolabeled and non-

labeled treatments were processed separately but following the same extraction procedures. First, plants were mixed in a blender with water at 1% acetic acid solution, concentrated on a C18 cartridge (Waters C18, 10 g), vacuum dried overnight and resuspended in HPLC phase A solution. Then 200 µl injections were made on a HPLC system (Hitachi Instruments, Inc., San Jose, CA, USA), the column used was a C18 4.6 mm by 150 mm column (C18 Column; Zorbax Eclipse XDB-C18; Agilent Technologies, Santa Clara, CA, USA). The HPLC was attached to a radio-detector (FlowStar LB 513; Berthold Technologies GmbH & Co., Bad Wildbad, Germany) with a flow cell YG-150-U5D solid cell YG-Scintillator (150 μl, Berthold Technologies). Metabolite extracts were run using phase A containing 89.9% water, 10% acetonitrile, and 0.1% formic acid and phase B containing 99.9% acetonitrile and 0.1% formic acid, as the solvent system. The gradient used for all runs was 30 min starting at 100% phase A and finishing at 100% phase B. Metabolite fractions from both populations were collected based on the radioactive signals generated from radiolabeled treated plants. Due to the large number of impurities from each fraction collected on the first column purification, after vacuum drying each fraction, the samples were resuspended again in phase A and re-purified using a CN column (MACHEREY-NAGEL NUCLEOSIL 100-5 C18 – 250 X 4 mm), with the same solvent system and gradient described above. Then a final purification was done by reinjecting pre-purified fractions into a long C18 column (Agilent ZORBAX SB-CN –250 X 4.6 mm) and a final vacuum drying was done.

For the main metabolites produced by resistant plants, the purified extracts were not sufficient for NMR resolution, so metabolites were chemically synthesized and their retention time and mass spectrometry were compared to the purified fractions from susceptible plant tissue, confirming that both had the same RT and MS profile. Metabolites from R plants were

characterized by NMR (BRUKER US400). Deuterium oxide (D2O) was used as solvent in all cases. The ^{1}H-NMR, zTOCSY, ROESYAD, c2hsqcse and gHMBC spectra were obtained with a 5-mm probe. For 1H, the solvent peak was referenced to 4.65 ppm (D2O). Chemical shifts (δ) expressed in ppm and coupling constants in Hertz (Hz). High-resolution mass spectrometry (HRMS), was done using an AGILENT 6520 TIME OF FLIGHT (TOF) LC-MS Q-TOF, under negative ionization mode, nebulizing nitrogen gas at 35 psi. A C18 column was used (Kinetex 2.6 µm 100 Å – 100X4.6 mm), with the same solvents and gradient described above. The exact mass measurements were calibrated using formic acid.

Plant metabolic profile analysis

To quantify and characterize the production of the main metabolites in waterhemp, two experiments were done. In the first, both genotypes were treated post-emergence, where the fourth expanded leaf was covered with aluminum paper and plants were sprayed with commercial 2,4-D. Subsequently, the leaf was treated with radiolabeled 2,4-D (8.333 KBq – 500,000 dpm) as described above. In the second experiment, plants of each population were collected from soil and roots were carefully washed. Then leaves, stems, and roots were separated, cut in 2 cm pieces and placed separately into 6 well plates containing 5 ml of water solution with 100 kBq (6,000,000 dpm) of [^{14}C] 2,4-D. After 96 hr, the content of each well was collected and washed with water to remove the non-absorbed herbicide. Each tissue was then extracted using the same methods described above, vacuum evaporated, resuspended in 300 µL of phase A, and 200 µL was injected into the HPLC for metabolism quantitation. Purified C14 metabolites were run for metabolite characterization based on retention time. A similar experiment was done using non-labeled 2,4-D and the extracts were run in LC-MS Q-TOF to

confirm the structure characterization of the metabolites found on the radiolabeled chromatograms.

Metabolite synthesis

To investigate the toxicological aspect of the main 2,4-D primary metabolites found in waterhemp, 2,4-D-Asp and 5-OH-2,4-D were synthesized (Supplementary figure 3.1). 2,4-D aspartate was produced by a carbodiimide-mediated amine coupling conjugation following the protocol described in Eyer et al. (2016). 5-OH-2,4-D was synthesized adapting the Williamson ether reaction described for 2,4-D synthesis (Ebel et al., 1947). 122 mmol of 4,6-chlororesorcinol and 122 mM of monochloroactic acid were boiled with 290 mmol of sodium hydroxide in 60 ml of water under a reflux system for 12 hr. After cooling to room temperature, the pH was adjusted to 6 with HCl and extracted with ether to remove the unreacted 4,6-chlororesorcinol. The inorganic phase was acidified at pH 1 and extracted with ether. Sodium sulfate was used to remove water from the ether that was posteriorly evaporated under nitrogen flux. The product, a brown-red powder, was then resuspended in ethyl acetate and silica was added until the complete absorption of the material. Subsequently, the ethyl acetate was carefully evaporated under gentle nitrogen flux and submitted to chromatography purification. A glass column (size 50 × 150 mm) was packed with silica gel and the silica containing the product of the reaction was placed on top. A first run using 5 volumes of column was done using 100% dichloromethane to remove the remaining 4,6-chlororesorcinol. 5-OH-2,4-D was recovered on the 10 % ethyl acetate, 90% dichloromethane and 0.01% acetic acid. The structure was confirmed by NMR using Dimethyl sulfoxide-d6 as solvent and mass spectrometry. The final purity was about 90%.

Root assays

Toxicological studies were performed using 2,4-D and the synthesized metabolites on agar plates (120 mm Square Petri Dishes – Fisher Scientific) with the dosage of 0; 0.01; 0.1; 0.5; 1; 10; 100; and 1000 µM. For waterhemp, gas sterilized seeds were planted on media with agar (10 g L^{-1}) and incubated at 4ºC for one wk to break dormancy and moved to light (16-hr day; 23ºC, humidity 65% and light intensity of 200 µMol m^2). After 7 d, 12 seedlings were transplanted to agar plates containing the respective auxin treatment and roots were measured 2 wk later. For experiments using Arabidopsis, a DR5::GUS line (Ulmasov et al., 1997b) was used for histological analysis of auxin response. Gas sterilized seeds were plated on half MS, scarified at 4ºC for 3 days, and moved to light conditions similar to the waterhemp plate, but lower light intensity (180 µMol m^2). Twelve one wk old seedlings were moved to plates with auxin and evaluated one week later. After root measurements, four plants of each treatment were incubated in X-Gluc stain solution (50 mM Phosphate buffer, pH 6 and 1 mM X-Gluc) at 37ºC overnight. Then, chlorophyll was removed using 70% ethanol and pictures were obtained using a Nikon camera D40 and a magnifying glass microscope Nikon SMZ800 attached to a camera Nikon DS-Li1. Roots were measured using rootdetection-0.1.3-beta-2 and the logistic model was calculated using the package DRC from R program and different models were adjusted depending on growth response (Supplementary table 3.2). All the experiments were repeated at least 2 times.

RESULTS

2,4-D metabolic profile characterization and quantitation

In previous work five different metabolites were characterized in resistant plants, named 1 to 5 (Figueiredo et al., 2018). Since it was not possible to purify or characterize two metabolites that were produced in small quantities, the three main metabolites were renumbered

(1 to 3) to characterize the three that were highly produced in the two waterhemp populations. The main metabolites of resistant and susceptible populations were purified and characterized on MS/MS and NMR. In susceptible plants, the main metabolite (met1; RT of 10.40 min – Figure 3.1A and B) produced was an aspartyl conjugate of 2,4-D. The main isotopic signals for MS of that metabolite was *m/z* of 333.9886 and the MS/MS of 160. 9558, corresponding to 2,4-Dichlorophenoxy moiety (Supplementary table 3.1). Since it was not possible to purify enough material to obtain good resolution on NMR, the validation of 2,4-D-Asp structure was done by chemical synthesis as done by Eyer et al. (2016). Both synthesized and plant purified 2,4-D-Asp had same RT and MS profile.

An additional class of metabolites was identified in resistant plants, where both metabolites 2 and 3 came from a primary metabolic transformation, in which 2,4-D underwent phenoxy hydroxylation forming 5-OH-2,4-D. Metabolite 2 (RT – 8.7 min, Figure 3.1A) was characterized as a 5-OH-2,4-D-(6-O-malonyl)-glucoside and metabolite 3 (RT – 8 min, Figure 3.1A) was a 5-OH-2,4-D-gucosyl (Figure 3.1A and B; Supplementary table 3.1). For hydroxylated metabolites, the main MS/MS signal was 176.9518, corresponding to 4,6-Dichlororesorcinal moiety, which mass corresponds to an addition of an oxygen to the 2,4-D aryl group (Supplementary table 3.1- Mets 2 and 3). The ^{1}H-NMR on this metabolite confirmed the loss of the hydrogen on position 5 of the aryl group, where the original three signals of hydrogen on positions 3, 5, and 6 (δ 7.48, 7.25 and 6.93 ppm) of 2,4-D changed to just two singlets at δ 7.47 and 6.72 ppm (Supplementary table 3.1- 2,4-D, Met2 and Met3). For metabolite 3 (*m/z* of 397.0094), HMBC data further confirmed the hydroxylation, showing correlation between the hydrogen on the 17’ hydrogen of the glucose group at 4.97 ppm and the carbon of 5-OH group of the aryl group at δ 151.25 ppm on ^{13}C-NMR (Supplementary table 3.1 – Met 3). From ^{1}H-NMR,

the additional signals corresponding to the glucose hydrogen groups (14', 15', 18', 19', 23') were shifted downfield at δ 3.86 – 3.43 ppm. The hydrogens from the sugar methyl protons (23'', 23') absorbed as two double doublets with chemical shifts of δ 3.86 and 3.67 ppm, c2hsqcse characterized those two hydrogens as CH_2 correlated to the same carbon. HRMS was *m/z* of 397.0094 that generated a molecular formula corresponding to the sugar conjugate (Supplementary table 3.1 – Met 3). The second main metabolite produced by R plants (Met 2) had just a difference of 86.0006 units of *m/z* which corresponds to the addition of a malonyl group ($C_3H_2O_3$). That metabolite was identified as a 5-OH-2,4-D-(6-O-malonyl)-glucoside, with a MS of *m/z* of 483.0100 and MSMS of 176.9518 (Supplementary table 3.1 – Met 2). The 1H-NMR showed a similar profile to Met 3 with changes on the glucose methyl group that turned to a singlet upfield at δ 4.37 ppm. On HMBC data, there is a correlation between the sugar CH2 group (6') and the malonyl C=O first group, confirming the malonylation position on the primary glycosylated metabolite (δ 170.27 ppm). Overall based on the characterization of the metabolites between resistant and susceptible plants, it was confirmed that there are two distinct routes of herbicide detoxification, where susceptible plants predominantly produce an aspartyl conjugate metabolite and resistant plants are distinctively able to hydroxylate 2,4-D.

After chemical characterization, a relative quantitation was done in plants sprayed post-emergence and in different isolated plant parts incubated in water with radiolabeled 2,4-D. In post-emergence treated plants, 43% of the radioactive material recovered was intact 2,4-D, 30% was 2,4-D-Asp, 11% was the sum of metabolites that occurred in small amounts and were not able to be characterized, and 14% of the radioactive material applied in the plants was insoluble, likely representing the portion of herbicide that is incorporated into the cell wall structure. In resistant plants, the highest portion of radioactive material recovered was 5-OH-2,4-D-Glucosyl

(37%), 17% was intact 2,4-D, 9% was 2,4-D-Asp, 9% was 5-OH-2,4-D-Malonyl-Glucosyl, 7% was undefined metabolites, and insoluble radioactive residues were 17% (Figure 3.1 C). Herbicide metabolism for different parts after 96 hr of incubation in 2,4-D radiolabeled solution showed that in susceptible plants, all organs metabolized about 50% of 2,4-D into 2,4-D-Asp (Supplementary Figure 3.2). Leaves produced small amounts of two other metabolites and those were hard to characterize from MS data because apparently they were 2,4-D sugar conjugates, but none of them showed fragments similar to hydroxylated metabolites as was found in resistant populations. In resistant plants, all the tissues presented high percentages of hydroxylated metabolites. Leaves metabolized mostly 5-OH-2,4-D- malonyl-glucosyl (59%), similar percentages of 5-OH-2,4-D-glucosyl and 2,4-D-Asp (6%) were recovered, and 29% of the radioactive material remained as 2,4-D. Stems from resistant plants were less efficient in 2,4-D metabolism (total of parent compound recovered = 41%), hydroxylated metabolites corresponded to 45%, amino acid conjugates were 10%, and 4% was other metabolites. In roots, 21% of the parent compound was detected, and 70% of the radioactive material was converted to 5-OH-2,4-D products (30% glucosyl and 40% glucosyl-malonyl conjugates). No 2,4-D-Asp was detected in the roots and just 9% of the radioactive material corresponded to non-characterized metabolites (Supplementary Figure 3.2). These results show that all tissues are capable of metabolizing 2,4-D as both populations conjugate 2,4-D into aspartyl metabolite, but hydroxylated compounds are exclusively present in resistant plants.

Toxicological studies on 2,4-D metabolites

2,4-D-Asp and 5-OH-2,4-D were synthesized and their structure was confirmed by NMR and mass spectrometry (Supplementary figure 3.1 – synthesized metabolite 1 and 2). Resistant and susceptible waterhemp seedlings were exposed to different doses of 2,4-D, 2,4-D-Asp, and

5-OH-2,4-D, and evaluated 14 d later. Resistant plants treated with 2,4-D had normal root growth up to 1 μM dose and at 10 μM, there was no root development. Susceptible seedlings grew more than the control at 0.01 μM, but they showed 50 % growth inhibition at 1 μM and no growth at 10 μM (Figure 3.2 AI). The 2,4-D-Asp induced more root growth compared to untreated plants of both R and S populations at 1 μM (around 175%). At 10 μM, resistant seedlings maintained the same growth as the other doses and susceptible started to have inhibitory effects. The dose causing 50% root inhibition was estimated as 100 μM for both genotypes and total inhibition was reached at 1000 μM (Figure 3.2 AII). 5-OH-2,4-D stimulated increased root growth up to the dose of 100 μM, and total inhibition was achieved at 1000 μM for both genotypes (Figure 3.2 AIII). Arabidopsis was tested for the herbicide and the main metabolites produced by waterhemp. 2,4-D inhibitory effects on root growth of 75% was at 0.012 μM, 2,4-D-Asp had the same inhibition at 1.2 μM and 232 μM for the 5-OH-2,4-D. Those results show that, to achieve the same level of growth inhibitory effect comparing to the parent herbicide, 2,4-D-Asp needs to be applied 100 times more concentrated and the 5-OH-2,4-D needs to be 19,339 times more concentrated in Arabidopsis seedlings (Figure 3.2 B). 2,4-D-Asp and 5-OH-2,4-D have less toxicological effects on plants than the parent herbicide 2,4-D. 5-OH-2,4-D produced by resistant plants was less toxic than the 2,4-D-Asp conjugate, which was the main metabolite found in susceptible plants.

The auxin gene transcription induction of 2,4-D and the waterhemp metabolites in Arabidopsis was studied using the synthetic auxin responsive element DR5 tagged with GUS reporter system that forms a blue precipitate on tissues where auxin induces the transcription of the DR5 promoter (Figure 3.3). Untreated plants had histological signs only on root tips. 2,4-D and 2,4-D-Asp started to have an increment of auxin trigged transcription at 0.01 μM (2,4-D)

and 0.5 μM (2,4-D-Asp). GUS staining over the root tips, lateral roots, stems, and leaves became more intense at the higher doses. 5-OH-2,4-D did not induce auxin triggered transcription in roots in most of the doses tested. The only treatment with intense GUS staining was at the stem at 1,000 μM treatment. Overall, 2,4-D and 2,4-D-Asp have auxin transcription activity, while 5-OH-2,4-D did not show auxin activity in most of the doses tested.

DISCUSSION

A 2,4-D resistant *A. tuberculatus* population was previously shown to have P450-mediated enhanced metabolism of 2,4-D (Figueiredo et al., 2018). Metabolites produced by resistant and susceptible populations of waterhemp were characterized by NMR and HRMS. Susceptible plants perform aspartic acid conjugation and resistant plants produce 5-OH-2,4-D related metabolites as a detoxification reaction (Figure 3.1). Several studies on 2,4-D metabolism in plants were performed starting in the 1960s. Those studies showed that there are differences in 2,4-D metabolic fate depending on the species. In *Avena sativa* and *Raphanus raphanistrum*, the main metabolite yielded in plants treated with radiolabeled 2,4-D was a glucose ester conjugation (Thomas et al., 1964; Goggin et al., 2018). Distinctively, in Fabaceae species like *Phaseolus vulgaris* and *Glycine max*, the main metabolites were amino acid conjugates of 2,4-D (glutamic acid, aspartic acid and phenylalanine) and glucoside of a ring hydroxylated metabolite (Thomas et al., 1964; Witham et al., 1971). Several works show the capacity of both monocot and dicot species to perform amino acid conjugation and ring hydroxylation detoxification reactions. The predominant reactions performed between plants species are considerably different (Ercegovich et al., 1971; Feung et al., 1975a; Feung et al., 1978). Analyzing callus tissue culture of different plant species treated with 2,4-D, monocots showed higher percentages of hydroxylated metabolites compared to dicot species. In corn plants, just 13% of radioactive applied 2,4-D was

converted to amino acid conjugates and 54.4% was converted to aryl hydroxylated metabolites, 22.7% remained the parent 2,4-D. In dicot species (carrot, jackbean and sunflower), generally 50% remained as intact 2,4-D and amino acid conjugation was higher (around 40%) than hydroxylated products (approximately 10 to 15% depending on the species – Feung et al., 1975a). Waterhemp resistant plants metabolized approximately 43 % of applied radioactive 2,4-D to hydroxylated compounds, while 9% was conjugated to aspartic acid metabolite. Susceptible plants did not produce hydroxylated metabolites and 30% was 2,4-D-Asp (Figure 3.1C).

The production of 2,4-D aspartic acid conjugate was detected in both waterhemp populations. In plants, amino-acid conjugation reactions are performed by GRETCHEN HAGEN 3 (GH3), a class of enzymes involved in the formation of hormone amino acid conjugates that are rapidly transcriptionally activated under high auxin concentrations, having a key role in auxin regulation and homeostasis in the plant cell (; Ulmasov et al., 1999b; Staswick et al., 2002). GH3 enzymes use ATP to adenylate the 2,4-D carboxyl group, releasing pyrophosphate and forming 2,4-D-AMP (Supplementary figure 3.3). After that, a transferase reaction occurs where the NH_3^+ nucleophilic group of an aspartic acid attacks the carbonyl group of 2,4-D-AMP acyl acid, yielding 2,4-D-Asp (Staswick et al., 2002; Chen et al., 2010; Westfall et al., 2012). In Arabidopsis, an extensive study analyzed the activity of 2,4-D conversion to 2,4-D amino acid conjugation of 76 different GH3 proteins from several plant species. Most of the GH3 tested were able to make 2,4-D-Asp conjugation, but the levels of conversion were very low, except for *Gm*GH3.26 from soybean that had an efficient conjugation activity. While most of the studies on amino-acid conjugation show that plants produce 2,4-D aspartyl and glutamine conjugates (Witham et al., 1971; Feung et al., 1972; Eyer et al., 2016; Chiu et al., 2018), in the waterhemp

populations used in this study, only the aspartyl conjugate was detected (Figure 3.1C and Supplementary figure 3.2).

In 1954, the activity of several synthesized amino acid conjugates of the synthetic auxinic herbicide Methyl-4-Chlorophenoxyacetic acid (MCPA) showed auxin activity for both L- and D-isomers of aspartic acid conjugates in monocot and dicot species (Krewson et al., 1954). In soybean callus, 2,4-D-Asp showed less auxin activity than 2,4-D in tissue growth (Feung et al., 1972). In waterhemp, 2,4-D-Asp showed inhibitory root effects on resistant and susceptible populations at 10 and 100 µM respectively. In Arabidopsis, 2,4-D-Asp had root inhibition and expression of DR5::GUS at the dose of 0.5 µM. The auxinic effect of 2,4-D-Asp is due to the conversion of the metabolite to the parent herbicide. In Arabidopsis seedlings, 35% of 2,4-D-Asp was hydrolyzed back to 2,4-D parent 9 d after treatment (Eyer et al., 2016) and this reaction is catalyzed by two amidohydrolases, *At*ILL5 and *At*IAR3 (Chiu et al., 2018). Amino acid conjugates of other auxinic herbicides are probably not active as demonstrated for the synthetic auxin dicamba, where amidohydrolases were not able to convert dicamba-amino acid conjugates back to the parent compound. Dicamba conjugates did not have any effects when sprayed on soybean, while 2,4-D amino acid conjugates were converted to the parent herbicide and had herbicide effects on treated plants (Chiu et al., 2018). In susceptible waterhemp plants, 2,4-D is mainly converted into 2,4-Asp in amounts up to 50%, depending on the tissue (Figure 3.1C and Supplementary figure 3.2). The inefficiency of herbicide conjugation, which is five times slower in susceptible plants than in resistant (Figueiredo et al., 2018) and the hydrolyzation of 2,4-D-Asp back into the parent herbicide (Figures 3.2 and 3.3) show that the intrinsic mechanisms of herbicide metabolism are not sufficient to protect susceptible waterhemp populations against 2,4-D herbicide action, causing severe injury and death.

In resistant waterhemp plants, 2,4-D epinasty effects occur in the first 3 d after treatment, but after that period, leaves start to recover from the primary herbicide symptoms, with complete recovery in 7 d. 2,4-D action was restored in resistant waterhemp plants when pretreated with the P450 inhibitor malathion and a metabolic analysis confirmed the reduction of 2,4-D metabolism (Figueiredo et al., 2018). Here we demonstrated that the resistant population evolved a different metabolic pathway, where 2,4-D undergoes ring hydroxylation. This reaction is typically performed by cytochrome P450s that contain a heme structure with an electrophilic FeO^{3+} that attacks the C5 of the phenoxy group of 2,4-D, forming a tetrahedral intermediate σ-complex. This arrangement induces the existing hydrogen to be abstracted by the porphyrin structure and bounce back to the carbonyl oxygen inserted at C5, forming 5-OH-2,4-D (Supplementary figure 3.3 – Bathelt et al., 2008). Phenoxy hydroxylation on the carbons C-4,5 is more predominant in dicot species forming three possible products 4-OH-2,5-D, 4-OH-2-Cl, and 5-OH-2,4-D, while in monocots it occurs predominantly at C-3,4, which will form hydroxylated products such as 4-OH-2,3-D, 4-OH-2-Cl, and 3-OH-2,4-D (Feung et al., 1975a). In terms of auxin activity, a study done in *Avena fatua*, showed that 3-OH-2,4-D induced higher auxinic growth effects than the parent 2,4-D. Other hydroxylated metabolites, as 5-OH-2,4-D, 6-OH-2,4-D, 4-OH-2,5-D and 4-OH-2,3-D did not show any effects on coleoptile elongation and are considered inactivated products (Wightman and Setterfield, 1968; Witham et al., 1971). In 2,4-D resistant lines of soybean, there was higher accumulation of ring hydroxylated glycosides than the nonresistant control tissue (Feung et al., 1978). In the present study, both waterhemp populations and Arabidopsis did not show strong root or auxin effects after treatment with high doses of 5-OH-2,4-D, confirming the results reported previously in *Avena*. One question that remains is if the

hydroxylated metabolite would lose its auxinic effects because of the change in its chemical structure or if rapid 5-OH-2,4-D glucosylation prevents the metabolite to be in its active form.

In waterhemp, 5-OH-2,4-D is rapidly glucosylated and posteriorly the sugar conjugate is malonylated, which are typical reactions of the phase 2 in xenobiotics metabolism and these reactions occur to chlorophenols in diverse plant species (Day and Saunders, 2004; Laurent et al., 2007; Pascal-Lorber et al., 2008). Glucosylation reactions in xenobiotic hydroxyl nucleophilic groups are catalyzed by O-glucosyltransferases (OGT) enzymes using UDP-glucose as the sugar donor molecule (Supplementary figure 3.3). In Arabidopsis, an OGT called UGT72B1 showed high activity on chlorophenol glucosylation, due its hydrophobic and flexible binding pocket (Brazier-Hicks et al., 2007). In waterhemp resistant populations, 5-OH-2,4-D is rapidly glucosylated by OGTs because there was no detection of the primary 5-OH-2,4-D metabolite in the LC-MS chromatograms of 2,4-D treated plants. Glucoside metabolites are mobile in the apoplast due their hydrophilicity, which may explain the higher amounts of translocated radioactive 2,4-D observed in resistant waterhemp (Figueiredo et al., 2018).

Malonylation of glucoside xenobiotics can be a subsequent step of phase 2 metabolism and is important to trap those molecules into the apoplast and promote vacuolar compartmentalization (Schmitt and Sandermann, 1982; Schmitt et al., 1985; Farlane and Trapp, 1994). In Arabidopsis and tobacco, two malonyl transferase enzymes (MaT1 and MaT2) showed substrate specificity to phenolic glucosides. Malonyl glucoside metabolite accumulation was lower in knockout mutant lines for those enzymes. The overexpression of *pmat1* in Arabidopsis reduced cell excretion of the glucoside metabolites to the culture media and increased accumulation of malonylated glucosides in the protoplast cytosol. Structural analysis of tobacco *Nt*MAT1 showed that the enzyme has a flexible and large binding pocket, which may explain its

substrate versatility for diverse glucosylated flavonoid and xenobiotics binding (Taguchi et al., 2010; Manjasetty et al., 2012). In resistant waterhemp plant tissues incubated in ^{14}C-2,4-D water solution, large fractions of 5-OH-2,4-D-(6-O-malonyl)-glucoside were detected in all tissues (Figure 3.1C and Supplementary Figure 3.2). In post-emergence treated plants, malonylated conjugates correspond to just 7% of the characterized radioactive material. The main metabolite produced in 264 hr after 2,4-D application was 5-OH-2,4-D-Glucosyl (37% - Figure 3.1C), where plants were already fully recovered from the primary herbicide symptoms. A previous work shows that resistant waterhemp translocate more radioactive material compared to susceptible (Figueiredo et al., 2018). This may occur as a mechanism to export hydroxylated sugar metabolites to stems and roots for local excretion into those storage organs. Vacuolar storage of herbicide metabolites in waterhemp plants may occur several days after herbicide treatment, when almost 100% of 2,4-D parent is already metabolized (Figure 3.1C).

After malonylation, the final phase 3 of 2,4-D metabolism in plants corresponds to sequestration to the vacuole as a pathway of "local excretion". In plants, there is no identification of specific xenobiotic vacuolar transporters yet, however a class of ABC-type transporter known as multidrug and toxin extrusion transporters (MATE) showed the transported glucosylated and malonylated glucoside flavonoids in *Medicago truncatula*. Those endogenous compounds can undergo glycosylation and malonylation reactions by the same families of enzymes that conjugate xenobiotics. Additionally, MATE transporters are related to detoxification mechanisms in eukaryotes and prokaryotic organisms (review at Martinoia, 2018). Incorporation of xenobiotics into the cell wall lignin is an additional pathway in phase 3 that can happen to chlorinated phenols. Incorporation of xenobiotics generally consists of co-polymerization of nucleophilic addition of the xenobiotic (-OH and -COOH in the case of 2,4-D and its

hydroxylated metabolites) to the benzylic α-carbon of lignol quinone-methide intermediates (Figure 3.4; Trenck et al., 1981). Measurements of incorporated metabolites transformed from original radiolabeled 2,4-D in soybean and wheat cell suspension cultures showed that most of the incorporated radioactive material into lignin corresponded to intact 2,4-D and its ring hydroxylated metabolites (4-OH-2,5-D; Scheel and Sandermann, 1981a). Solvent unextractable metabolites are structurally incorporated to the lignin needing long acid digestion treatments to release (Scheel and Sandermann, 1981a). In the present work, the unextractable incorporated metabolites were quantified by oxidizing the treated plant tissue after solvent extraction and quantifying the amount of radioactive material recovered. Based on prior studies, it can be considered that those incorporated metabolites correspond both to 2,4-D and 5-OH-2,4-D in resistant plants (Scheel and Sandermann, 1981a). Resistant and susceptible populations of waterhemp had similar rates of unextracted radioactive material (15-17% – Figure 3.1 C). At 264 hr after 2,4-D treatment, percentages of unextracted radioactive material were higher than 5-OH-2,4-D-(6-O-malonyl)-glucoside, suggesting that lignin incorporation pathways were the predominant pathway in phase III of 2,4-D metabolism in this resistant population.

Our results demonstrate the gain of a metabolic detoxification response evolved in a 2,4-D resistant waterhemp population, leading to high adaptation of the weed in agronomic systems in which the herbicide is used. In susceptible plants, aspartic acid was the predominant metabolic reaction and toxicological studies showed that the metabolite has less auxin activity and plant inhibitory growth effects compared to the parent herbicide. Based in previews literature, the herbicide effect is probably due to the conversion of 2,4-D-Asp to 2,4-D by amidohydrolases (Eyer et al., 2016; Chiu et al., 2018). Resistant plants presented a different metabolic profile, where 5-OH-2,4-D glucosyl and malonyl-glucosyl conjugates were predominantly found. Those

are likely formed through a cytochrome P450 mediated detoxification reaction, where the phenoxy group of 2,4-D is hydroxylated. Toxicological studies confirmed the low auxinic inhibitory effects in root growth and lack of auxin transcriptional responses of 5-OH-2,4-D in plants. A general scheme with the potential enzymes involved on each step of 2,4-D metabolism in resistant waterhemp was generated based on the chemical structure of the metabolites described above and the potential enzymes that would be governing the metabolic reactions in waterhemp populations (Figure 3.4). Those findings open new perspectives for a better understanding of the evolutionary adaptation of weeds in agronomic systems and, more precisely, in novel metabolic enzymatic functions that can be gained in the process of adaptation. Gene function validation in non-model plants is still a great challenge for the proper understanding of the mechanisms of weed adaptation, which are, in some cases, impossible to be tested in heterologous organisms. Those challenges urge the development of specific genetic, molecular biology, and bioinformatics tools to study those molecular functions in the weed species itself.

REFERENCES

Bak S, Beisson F, Bishop G, Hamberger B, Höfer R, Paquette S, Werck-Reichhart D (2011) Cytochromes p450. Arabidopsis Book 9:e0144-e0144

Bathelt CM, Mulholland AJ, Harvey JN (2008) QM/MM Modeling of Benzene Hydroxylation in Human Cytochrome P450 2C9. The Journal of Physical Chemistry A 112:13149-13156

Bernards ML, Crespo RJ, Kruger GR, Gaussoin R, Tranel PJ (2012) A Waterhemp (Amaranthus tuberculatus) Population Resistant to 2,4-D. Weed Science 60:379-384

Brazier-Hicks M, Offen WA, Gershater MC, Revett TJ, Lim E-K, Bowles DJ, Davies GJ, Edwards R (2007) Characterization and engineering of the bifunctional N- and O-glucosyltransferase involved in xenobiotic metabolism in plants. Proceedings of the National Academy of Sciences 104:20238-20243

Chen Q, Westfall CS, Hicks LM, Wang S, Jez JM (2010) Kinetic basis for the conjugation of auxin by a GH3 family indole-acetic acid-amido synthetase. J Biol Chem 285:29780-29786

Chiu L-W, Heckert MJ, You Y, Albanese N, Fenwick T, Siehl DL, Castle LA, Tao Y (2018) Members of the GH3 Family of Proteins Conjugate 2,4-D and Dicamba with Aspartate and Glutamate. Plant and Cell Physiology 59:2366-2380

Costea M, Weaver SE, Tardif FJ (2005) The Biology of Invasive Alien Plants in Canada. 3. Amaranthus tuberculatus (Moq.) Sauer var. rudis (Sauer) Costea & Tardif. Canadian Journal of Plant Science 85:507-522

Davies K (2013) Weed Science: A Plea for Thought—Revisited. By R. L. Zimdahl. Heidelberg, Germany: Springer (2012), pp. 73, £44.99. ISBN 978-94-007-2087-9. Experimental Agriculture 49:149-150

Day JA, Saunders FM (2004) Glycosidation of chlorophenols by Lemna minor. Environmental Toxicology and Chemistry 23:613-620

Devine MD, Shukla A (2000) Altered target sites as a mechanism of herbicide resistance. Crop Protection 19:881-889

Dinesh DC, Villalobos LIAC, Abel S (2016) Structural Biology of Nuclear Auxin Action. Trends in Plant Science 21:302-316

Ebel E, Bell J, Fries A, Kasey C, Berkebile JM (1947) Preparation of 2,4-D(2,4-dichlorophenoxyacetic acid) from phenol and monochloracetic acid. Journal of Chemical Education 24:449

Ercegovich CD, Hamilton RH, Hurter J, Hall JK (1971) Metabolism of phenoxyacetic acids. Metabolism of 2,4-dichlorophenoxyacetic acid and 2,4,5-trichlorophenoxyacetic acid by bean plants. Journal of Agricultural and Food Chemistry 19:480-483

Eyer L, Vain T, Pařízková B, Oklestkova J, Barbez E, Kozubíková H, Pospíšil T, Wierzbicka R, Kleine-Vehn J, Fránek M, Strnad M, Robert S, Novak O (2016) 2,4-D and IAA Amino Acid Conjugates Show Distinct Metabolism in Arabidopsis. PLOS ONE 11:e0159269

Farlane CM, Trapp S (1994) Plant Contamination: Modeling and Simulation of Organic Chemical Processes: Taylor & Francis

Feung C-S, Hamilton RH, Mumma RO (1975) Metabolism of 2,4-dichlorophenoxyacetic acid. VII. Comparison of metabolites from five species of plant callus tissue cultures. Journal of Agricultural and Food Chemistry 23:373-376

Feung CS, Hamilton RH, Witham FH, Mumma RO (1972) The relative amounts and identification of some 2,4-dichlorophenoxyacetic Acid metabolites isolated from soybean cotyledon callus cultures. Plant physiology 50:80-86

Feung CS, Loerch SL, Hamilton RH, Mumma RO (1978) Comparative metabolic fate of 2,4-dichlorophenoxyacetic acid in plants and plant tissue culture. Journal of Agricultural and Food Chemistry 26:1064-1067

Figueiredo MR, Leibhart LJ, Reicher ZJ, Tranel PJ, Nissen SJ, Westra P, Bernards ML, Kruger GR, Gaines TA, Jugulam M (2018) Metabolism of 2,4-dichlorophenoxyacetic acid contributes to resistance in a common waterhemp (Amaranthus tuberculatus) population. Pest Management Science 74:2356-2362

Gaines TA, Lorentz L, Figge A, Herrmann J, Maiwald F, Ott M-C, Han H, Busi R, Yu Q, Powles SB, Beffa R (2014) RNA-Seq transcriptome analysis to identify genes involved in metabolism-based diclofop resistance in Lolium rigidum. The Plant Journal 78:865-876

Gaines TA, Zhang W, Wang D, Bukun B, Chisholm ST, Shaner DL, Nissen SJ, Patzoldt WL, Tranel PJ, Culpepper AS, Grey TL, Webster TM, Vencill WK, Sammons RD, Jiang J, Preston C, Leach JE, Westra P (2010) Gene amplification confers glyphosate resistance in Amaranthus palmeri. Proceedings of the National Academy of Sciences 107:1029-1034

Ghanizadeh H, Harrington KC (2017) Non-target Site Mechanisms of Resistance to Herbicides. Critical Reviews in Plant Sciences 36:24-34

Goggin DE, Nealon GL, Cawthray GR, Scaffidi A, Howard MJ, Powles SB, Flematti GR (2018) Identity and Activity of 2,4-Dichlorophenoxyacetic Acid Metabolites in Wild Radish (Raphanus raphanistrum). Journal of Agricultural and Food Chemistry 66:13378-13385

Grossmann K (2010) Auxin herbicides: current status of mechanism and mode of action. Pest Management Science 66:113-120

Guo F, Iwakami S, Yamaguchi T, Uchino A, Sunohara Y, Matsumoto H (2019) Role of CYP81A cytochrome P450s in clomazone metabolism in Echinochloa phyllopogon. Plant Science 283:321-328

Hatzios KK (1997) Regulation of enzymatic systems detoxifying xenobiotics in plants: Springer Science & Business Media

Heap I (2020) The International Survey of Herbicide Resistant Weeds. 2020

Iwakami S, Endo M, Saika H, Okuno J, Nakamura N, Yokoyama M, Watanabe H, Toki S, Uchino A, Inamura T (2014) Cytochrome P450 CYP81A12 and CYP81A21 Are Associated with Resistance to Two Acetolactate Synthase Inhibitors in Echinochloa phyllopogon. Plant Physiology 165:618-629

Iwakami S, Kamidate Y, Yamaguchi T, Ishizaka M, Endo M, Suda H, Nagai K, Sunohara Y, Toki S, Uchino A, Tominaga T, Matsumoto H (2019) CYP81A P450s are involved in concomitant cross-resistance to acetolactate synthase and acetyl-CoA carboxylase herbicides in Echinochloa phyllopogon. New Phytologist 221:2112-2122

Krewson CF, Neufeld CHH, Drake TF, Fontaine TD, Mitchell JW, Preston WH (1954) Synthetic Plant-Growth Modifiers. IV. 2-Methyl-4-Chlorophenoxyacetyl Derivatives of Amino Acids. Weeds 3:28-37

Küpper A, Peter F, Zöllner P, Lorentz L, Tranel PJ, Beffa R, Gaines TA (2018) Tembotrione detoxification in 4-hydroxyphenylpyruvate dioxygenase (HPPD) inhibitor-resistant Palmer amaranth (Amaranthus palmeri S. Wats.). Pest Management Science 74:2325-2334

Laurent F, Canlet C, Debrauwer L, Pascal-Lorber S (2007) Metabolic fate of [14C]-2,4-dichlorophenol in tobacco cell suspension cultures. Environmental Toxicology and Chemistry 26:2299-2307

Lu H, Yu Q, Han H, Owen MJ, Powles SB (2019) Non-target-site resistance to PDS-inhibiting herbicides in a wild radish (Raphanus raphanistrum) population. Pest Management Science n/a

Manjasetty BA, Yu X-H, Panjikar S, Taguchi G, Chance MR, Liu C-J (2012) Structural basis for modification of flavonol and naphthol glucoconjugates by Nicotiana tabacum malonyltransferase (NtMaT1). Planta 236:781-793

Martinoia E (2018) Vacuolar Transporters – Companions on a Longtime Journey. Plant Physiology 176:1384-1407

Obenland OA, Ma R, O'Brien SR, Lygin AV, Riechers DE (2019) Carfentrazone-ethyl resistance in an Amaranthus tuberculatus population is not mediated by amino acid alterations in the PPO2 protein. PLOS ONE 14:e0215431

Oerke EC (2006) Crop losses to pests. The Journal of Agricultural Science 144:31-43

Oliveira MC, Gaines TA, Jhala AJ, Knezevic SZ (2018) Inheritance of Mesotrione Resistance in an Amaranthus tuberculatus (var. rudis) Population from Nebraska, USA. Front Plant Sci 9:60-60

Pascal-Lorber S, Despoux S, Rathahao E, Canlet C, Debrauwer L, Laurent F (2008) Metabolic Fate of [14C] Chlorophenols in Radish (Raphanus sativus), Lettuce (Lactuca sativa), and Spinach (Spinacia oleracea). Journal of Agricultural and Food Chemistry 56:8461-8469

Preston C (2004) Herbicide resistance in weeds endowed by enhanced detoxification: complications for management. Weed Science 52:448-453

Scheel D, Sandermann H (1981) Metabolism of 2,4-dichlorophenoxyacetic acid in cell suspension cultures of soybean (Glycine max L.) and wheat (Triticum aestivum L.). Planta 152:253-258

Schmitt R, Kaul J, Trenck Tvd, Schaller E, Sandermann H (1985) β-d-Glucosyl and O-malonyl-β-d-glucosyl conjugates of pentachlorophenol in soybean and wheat: Identification and enzymatic synthesis. Pesticide Biochemistry and Physiology 24:77-85

Schmitt R, Sandermann H (1982) Specific Localization of β-D-Glucoside Conjugates of 2, 4-Dichlorophenoxyacetic Acid in Soybean Vacuoles. Zeitschrift für Naturforschung C 37:772-777

Shergill LS, Barlow BR, Bish MD, Bradley KW (2018) Investigations of 2,4-D and Multiple Herbicide Resistance in a Missouri Waterhemp (Amaranthus tuberculatus) Population. Weed Science 66:386-394

Shyam C, Jhala AJ, Kruger G, Jugulam M (2019) Rapid metabolism increases the level of 2,4-D resistance at high temperature in common waterhemp (Amaranthus tuberculatus). Scientific Reports 9:16695

Siminszky B (2006) Plant cytochrome P450-mediated herbicide metabolism. Phytochemistry Reviews 5:445-458

Staswick PE, Tiryaki I, Rowe ML (2002) Jasmonate Response Locus JAR1 and Several Related Arabidopsis Genes Encode Enzymes of the Firefly Luciferase Superfamily That Show Activity on Jasmonic, Salicylic, and Indole-3-Acetic Acids in an Assay for Adenylation. The Plant Cell 14:1405-1415

Taguchi G, Ubukata T, Nozue H, Kobayashi Y, Takahi M, Yamamoto H, Hayashida N (2010) Malonylation is a key reaction in the metabolism of xenobiotic phenolic glucosides in Arabidopsis and tobacco. The Plant Journal 63:1031-1041

Tan X, Calderon-Villalobos LIA, Sharon M, Zheng C, Robinson CV, Estelle M, Zheng N (2007) Mechanism of auxin perception by the TIR1 ubiquitin ligase. Nature 446:640-645

Thomas EW, Loughman BC, Powell RG (1964) Metabolic Fate of some Chlorinated Phenoxyacetic Acids in the Stem Tissue of Avena sativa. Nature 204:286-286

Torra J, Rojano-Delgado AM, Rey-Caballero J, Royo-Esnal A, Salas ML, De Prado R (2017) Enhanced 2,4-D Metabolism in Two Resistant Papaver rhoeas Populations from Spain. Front Plant Sci 8

Trenck KTvd, Hunkier D, Sandermann H (1981) Incorporation of Chlorinated Anilines into Lignin. Zeitschrift für Naturforschung C 36:714-720

Ulmasov T, Hagen G, Guilfoyle TJ (1999) Activation and repression of transcription by auxin-response factors. Proceedings of the National Academy of Sciences 96:5844-5849

Ulmasov T, Murfett J, Hagen G, Guilfoyle TJ (1997) Aux/IAA proteins repress expression of reporter genes containing natural and highly active synthetic auxin response elements. The Plant Cell 9:1963-1971

Westfall CS, Zubieta C, Herrmann J, Kapp U, Nanao MH, Jez JM (2012) Structural Basis for Prereceptor Modulation of Plant Hormones by GH3 Proteins. Science 336:1708-1711

Wightman F, Setterfield G (1968) Biochemistry and physiology of plant growth substances: proceedings: The Runge

Witham FH, Feung C-S, Hamilton RH (1971) Metabolism of 2,4-dichlorophenoxyacetic acid by soybean cotyledon callus tissue cultures. Journal of Agricultural and Food Chemistry 19:475-479

Yamada T, Kambara Y, Imaishi H, Ohkawa H (2000) Molecular Cloning of Novel Cytochrome P450 Species Induced by Chemical Treatments in Cultured Tobacco Cells. Pesticide Biochemistry and Physiology 68:11-25

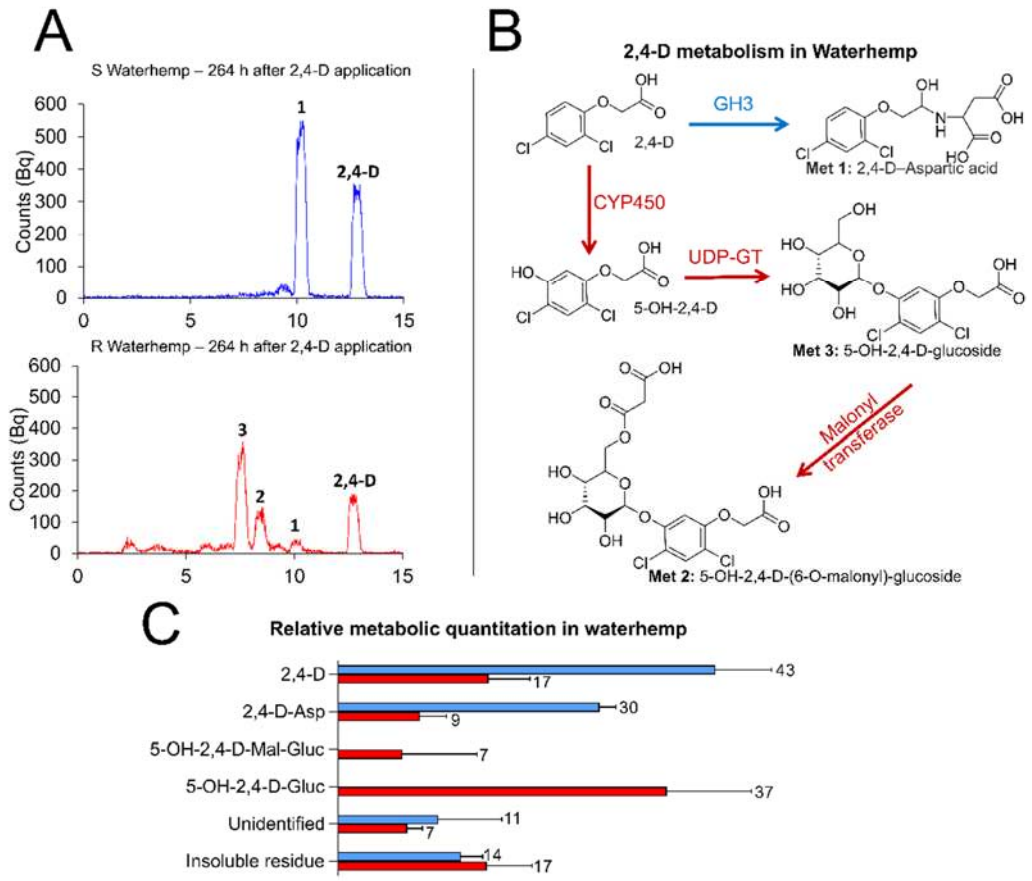

Figure 3.1: Chemical characterization of metabolites produced by resistant and susceptible populations. A) HPLC chromatograms of [^{14}C] 2,4-D metabolism at 264 hr after treatment (radioactive units in Bq versus retention time in minutes) in susceptible (Blue) and resistant (Red). The last peak corresponds to the parent herbicide 2,4-D and other peaks correspond to metabolites with their respective number. B) Metabolism pathways based on NMR and HRMS chemical characterization of 2,4-D metabolites. Susceptible plants perform aspartyl conjugation reactions (Met. 1) of 2,4-D mediated by GH3 enzymes In resistant plants, a CYP450 enzyme performs ring hydroxylation at position 5 and a UDP-GT rapidly transfers a glucosyl group, forming 5-OH-2,4-D-glucoside (Met. 3). Subsequently, a malonyl transferase transfers a malonyl group to 5-OH-2,4-D-glucoside forming 5-OH-2,4-D-(6-O-malonyl)-glucoside (Met. 2). C) Hydroxylated metabolites were found only in resistant plants. Relative percentage of 2,4-D parent, characterized and undefined metabolites, and unrecovered radioactive material from waterhemp plants harvested 264 hr after herbicide treatment. Plotted values on each bar corresponds to the average percentage recovered of the respective radioactive product (n=3).

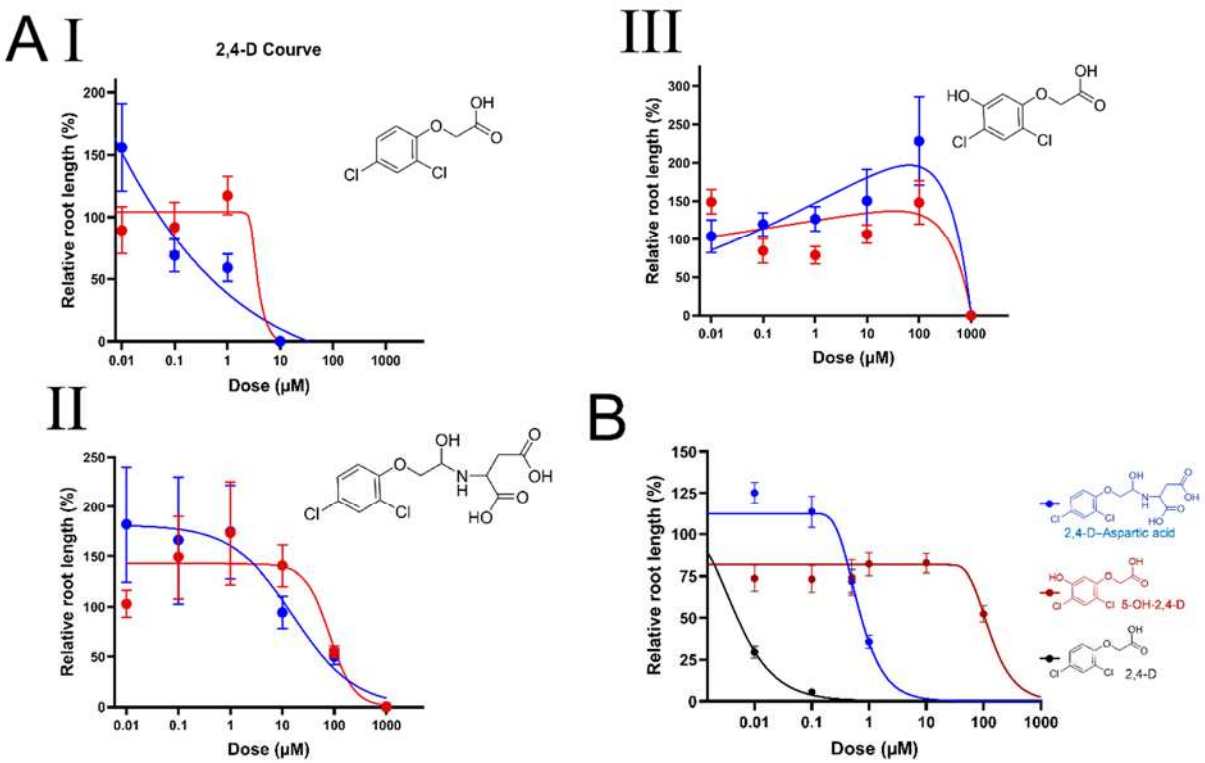

Figure 3.2: Toxicological characterization of 2,4-D, 2,4-D-Asp, and 5-OH-2,4-D on resistant and susceptible *Amaranthus tuberculatus* and *Arabidopsis thaliana*. A) Root growth in *A. tuberculatus* resistant (red) and susceptible (blue) treated with the doses of 0.01, 0.1, 1, 10, 100, and 1000 µM of 2,4-D (AI), 2,4-D-Asp (AII), and 5-OH-2,4-D (AIII). B) Dose response on Arabidopsis with 2,4-D (black), 2,4-D-Asp (blue), and 5-OH-2,4-D (red). Root growth was evaluated with the doses of 0.01, 0.1, 0.5, 1, 10, 100, and 1000 µM. For all experiments 7-d old seedlings were transferred to agar plates containing auxin treatment and root growth was evaluated 7 d later. The percentage of root length was calculated based on root growth in DMSO media (10 µL ml^{-1}). Error bars correspond to standard error of the mean (for all experiments n = 12).

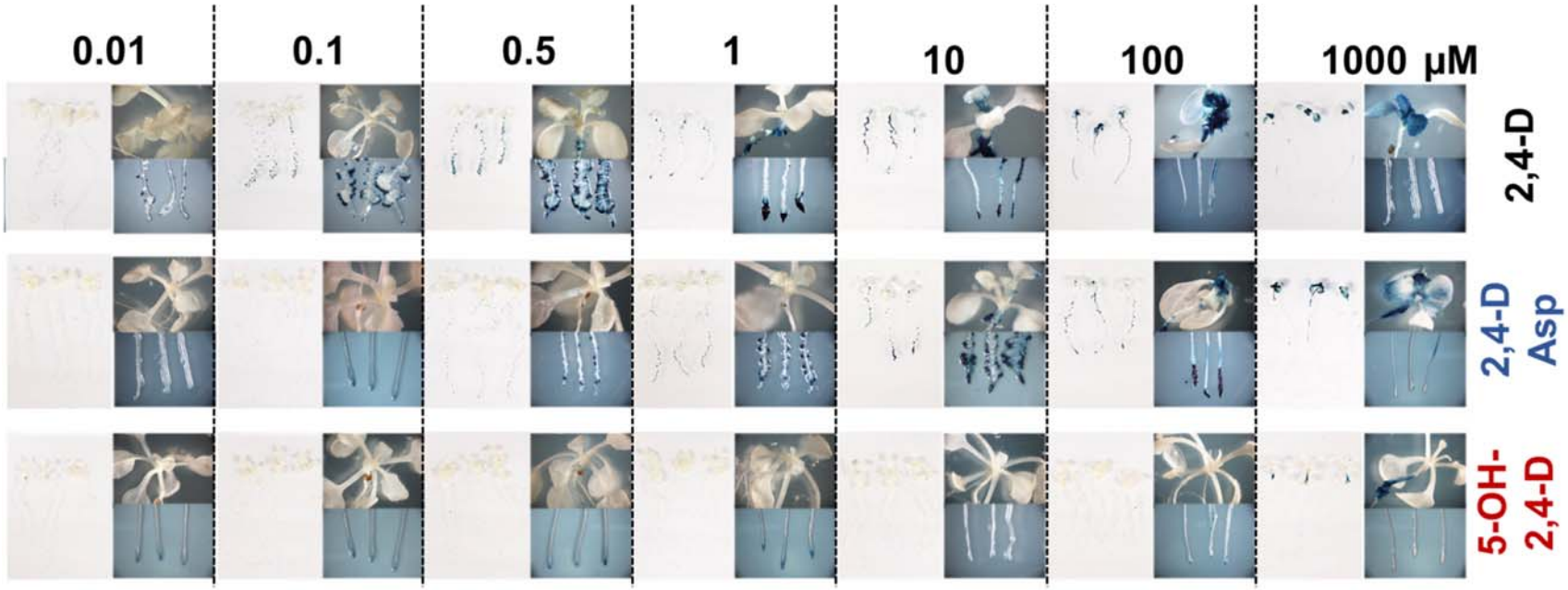

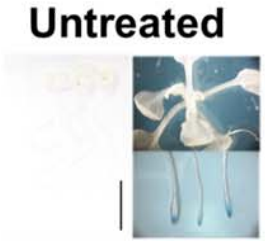

Figure 3.3: *DR5::GUS* auxin reporter system showing phytohormone activity of 2,4-D and waterhemp metabolites under different doses. Representative images of Col-0 carrying the *DR5::GUS* reporter (Ulmasov et al., 1997b) on 16-d-old seedlings, rosettes, and primary roots, 7 d after treatment exposure. Column numbers correspond to the auxin concentration used (µM) of 2,4-D, 2,4-D-Asp, and 5-OH-2,4-D. Untreated plants contained DMSO at 10 µl ml^{-1}.

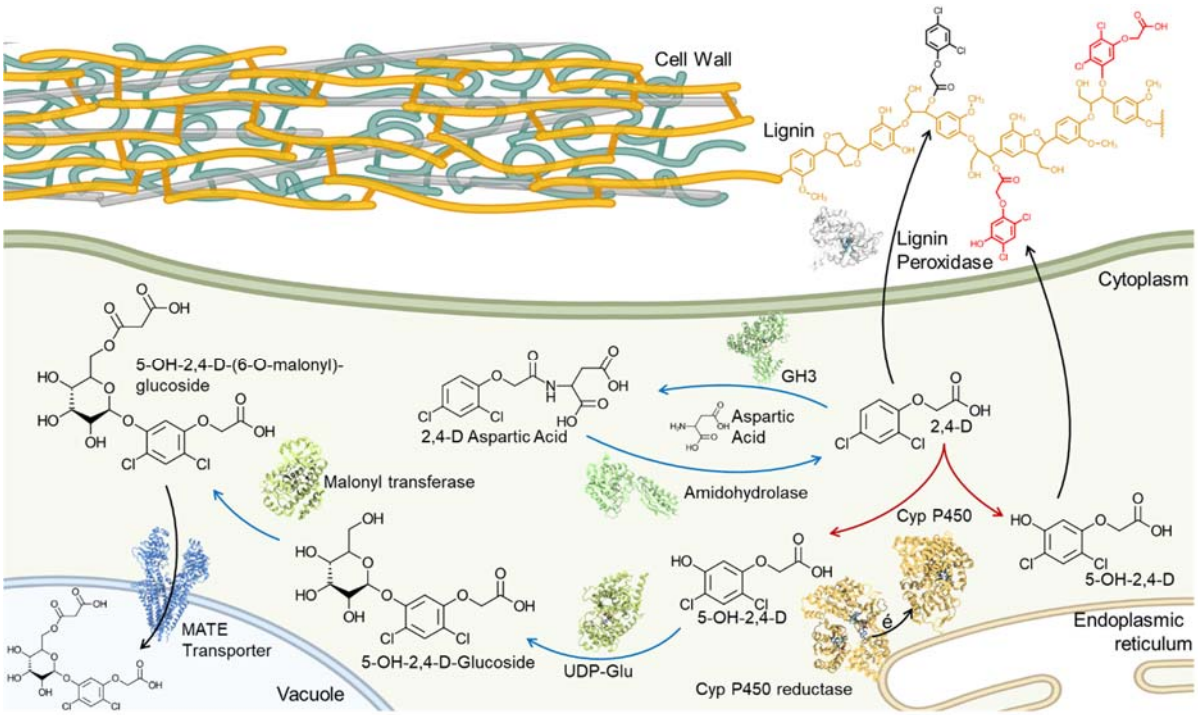

Figure 3.4: Proposed general model for 2,4-D metabolism in resistant waterhemp plant cells. Red arrows correspond to phase I, blue is phase II, and black is phase III of herbicide metabolism reactions. In susceptible and resistant populations, GH3 enzymes mediate an aspartyl conjugation reaction, producing 2,4-D-Aspartic acid. That metabolite can be turned back into 2,4-D through amidohydrolases. For detoxification reaction in phase I, 2,4-D undergoes hydroxylation by a cytochrome P450, forming 5-OH-2,4-D. In phase II, the nucleophilic -OH group at C5 is attacked by a UDP-Glucosyl transferase, making 5-OH-2,4-D-Glucoside. Posteriorly, a malonyl transferase will catalyze the formation of 5-OH-2,4-D-(6-O-malonyl)-Glucoside. This malonylated final conjugate will undergo vacuolar compartmentalization through The Multidrug and Toxin Extrusion (MATE) like active transporter in phase III. A consistent part of insoluble metabolites were detected in waterhemp tissue, indicating the incorporation of 2,4-D acid and 5-OH-2,4-D into the cell wall structure mediated by the action of lignin peroxidases corresponding to an additional "local excretion" pathway in phase III of 2,4-D metabolism. Overall, rapid hydroxylation and sugar conjugation of 2,4-D reduces the auxinic toxic effects of the original herbicide, leading to herbicide resistance.

Chapter IV – Resistance to the herbicide 2,4-D in *Sisymbrium orientale* conferred by a deletion mutation in the degron tail of IAA2

INTRODUCTION

Auxins are a group of plant hormones that regulate plant growth and morphogenesis. The natural auxin indole-3-acetic acid (IAA) is a product of the tryptophan pathway. The level of active IAA is highly regulated by metabolic processes including conjugation and degradation. Synthetic auxin herbicides mimic the effects of IAA, but due to their high stability induce strong auxinic responses in plants. Auxin signaling occurs in the cell nucleus and is mediated by transcription factors called Auxin Response Factors (ARF) that bind to auxin-responsive elements at the promoter regions of auxin-related genes (Ulmasov *et al.*, 1995). ARFs are regulated by transcriptional repressors called Aux/IAA proteins. Those repressor proteins can be degraded by a class of SCF-E3 protein complexes that contain an F-box protein co-receptor family called Transport Inhibitor Response 1/Auxin Signaling F-box (TIR1/AFB). Auxins act as a "molecular glue" in bringing together $SCF^{TIR1/AFB}$ and Aux/IAA. This process leads to Aux/IAA ubiquitination and subsequent degradation of these repressors by the 26S proteasome and activation of ARFs, resulting in the transcription of auxin early responsive genes (Tan et al., 2007; Dinesh et al., 2016).

Aux/IAA have four characteristic domains. Domain I is important for transcriptional repression. Domain II contains the degron motif, which is a 13 amino acid sequence that binds to $SCF^{TIR1/AFB}$ and auxin. Domains III and IV are called Phox and Bem1p (PB1) domain, which have homology to the DIII and DIV of ARFs forming homo and heterodimers that lead to transcriptional repression (Dinesh et al., 2015). Only the PB1 domain within the Aux/IAA structure has a defined crystal structure (Dinesh et al., 2015), while the other regions are

characterized as intrinsically disordered regions (IDR). Mutations in certain regions of Aux/IAA genes can lead to auxin insensitivity due to changes in protein stability, which can cause strong phenotypes with changes in leaf shape, plant size, root development, underdeveloped reproductive systems and low seed production (Hamann et al., 1999; Tian and Reed, 1999; Nagpal et al., 2000; Ouellet et al., 2001; Rogg et al., 2001; Fukaki et al., 2002; Hamann et al., 2002; Tatematsu et al., 2004; Yang et al., 2004; Overvoorde et al., 2006; Walsh et al., 2006; Rinaldi et al., 2012; Calderón Villalobos et al., 2012). A mutation causing a Gly127Asn amino acid substitution in degron motif of the *Aux/IAA16* gene of the weed species *Kochia scoparia* caused resistance to the synthetic auxin herbicide dicamba, showing the practical importance that changes to Aux/IAA repressors can have for auxin responses and herbicide resistance (LeClere et al., 2018). Currently, there are 41 different species that have evolved resistance to synthetic auxin herbicides and in most of the resistance cases the mechanism is unknown (Heap, 2020).

In that context, *Sisymbrium orientale* is an important weed in crops and pastures of Australia. This species is monoecious, primarily self-pollinating diploid (2n=14), and a member of the *Brassicaceae* family. In 2005, a population resistant to the synthetic auxin herbicides 2,4-Dichlorophenoxyacetic acid and 2-methyl-4-chlorophenoxyacetic acid (MCPA) was reported near Port Broughton in South Australia (Preston et al., 2013). The plants did not show epinasty symptoms or tissue necrosis following 2,4-D treatment. Progeny tests revealed that the resistance was inherited as a single dominant allele (Preston and Malone, 2015). Subsequently, two other resistant populations from the same area were characterized. In both populations, resistance was the result of a single, dominant allele. No reductions in 2,4-D absorption were found in the resistant plants; however, reduced translocation of 2,4-D out of the treated leaf was observed from 24 hr after treatment in both resistant populations (Dang et al., 2018).

Given the management importance of synthetic auxins in agriculture and the recent introduction of synthetic auxin resistant soybean and cotton (Busi et al., 2018), our objective in this study was to determine the 2,4-D resistance mechanism in this species. Here we performed a transcriptome analysis on Recombinant Inbred Lines (RILs) derived from a cross between 2,4-D-resistance (R) and -sensitive (S) genotypes and found a 27 bp deletion in the degron tail (DT) of Aux/IAA2 (*SoIAA2*) to confer auxin insensitivity. The DT deletion reduced *in vitro* auxin binding to TIR1 and AFB5. We further show the importance of IAA2 for auxin homeostasis and confirm the importance of the DT in the process of Aux/IAA degradation. These results advance the understanding of Aux/IAA functions in auxin signaling and demonstrate a novel mechanism of targeted mutation that confers field-evolved auxinic herbicide resistance.

MATERIAL AND METHODS

Plant material

One population of 2,4-D-resistant *S. orientale* was collected from a wheat field in Port Broughton (PB-R), a second 2,4-D resistant population was collected 9.2 km away (PB-R2), while the susceptible population originated from Roseworthy (S), Australia, about 120 km away from the resistant populations (Preston et al., 2013; Preston and Malone, 2015). PB-R plants were reported to be 22-fold more resistant to 2,4-D and 20-fold more resistant to MCPA compared to S plants (Preston et al., 2013; Dang et al., 2018).

Two biparental crosses were made to study inheritance of 2,4-D resistance (Dang et al., 2018), using PB-R as the male parent for Cross A and PB-R2 as the male parent for Cross B, with S as the female parent for both crosses. Crosses were performed by hand emasculation of S and hand pollination with pollen from the R parent as previously described (Preston and Malone,

2015; Dang et al., 2018). The F1 progeny were self-pollinated to produce F2 progeny, and F2 individuals were self-pollinated to produce F3 progeny. The F3 progeny were sprayed with 150 g a.i. ha^{-1} 2,4-D (2,4-D amine, Shredder, Winfield) using an overhead track sprayer (DeVries Manufacturing) equipped with a flat-fan nozzle tip (Teejet® 8002EVS, Spraying System) calibrated to deliver 187 L ha^{-1} of spray solution at 172 kPa to visually determine segregation of 2,4-D resistance, evaluated 21 days after treatment (DAT). Homozygous resistant and homozygous susceptible F3 lines were inbred via single-seed descent to create recombinant inbred lines (RILs) to the F4 generation (Cross A). The F3 generation was used for Cross B.

RNA-Sequencing

RNA-Sequencing was performed on a total of 12 individuals, one individual from each of six F4 RILs from Cross A and one individual from each of six F3 RILs from Cross B. From Cross A, three RILs were homozygous 2,4-D-resistant and three RILs were homozygous 2,4-D-susceptible. From Cross B, two RILs were homozygous 2,4-D-resistant and four RILs were homozygous 2,4-D-susceptible. The lines used for RNA-Sequencing were first germinated on agar plates, transplanted to 3×3cm pots filled with potting soil (Fafard, Sun Gro Horticulture), and grown in a growth chamber at 25/20 °C, 16/8 h light/dark photoperiod. At the four-leaf stage, the youngest expanded leaf was collected. Samples were frozen immediately in liquid nitrogen and total RNA was extracted using the RNeasy Plant Mini Kit (Qiagen). Sample quality was assessed by RIN score (Agilent TapeStation) as well as by gel electrophoresis. DNase treatment, library preparation, and sequencing were conducted at the Roy J. Carver Biotechnology Center at the University of Illinois. Libraries were prepared using the TruSeq Stranded mRNA Sample Prep Kit (Illumina). Sequencing was performed on a HiSeq 4000 (Illumina) using bar-coded adapters in two lanes of the Illumina flow-cell, yielding 1.6 billion

paired-end 100 bp reads. Individual library yields ranged from 52 to 75 million paired-end reads. Fastq files were generated and demultiplexed with bcl2fastq v2.17.1.13 conversion software (Illumina) and adaptors were trimmed from the 3'-end reads.

A *de novo* reference transcriptome was obtained by separately assembling Illumina reads from a Cross A 2,4-D-resistant RIL (R206) and a susceptible RIL (S242) with Trinity (Li and Godzik, 2006). The assembled contigs were filtered for minimum contig length of 500 bp. The two assemblies were compared using CDHit v4.6.6 (Li and Godzik, 2006) with a 95% confidence interval to eliminate redundant contigs and retain all contigs unique to either the R or S assembly. This resulted in a 72-Mb transcriptome with 37,223 contigs. Putative annotations were assigned using Trinotate (Haas et al., 2013) and the TAIR10 protein database (Berardini et al., 2015). Read alignments to the *de novo* reference transcriptome were conducted with Bowtie2 (Langmead and Salzberg, 2012) using the default "end-to-end" mode and the "sensitive" option. The minimum allowed fragment length was set to 100 and the maximum to 800 bp.

Differential expression and SNP analysis

Raw read counts were extracted using SAMtools (Li et al., 2009). Counts-per-million (CPM) and gene expression differences were calculated with the package 'edgeR' (Robinson et al., 2010) using the statistical software R v3.3 (Team, 2013) and an expression threshold of ≥1 CPM in at least two samples. After normalization of the read depth the data was analyzed using the 'classic approach'. Expression differences were compared between 2,4-D resistant and susceptible RILs within Cross A and B, respectively, as well as between all 2,4-D-resistant and -susceptible RILs. Differentially expressed transcripts were then filtered for a fold-change of ≥ |2| and a false discovery rate (FDR) adjusted p-value ≤ 0.05. Single nucleotide polymorphism (SNP)

calling was performed using SAMtools (v. 1.3.1) with the default options and the "mpileup" command. The command "bcftools" was used to retain only SNPs that had a quality score higher than 10 and read depth higher than 10. An additional filtering step was for SNPs that were heterozygous or homozygous in at least three individuals of all R and all S RILs. Contigs with annotations in the TIR1/AFB family and the Aux/IAA gene family were manually inspected for sequence variants between R and S RILs using IGV to view BAM file read alignments (Thorvaldsdóttir et al., 2013).

Sequence verification of *IAA2* deletion

The IAA2 deleted region was sequenced from R and S RILs samples used in the RNAseq. cDNA was synthesized using Iscript (Bio-Rab) and a PCR was performed using EconoTaq 2X master mix with primers (Supplementary table 4.1) spanning the predicted deletion in IAA2, to produce a predicted 239 bp amplicon from S and a 212 bp amplicon from R containing a 27 bp deletion (PCR conditions – 94ºC (2 min), 30 cycles of 94ºC (30 sec) 54ºC (30 sec) and 72ºC (15 sec); followed by 72ºC (5 min). The sequence of amplicons was determined by Sanger sequencing.

A KASP genotyping assay was developed using a forward primer specific to the R allele appended with a linker sequence for the HEX fluorophore and a forward primer specific to the S allele appended with a linker sequence for the FAM fluorophore, together with a universal reverse primer (Supplementary table 4.1). The analysis was performed by mixing a primer master mix containing the three primers and a KASP master mix (12 nM of primers and 432 µL of KASP solution from LGC Biosearch Technologies). Four µl of the master mix was added to 4 µl of plant DNA at 20 ng μL^{-1}. The PCR was run on a Biorad CFX at conditions of 94 ºC for 15 min; followed by 10 cycles of 94 ºC for 20 sec, 61 decreasing to 55 ºC for 60 Sec (0.6 ºC

touchdown per cycle); followed by 26 cycles of 94 ºC for 20 sec, and 55 ºC for 60 sec. FAM and HEX fluorescence was obtained and corrected by removing background fluorescence obtained in a non-template control.

Segregation analysis

A progeny test segregation analysis was performed on 219 F3 plants derived from self-pollination of a heterozygous F2 individual from cross B, identified via progeny test due to segregation of 2,4-D resistance in the F3 progeny. Plants were sprayed with 200 gai ha^{-1} 2,4-D at the 5 true leaf stage. Damage percentage was evaluated at 28 DAT. Leaf tissue was harvested and genomic DNA was extracted by CTAB (Doyle and Doyle, 1987). A KASP assay was performed with primers and methods as described above. To further test the co-segregation between the resistant phenotype and $IAA2_{\Delta 27}$, nine each of R and S RILs from cross A and three each of R and S RILs from cross B were genotyped using the KASP assay. Two individuals were genotyped from each RIL.

Analysis of *IAA2* deletion in other resistant *S. orientale* populations

Seeds of additional *S. orientale* populations collected in South Australia were germinated by sowing directly onto the soil surface of seedling trays containing standard potting mix (Boutsalis et. al. 2012). Once emerged, seedlings were transplanted into 9.5 × 8.5 × 9.5 cm punnet pots (Masrac Plastics, South Australia, Australia) and grown outdoors at the Waite Campus, University of Adelaide, Australia. At the 4-leaf stage, plants were treated with a single rate of 250 g a.i. ha^{-1} 2,4-D (2,4-D amine 650, FMC) to screen for resistance. Herbicide was applied using a laboratory moving boom pesticide applicator and applied at an equivalent of 109 L ha^{-1} of water at a pressure of 250 kPa and a speed of 1 m s^{-1} using Tee-Jet 001 nozzles (Tee-

Jet 8001E; Spraying Systems Co., Wheaton, IL). Leaf curl was assessed 48 h after treatment, with any plants showing leaf epinasty considered susceptible and tissue harvested, while the remaining plants were considered resistant and allowed to grow for a further 21 d to confirm resistance and tissue subsequently harvested.

Genomic DNA was extracted using the Isolate II Plant DNA kit (Bioline, Alexandria, New South Wales, Australia) according to the manufacturer's instructions. The concentration of DNA was determined spectrophotometrically on a Nanodrop ND-1000 (Thermo Scientific, Wilmington, DE, USA). For polymerase chain reaction (PCR) amplification, ~100 ng of gDNA was added to a standard 25 µL PCR reaction mix containing 1× MyFi reaction buffer (containing 0.2 mM of dNTPs and 0.6 mM of $MgCl_2$), 0.4 µM of each gene-specific primer (as above – Supplementary table 4.1) and 1 µL of MyFi DNA polymerase (Bioline). Amplification was carried out in an automated DNA thermal cycler (GeneTouch, Bioer Technology, Binjiang, Hangxhou, China) with PCR conditions as follows: 1 min denaturing at 95 ºC; 35 cycles of 15 s denaturation at 95 ºC, 30 s annealing at 58 ºC, 15 s elongation at 72 ºC and a final extension for 7 min at 72 ºC. PCR products were prepared with 1× Ficoll loading dye [15% (w/v) Ficoll 4000, 0.25% (w/v) bromophenol blue, 0.25% (w/v) xylene cyanol FF] and visualized on SYBR Safe (Life Technologies, Mulgrave, Victoria, Australia) stained agarose gels. Samples were electrophoresed in 1× TAE buffer (40 mM of Trizma base, 1 mM of Na_2EDTA, pH to 8 with glacial acetic acid) at 100 V and photographed under UV light (λ = 302 nm). DNA fragment sizes were estimated by comparing their mobility with bands of known sizes of a low-molecular-weight marker (EasyLadder & HyperLadder; Bioline).

Amplified fragments were cloned using the Topo TA cloning kit (Life Technologies) according to the manufacturer's instructions to facilitate sequencing. Colony PCR was performed

to determine positive clones carrying the fragment, using the same PCR protocol as used for amplification, but replacing the template DNA with a single clone colony, and increasing the initial denaturing step to 10 min to aid cell lysis. Before adding to the PCR reaction, colonies were streaked onto standard LB/kan plates and plasmid DNA of positive clones isolated from the regrown streaked colonies (Isolate II Plasmid Mini Kit, Bioline). Plasmids were sequenced using the standard M13 vector primers with sequencing conducted by the Australian Genome Research Facility (AGRF). Sequence data were analyzed using ContigExpress from the Vector-NTI Suite 6 programs (Life Technologies).

Functional validation of *IAA2* deletion in Arabidopsis

Arabidopsis transformation was performed using the established protocols (Clough and Bent, 1998) with modifications (Bechtold and Bouchez, 1995). *IAA2* alleles were amplified by PCR from cDNA generated from RNA extracts of homozygous R and S F5 lines (Cross A). RNA was extracted using Direct-zol RNA Miniprep Plus Kit (Zymo). cDNA synthesis was performed with oligo(dT)$_{20}$ primers using SuperScript™ II Reverse Transcriptase kit (Invitrogen). Wild-type (WT) and mutant alleles were amplified by PCR using PrimeSTAR HS Premix (Takara) using primers linked with *AscI* and *BamHI* restriction enzyme sites for cloning (Supplemental Table 4.1). Purified PCR amplicons were ligated into the pGEM-T Easy Vector (Promega), transformed into *E. coli*, sequenced by Sanger sequencing, and digested using the restriction enzymes *AscI* and *BamHI* (New England BioLabs). The digested product was then ligated into the binary vector pFGC5941, which was also digested with *Asc*I and *BamH*I and transformed into *Agrobacterium tumefaciens* (strain GV3101). For plant transformation, a single colony of *Agrobacterium tumefaciens* carrying pFGC5941 plasmid with *IAA2* alleles was inoculated into 5 ml of LB medium with appropriate antibiotics for 24 hr to obtain primary

culture. 500 µl of primary culture was added to 500 mL of liquid LB medium and incubated on a shaker (200 rpm) at 28ºC for 24 to 36h to obtain secondary culture for transformation of Arabidopsis wild type plants. Bacterial culture was pelleted by centrifugation at 6000xg for 15 min at 4ºC. The pellet was resuspended in ~300 mL solution containing 5% sucrose and 0.02% Silwet L-77 to obtain an OD of 0.8 to 0.9 at Abs $_{600}$ nm. Each allele of *IAA2* was transformed into *Arabidopsis thaliana* (Col-0) by floral dip method and grown for seed production.

For transformant selection, 40 mg of transformed seeds for each *IAA2* allele were sterilized with bleach solution (12.5%) and plated on ½ MS selection medium with Cefotaxime (200 mg/L) and glufosinate-ammonium (7.5 mg/L). After two weeks, putative transgenic plants were selected and transferred to a second selection plate with ½ MS medium with Cefotaxime (100 mg/L), and glufosinate-ammonium (5 mg/L). After a second round of selection, plants were transferred to soil and grown until seed production. For T2 selection, 36 seeds were cleaned and grown on ½ MS with glufosinate-ammonium (5 mg/L). T3 homozygous plants containing one copy of the T-DNA vector were selected and *So*IAA2 expression was analyzed using the same primers from the *So*IAA2 expression assay (Supplementary table 4.1) and *At*Cyclophilin and *At*Actin2 were used for normalization. The expression of *So*IAA2 was measured in Col-0 plants (n=3), as negative control. Two expressing homozygous lines that exhibited good expression of each version of the IAA2 WT or *SoIAA2*$_{\Delta 27}$ and contained a single copy of the T-DNA insertion were selected and used for the root growth experiments.

Root assay and gene expression analysis of *IAA2* after auxin treatment

Root assays were performed on 120 mm square petri dishes with ½ MS and 1% phytoagar with natural and synthetic auxins (2,4-D, dicamba, and IAA, Caisson Labs). Stock

solutions were made in DMSO at 1 mM and 0.001 mM and finally diluted into 100 ml depending on the final concentration of the treatment. For the auxin treatments 2,4-D (0.5 μM), dicamba (5 μM), IAA (10 μM) and DMSO at 1 μL mL^{-1} was used for the control. Seeds of Arabidopsis transgenic lines were surface sterilized, plated directly in media with or without auxin, incubated at 4ºC in dark for seed stratification and moved to the growth chamber after 3 days (60% RH, 21/18 °C, 16/8 h light/dark photoperiod). In this study, T3 homozygous plants of *35*::*SoIAA2*, 35:: $SoIAA2_{\Delta 27}$, pFGC5941 vector control and Col-0 as a non-transgenic control, were used. Twelve plants per construct were used in total and roots were measured two weeks after the plates were moved to the growth conditions. Seeds were gas sterilized for 6 hr using bleach and hydrochloric acid.

To study *IAA2* expression under auxin treatments, *S. orientale* sterilized seeds from F5 RILs for each phenotype were planted in ½ MS and grown until expanded cotyledon stage (size was about 2 cm from root to cotyledon tips). Four plants of each phenotype were then dipped in different 1/2 MS liquid media containing DMSO (10 μl ml^{-1}) as control, dicamba (5 μM), IAA (10 μM), or 2,4-D (0.5 μM) for 2 hr. After exposure, plants were collected into 2 ml centrifuge tubes and flash-frozen in liquid nitrogen. RNA was extracted using Direct-zol RNA Microprep from Zymo research, DNase treatment was done using DNaseI (Invitogen –ThermoFisher) and cDNA was generated using iScript according to each manufacturer protocol. q-PCR (CFX Connect TM Real-Time PCR Detection System thermal cycler, BioRad, Hercules, CA) was used to determine *IAA2* expression. The qPCR reaction contained 12.5 μl of SYBR Green (PerfeCTa SYBR Green FastMix), 1 μl each of forward and reverse primers (5 μM) and 1 μL of cDNA for a final reaction volume of 25 μl. q-PCR parameters were 50°C for 2 min, 95°C for 10 min, and 40 cycles of 95°C for 30 s and 60°C for 1 min. Relative expression quantification was calculated

by Expression = $2^{\Delta Ct}$, where $\Delta C_T = C_T$ (average of Actin2 and Cyclophilin) – C_T(IAA2). Each biological sample was run with two technical replicates.

IAA2 proteins purification

The cDNAs corresponding to two alleles of *IAA2* were cloned into a pFN2A (GST) flexi vector (Promega) using the same methodology as described under Arabidopsis transformation. The restriction sites used were *SgfI* and *PmeI* (Supplementary table 4.1). Each version of the *GST-IAA2* vector was transformed into *E. coli* BL21 competent cells and incubated at 37ºC to an OD_{600} of 0.6 and induced with 1 mM of IPTG at 18ºC for 16 hours. The cells were then centrifuged at 4000×g under 4ºC for 20 min, the pellet was resuspended in 40 ml lysis buffer (25 mM Tris HCl pH 7.5, 300 mM NaCl, 10 mM EDTA and 7 mM DTT) and lysed at 12,500 KPa in a microfluidizer at 4ºC. The lysate was centrifuged at 12,500 xg in a Sorval SS-34 rotor, the supernatant was collected and filtered with 0.45 µm and 0.25 µm cellulose filters. The clarified lysate containing soluble protein was then incubated with 5 ml of GST beads (Glutathione Sepharose 4B from GE), washed in lysis buffer, and incubated for 1 hr at 4ºC under rotation. After that, beads were washed 3 times with lysis buffer to remove unbound proteins. The GST-IAA2 proteins were recovered by adding elution buffer (50 mM Tris pH 8 and 15 mM of reduced glutathione at pH 8.0), gently mixed for 10 min, then beads were centrifuged at 500×g for 4 min, buffer was removed, and three more elutions were done. GST was then cleaved using TEV protease (100 µL at 400 µM – New England Biolabs) and the eluent was concentrated and resuspended in lysis buffer using Amicon Ultra Centrifugal Filters. GST beads were added for final purification and it was shaken for 10 min to eliminate GST and undigested proteins. The pure protein solution was recovered by pipetting out the supernatant from beads centrifuged at

500×g. The final purified IAA2 proteins were then quantified on nanodrop and separated on SDS-PAGE to verify the purity.

In silico protein structure predictions

Resistant and susceptible versions of *So*IAA2 amino acid sequences were used for IDRs predictions using PrDos (Ishida and Kinoshita, 2007), IUPred (Mészáros et al., 2018) and Spot2 (Hanson et al., 2016) algorithms. Kyte-Doolittle hydropathy maps were calculated by Expasy-linked ProtScale (Gasteiger et al., 2005).

Size exclusion chromatography (SEC) purification and retention volume studies

The cleaved IAA2 proteins were loaded into a GE superdex 75 equilibrated in CD buffer (10 mM Tris H_2SO_4 pH 7.0 and 150mM $NaClO_4$). Fractions containing different protein aggregates were quantified by UV 280 nm detector. The protein oligomers ware analyzed based on the retention volumes and compared to gel filtration standard proteins (15 – 600 KDa).

Circular dichroism (CD) analysis

CD analysis was performed using a MOS-500 spectrometer (Bio-logic, France) scanning 185-265nm with a 2 nm slit width at an acquisition rate of 2 sec/nm. Buffer and proteins were scanned in a PTFE stoppered 1mm UV quarts cuvette (fireflysci). Protein concentration was between 1 to 7 µM, the absorbance and voltage were 1 A.U and 500. CD measurements were conducted 3 times and the raw ellipticity values were averaged after buffer subtraction and converted to MRE or µMol ellipticity values.

Surface Plasmon Resonance (SPR) affinity binding analysis

Surface plasmon resonance (SPR) experiments were done according to the protocols described in (Lee et al., 2014). TIR1/AFB5 was expressed in insect cell culture using a recombinant baculovirus. The construct contained sequences for three affinity tags, namely 6 His, maltose-binding protein (MBP) and FLAG. Initial purification using the His tag was followed by clean-up using FLAG chromatography, the purified protein was used for SPR assays by passing it over a streptavidin chip loaded with biotinylated *So*IAA2 degron peptides (Thermo Fisher Scientific – Supplementary table 4.2).

The SPR buffer was Hepes-buffered saline with 10 mM Hepes, 3 mM EDTA, 150 mM NaCl and 0.05% Tween 20. Compounds to be tested were premixed with the protein to a final 50 μM concentration. Binding experiments were run at a flow rate of 30 μl min^{-1} using 2.0 min of injection time and 4.0 min of dissociation time. Data from a control channel (mIAA7) and from a buffer+DMSO-only run were subtracted from each sensogram following the standard double reference subtraction protocol.

Crystallography models Pymol for manual docking on *So*IAA2 and TIR1 association

A crystallographic model was made based on the available model of Arabidopsis ASK1-TIR1 in association with 2,4-D and a 13 amino acid degron motif (PDB: 2P1N) and a PB1 domain structure from pea (*Pisum sativum*, PDB: 2M1M). The PB1 domain was manually adjusted to the interaction moieties simulated by Niemeyer et al. (2020) including the amino acid positions for TIR1 of D119, D170, V171, S172, H174, H178, S199, and R220; and the amino acid positions for PB1 of Y196, R225, P237, and R238. The molecular distance corresponding to the length of the missing DT was measured based on the position of the last C-terminal amino-

acid of the core degron positioned on its binding pocket and the first amino acid of the PB1 domain positioned on its binding cluster.

RESULTS

Identification of *IAA2* as a candidate gene for herbicide resistance through RNA-seq

The transcriptome of six F4 recombinant inbred lines (RILs) from a cross between 2,4-D resistant PB-R and susceptible S (Cross A, 3 R RILs and 3 S RILs), and six F3 RILs from a cross between 2,4-D resistant PB-R2 and susceptible S (Cross B, 2 R RILs and 4 S RILs) was sequenced. Average reads per sample was 67,932,100 million with > 40 QC score.

Only three transcripts had differential expression between R and S RILs of both PB-R and PB-R2 populations based on cutoff criteria of FDR <0.05 and fold change of > |2|. These included Aux/IAA2 (*SoIAA2,* 3.3 fold lower in R than S, FDR<0.0001, showed highest sequence similarity to Arabidopsis IAA2 encoded by AT3G23030 – Supplementary figure 4.1), PRP39-2 (10 fold lower in R than S, FDR<0.0001, similar to AT5G46400 that encodes tetratricopeptide repeat (TPR-like) superfamily protein), and ABCB13 (6 fold higher in R than S, FDR <0.01, similar to AT1G27940 that encodes auxin efflux transporter). Notably, PRP39-2 and ABCB13 both had at least one RIL replicate inconsistent with the general pattern, while *So*IAA2 had lower read counts in all R RILs compared to all S RILs. No SNPs were identified that were shared among all R RILs and different from all S RILs from the two populations. However, inspection of the read alignments to *SoIAA2* identified a small gap in read coverage for all R RILs, suggesting a deletion in the R allele, whereas all S RILs had continuous read coverage at this position (Supplementary Figure 4.2).

SoIAA2 gene sequencing

To further investigate and validate the results found for *SoIAA2* through RNAseq, a region of the *SoIAA2* gene corresponding to the deletion was sequenced. A 239 bp region of the *SoIAA2* gene was amplified and sequenced for 3 R and 3 S RILs and the R allele was found to contain a 27 bp deletion (*So*IAA2$_{\Delta 27}$; Figure 4.1).The deletion results in a functional, in-frame *So*IAA2 protein lacking nine amino acids (aa 73 to 81) corresponding to most of the DT region located between the degron and the PB1 domain (Figure 4.1A). None of the S RILs contained a deletion in *SoIAA2*, suggesting the deletion was correlated with resistance.

The presence of *SoIAA2*$_{\Delta 27}$ in other 2,4-D resistant populations of *S. orientale* was also investigated. Eight populations from South Australia, including parent populations PB-R and PB-R2 were screened for resistance to 2,4-D, with four populations identified as resistant. The *SoIAA2* gene was sequenced to determine the presence or absence of *SoIAA2*$_{\Delta 27}$ in individual plants from each population (Supplementary Table 4.3). Only *So*IAA2 was present in individuals from four susceptible populations P15, P31, P49 and P50. All individuals from the two parent resistant populations, PB-R and PB-R2, contained *SoIAA2*$_{\Delta 27.}$ Individuals from resistant population P17 were found to be homozygous for *SoIAA2*$_{\Delta 27}$, or heterozygous for both *SoIAA2*$_{\Delta 27}$ and the WT *SoIAA2* with no deletion, suggesting a segregating population. Population P28, although resistant, did not contain *So*IAA2$_{\Delta 27}$.

Segregation of SoIAA2$_{\Delta 27}$

The heritable association between *SoIAA2*$_{\Delta 27}$ and the resistant phenotype was confirmed by a segregation analysis, where all sensitive progeny exhibited 70% visual injury and were homozygous for WT *SoIAA2*; heterozygous plants showed an average of 24% injury; and

homozygous resistant 12% (Figure 4.1B). This significant difference between heterozygous and homozygous R is probably due to semi-dominance for the resistant allele. The relative expression (RE) of *IAA2* also confirmed the results of the RNAseq, where untreated seedlings showed 3-fold higher expression in S (RE = 0.21) compared to R (RE = 0.07). Auxin treatment significantly increased the expression of *SoIAA2* in R (2.5-fold for 2,4-D and 9.5-fold for IAA) and S (4-fold for 2,4-D and 7-fold for IAA) seedlings compared to untreated plants and DMSO control. Treated susceptible plants (2,4-D RE = 0.55; IAA RE = 1) showed significantly increased expression compared to resistant (2,4-D RE = 0.16; IAA RE = 0.62) (Figure 4.1C).

Expression of SoIAA2$_{\Delta 27}$ in Arabidopsis confers 2,4-D and dicamba resistance

To test if *SoIAA2$_{\Delta 27}$* confers 2,4-D resistance, Arabidopsis was transformed with an empty PFGC5941 vector (Ø), *SoIAA2* and *SoIAA2*$_{\Delta 27}$ under a *CaMV35S* promoter (Supplementary Figure 4.3). The empty vector and WT *SoIAA2* did not show differences in plant phenotype. Heterozygous Arabidopsis transformed with *SoIAA2*$_{\Delta 27}$ showed leaves turned into lanceolate shape and minor reduction in plant size. Homozygous plants showed strong morphological abnormalities, dwarfism, low number of reproductive organs, and low seed production (Figure 4.2A).

A root growth assay in the presence and absence of natural and synthetic auxins was performed using the different transformed Arabidopsis lines. Col-0 (WT) and plants containing the null vector (Ø2 and Ø4) and *SoIAA2* (S1 and S7) were susceptible to inhibition by 2,4-D (0.5 µM) and dicamba (5 µM), having about 90% of root elongation inhibited compared to the control on DMSO (Figure 4.2B and C). Arabidopsis transformed with *So*IAA2$_{\Delta 27}$ (R1 and R38) exhibited high tolerance to 2,4-D and dicamba, showing root growth inhibition of 20 to 30%

compared to DMSO control. The levels of auxin resistance in *SoIAA2*$_{\Delta 27}$ lines were higher than the null vector and WT gene (p-value < 0.01). No differences in percentage root elongation occurred for any of the Col-0 or transgenic plants tested with the natural auxin IAA at 10 µM.

SoIAA2 protein structure and affinity binding analysis

According to Niemeyer et al. (2020), Aux/IAA DT helps in its interaction with TIR1, facilitating lysines to be ubiquitinated on the PB1 domain. Additionally, it was demonstrated that DTs can alter the binding affinity between the Aux/IAA and TIR1. Compared to other members of the Arabidopsis Aux/IAA proteins, *SoIAA2* has a shorter and relatively structured DT. As conducted by Niemeyer et al. (2020), models calculated by PrDos, IUPred, Spot2 to predict changes on protein structure, showed that the DT region of *SoIAA2* was slightly disordered to ordered. Based on the predicted models, loss of DT would make *SoIAA2*$_{\Delta 27}$ have a more ordered structure compared to the WT *SoIAA2*. Kyte-Doolittle hydropathy *in silico* predictions show the loss of a hydrophilic region corresponding to the DT (Supplementary figure 4.4). For a better understanding on the structural changes between proteins, both full versions of proteins were expressed and purified in a heterologous system and used to perform CD spectrometry and size exclusion chromatography. The *SoIAA2* CD spectra shows an alpha, beta, and other structures content of 12.9%: 38.4%: 48.7%, respectively, which is in agreement with a partial ordered structure from the PB1 domain but about half of the protein being disordered or "other". Both *So*IAA2 versions have near identical spectra for each, so it does not seem like the number of molecules or the deletion significantly alters the protein fold (Supplementary figure 4.6B). For size exclusion chromatography, both versions of *So*IAA2 were able to oligomerize in groups of around 6 to 12 molecules at retention volume between 11 and 12 ml, depending on protein concentration (Supplementary figure 4.5 and 4.6A). Dimers of both proteins elute at retention

volume next to 14 ml (Supplementary figure 4.5). Although there was not strong evidence of changes in protein structures, GST bound and purified *So*IAA2$_{\Delta 27}$ protein were more stable in buffer solution than the WT version. Based on these results, there were no apparent changes in protein structure and oligomerization when the DT is removed.

In order to have a better understanding on the mechanism whereby the deletion in *So*IAA2 interferes with auxinic herbicide action, a surface plasmon resonance (SPR) assay was performed using small biotinylated 24 aa peptides constituted by the degron core (9 aa), DT (9 aa), and a small fraction of PB1 (6 aa; Supplementary table 4.2). The assay showed lower binding association for *So*IAA2$_{\Delta 27}$ peptide compared to WT *So*IAA2, which resulted in lower recognition and binding interactions. Additionally, *So*IAA2$_{\Delta 27}$ peptide had more rapid dissociation of the complex indicating its higher instability of complex formation (Figure 4.3A). This was true in the presence of natural and synthetic auxins, where KD of *So*IAA2$_{\Delta 27}$ peptide was always higher compared to WT *So*IAA2 (IAA 40.7 vs 11.4 nM; 2,4-D 296 vs 135 nM; dicamba 694 vs 250 nM), which means the complex of TIR1-auxin- *So*IAA2$_{\Delta 27}$ tends to fall apart faster than with *So*IAA2. Similar results were found for AFB5, tested for 2,4-D and IAA (Figure 4.3B).

Protein model on Pymol

For better comprehension of the role of the DT on the association between TIR1 and IAA2, a manual docking was performed using available structures of the PB1 domain of IAAs and the ASK-TIR1-2,4-D-degron peptide complex. The PB1 and the DT were manually adjusted to the TIR1 interacting domain located on leucine-rich-repeat 3-6 (LRR3-6), also called Cluster 1 as was modeled by Niemeyer et al. (2020). By generating a mechanistic model, it was possible to

have a better understanding for how the loss of DT would interfere with the action of auxinic herbicides (Figure 4.4). The deleted region reduces the length of the DT between Domains II and III by approximately 28 Å (Figure 4.4B). This impairs the ability of the IAA protein to interact with the TIR1 protein, because it is no longer long enough to associate with LRR 3-6 sites in the TIR1 protein and still keep the core degron at its binding site. Based on that hypothesis, the IAA/herbicide/TIR1 complex tends to have less capacity for association and it dissociates faster giving the SoIAA2$_{\Delta 27}$ protein less chances of being ubiquitinated. Thus, *So*IAA2$_{\Delta 27}$ protein remains acting as a transcriptional repressor of ARFs, preventing the rapid increase in gene expression of auxin responsive genes. In susceptible plants, the WT *So*IAA2 is rapidly degraded in the presence of auxins, inducing the overexpression of auxin related genes, leading to auxin related plant injury.

DISCUSSION

The mechanism of synthetic auxin resistance in *S. orientale* was investigated. A transcriptome analysis pointed to a 27-nucleotide deletion that removed the *So*IAA2 DT in resistant individuals reducing the phytotoxicity of auxinic herbicides (Figure 4.1). A segregation study showed a strong correlation between the resistant phenotypes and the *So*IAA2$_{\Delta 27}$ allele. In terms of gene expression, *SoIAA2* tends to have low expression under natural conditions and it is rapidly transcriptionally activated after endogenous auxin application. Similar responses were observed in Arabidopsis Col-0 seedlings, where the expression of *At*IAA2 increased 6 fold in one hour after 20 μM of 2,4-D treatment (Yang et al., 2004).

Observing the differences in expression levels between resistant and susceptible plants, *So*IAA2 seems to be able to regulate its own expression depending on the rates of its degradation

in plants (Figure 4.1C). In resistant plants, the abundance of the repressor protein tends to be higher, due to its lower turnover. Based on that context, the transcriptional activation of *So*IAA2$_{\Delta 27}$ may be reduced by a self-negative feedback regulatory system, where the stable protein remains repressing transcription of auxin responsive genes. Overall, *So*IAA2 seems to play an important role in endogenous auxin homeostasis under hormonal dysregulation.

Usually, mutations inducing higher stability to Aux/IAA proteins lead to drastic morphological defects as was reported for *axr5-1*/IAA1 (Nagpal et al., 2000; Yang et al., 2015), shy2/IAA3 (Tian and Reed, 1999), *axr2/IAA7* (Nagpal et al., 2000)*, iaa16* (Rinaldi et al., 2012) and *iaa28* (Rogg et al., 2001). All these mutants were reported to be insensitive to natural and synthetic auxins. Core degron mutations in the weed *Bassia scoparia Ks*IAA16 also induced severe fitness penalty (LeClere et al., 2018). In Arabidopsis, IAA2 gene knockout lines did not show any visible changes in phenotype (Overvoorde et al., 2006). *So*IAA2$_{\Delta 27}$ heterologous constitutive over-expression in Arabidopsis induced strong phenotypes in homozygous plants compared to heterozygous (Figure 4.2 A). Resistant populations of *S. orientale* apparently do not show such morphological or reproductive defects, giving more evidence that *So*IAA2$_{\Delta 27}$ expression under natural endogenous auxin conditions is regulated to maintain its natural auxin repression levels while keeping normal plant development.

The deletion of the DT in *So*IAA2 is a novel mechanism of auxin target site mutation conferring herbicide resistance to weeds. These results confirm the importance of the DT for Aux/IAA stability. As it was first studied (Niemeyer et al., 2020) for the Arabidopsis *At*IAA7 and *At*IAA12, the deletion of DT led to more stable proteins, reducing the formation of the TIR1-Auxin-Aux/IAA complex in yeast two-hybrid system. In those studies, DT deletion induced less

Aux/IAA degradation in protoplast radiometric assays and lower levels of lysine ubiquitinated sites at *in vitro* ubiquitination.

CD and exclusion chromatography experiments did not show differences in protein structure, folding, or oligomerization between *So*IAA2$_{\Delta 27}$ and *So*IAA2, suggesting that in this case in particular, changes in binding to TIR1 in the presence of auxin are probably not defined by changes in protein folding due to the exclusion of DT. The interaction between the co-receptors could be additionally explained by the loss of specific ubiquitination sites at the DT. In 2015 (Moss et al.), found for the first time that deleting the C-terminal region, corresponding to DT and PB1, reduced the degradation of several Aux/IAA proteins in yeast two-hybrid system and *in planta*. In 2020, an interactome and docking analysis showed that interprotein cross-links occurred between K_{217} situated at TIR1 central cavity to K_{94} located at DT of IAA7 after the core degron (Niemeyer et al., 2020). This lysine is conserved in the DT of *So*IAA2, corresponding to K_{74}. The loss of this lysine could reduce the interaction between *So*IAA2 and TIR1, which would explain the results of SPR binding interaction analysis presented in this study. Moreover, in NMR studies on the interaction between TIR1 and an amino-terminal solution structure of the IAA17 containing DI, DII, and a DT fraction of 8 amino acids, significant changes were observed in the NMR signals for the DT-fraction bidning to TIR1, showing the importance of the binding interface between co-receptors in that region for Aux/IAA instability (Ramans Harborough et al., 2019).

A Pymol protein model using pre-existing crystallographic structures of TIR1 and PB1 domain showed that the loss of 9 amino acids at the DT reduced the molecular distance between the core degron and the PB1 by 28 Å, reiterating the hypothesis that DT amino acid length is important for interaction between TIR1-auxin-Aux/IAA. The reduction of the molecular distance

between degron and PB1, prevents the PB1 reaching its binding site located on LRR 3-6 at TIR1 and the degron to reach its binding pocket, reducing the accessibility of lysine sites to be ubiquitinated. Those findings open a question about what would be the "ideal" DT size for natural protein degradation rates and which specific amino acids would help for the protein degradation, in terms of ubiquitination sites and TIR1-IAA interprotein interaction that would facilitate that process. Further studies using yeast two-hybrid, in vitro ubiquitination and interactome assays can help to address those questions.

Putting everything together, we propose a model to explain why the deletion in the *So*IAA2 gene would likely result in varying levels of resistance to any herbicide that binds to the *So*IAA2/TIR1 complex, adapted on the model created by Niemeyer et al. (2020). In this model, the WT version of *So*IAA2 binds to TIR1 by interacting with the IDRs around the degron and the PB1 domain at the binding clusters at TIR1. Subsequently, *So*IAA2 degron core binds, in the presence of auxin, to its target site on TIR1, then the SCF-complex will ubiquitinate *So*IAA2 so it will be recognized and degraded by the 26S proteasome. In resistant populations, *So*IAA2$_{\Delta 27}$ does not reach the LRR side binding interface properly, probably because the reduction of the molecular distance between the core degron and PB1 domain and the loss of amino acids that facilitate interprotein interaction present at DT. This missing interaction probably impairs the capacity of the core degron to reach its binding site, reducing binding interactions and increasing the disassembling of the TIR1-Auxin- *So*IAA2$_{\Delta 27}$ complex.

Previously, an amino acid modification at the conserved Gly of the degron in IAA16 of *Kochia scoparia* was shown to provide resistance to dicamba (LeClere et al. 2018). This mutation provided high resistance to dicamba but only slightly changed yeast 2-hybrid interaction for 2,4-D, compared to the high level of resistance in *S. orientale* (Preston et al.

2013). Given the far greater effect that the 27 bp deletion has on the interaction of the IAA2 protein with the TIR1/auxin complex, this deletion, and possibly similar deletions in other Aux/IAA genes, will result in greater and more broad-spectrum resistance to auxinic herbicides compared to point mutations in the same region. In addition, the $IAA2_{\Delta 27}$ deletion also provides a novel way of generating crops with strong resistance to auxinic herbicides.

REFERENCES

Bechtold N, Bouchez D (1995) In planta Agrobacterium-mediated transformation of adult Arabidopsis thaliana plants by vacuum infiltration. Pages 19-23 Gene transfer to plants: Springer

Berardini TZ, Reiser L, Li D, Mezheritsky Y, Muller R, Strait E, Huala E (2015) The Arabidopsis information resource: Making and mining the "gold standard" annotated reference plant genome. Genesis 53:474-485

Busi R, Goggin DE, Heap IM, Horak MJ, Jugulam M, Masters RA, Napier RM, Riar DS, Satchivi NM, Torra J, Westra P, Wright TR (2018) Weed resistance to synthetic auxin herbicides. Pest Management Science 74:2265-2276

Calderón Villalobos LIA, Lee S, De Oliveira C, Ivetac A, Brandt W, Armitage L, Sheard LB, Tan X, Parry G, Mao H, Zheng N, Napier R, Kepinski S, Estelle M (2012) A combinatorial TIR1/AFB–Aux/IAA co-receptor system for differential sensing of auxin. Nature Chemical Biology 8:477-485

Clough SJ, Bent AF (1998) Floral dip: a simplified method for Agrobacterium -mediated transformation of Arabidopsis thaliana. The Plant Journal 16:735-743

Dang HT, Malone JM, Boutsalis P, Krishnan M, Gill G, Preston C (2018) Reduced translocation in 2,4-D-resistant oriental mustard populations (Sisymbrium orientale L.) from Australia. Pest Management Science 74:1524-1532

Dinesh DC, Kovermann M, Gopalswamy M, Hellmuth A, Calderón Villalobos LIA, Lilie H, Balbach J, Abel S (2015) Solution structure of the PsIAA4 oligomerization domain reveals interaction modes for transcription factors in early auxin response. Proceedings of the National Academy of Sciences 112:6230-6235

Dinesh DC, Villalobos LIAC, Abel S (2016) Structural Biology of Nuclear Auxin Action. Trends in Plant Science 21:302-316

Doyle JJ, Doyle JL (1987) A rapid DNA isolation procedure for small quantities of fresh leaf tissue.

Fukaki H, Tameda S, Masuda H, Tasaka M (2002) Lateral root formation is blocked by a gain-of-function mutation in the SOLITARY-ROOT/IAA14 gene of Arabidopsis. The Plant Journal 29:153-168

Gasteiger E, Hoogland C, Gattiker A, Duvaud Se, Wilkins MR, Appel RD, Bairoch A (2005) Protein Identification and Analysis Tools on the ExPASy Server. Pages 571-607 *in* Walker JM, ed. The Proteomics Protocols Handbook. Totowa, NJ: Humana Press

Haas BJ, Papanicolaou A, Yassour M, Grabherr M, Blood PD, Bowden J, Couger MB, Eccles D, Li B, Lieber M (2013) *De novo* transcript sequence reconstruction from RNA-seq using the Trinity platform for reference generation and analysis. Nat. Protoc. 8:1494

Hamann T, Benkova E, Bäurle I, Kientz M, Jürgens G (2002) The Arabidopsis BODENLOS gene encodes an auxin response protein inhibiting MONOPTEROS-mediated embryo patterning. Genes & Development 16:1610-1615

Hamann T, Mayer U, Jurgens G (1999) The auxin-insensitive bodenlos mutation affects primary root formation and apical-basal patterning in the Arabidopsis embryo. Development 126:1387-1395

Hanson J, Yang Y, Paliwal K, Zhou Y (2016) Improving protein disorder prediction by deep bidirectional long short-term memory recurrent neural networks. Bioinformatics 33:685-692

Heap I (2020) The International Survey of Herbicide Resistant Weeds. 2020

Ishida T, Kinoshita K (2007) PrDOS: prediction of disordered protein regions from amino acid sequence. Nucleic Acids Research 35:W460-W464

Langmead B, Salzberg SL (2012) Fast gapped-read alignment with Bowtie 2. Nat. Methods 9:357-359

LeClere S, Wu C, Westra P, Sammons RD (2018) Cross-resistance to dicamba, 2,4-D, and fluroxypyr in Kochia scoparia is endowed by a mutation in an AUX/IAA gene. Proceedings of the National Academy of Sciences 115:E2911-E2920

Lee S, Sundaram S, Armitage L, Evans JP, Hawkes T, Kepinski S, Ferro N, Napier RM (2014) Defining Binding Efficiency and Specificity of Auxins for SCFTIR1/AFB-Aux/IAA Co-receptor Complex Formation. ACS Chemical Biology 9:673-682

Li H, Handsaker B, Wysoker A, Fennell T, Ruan J, Homer N, Marth G, Abecasis G, Durbin R (2009) The sequence alignment/map format and SAMtools. Bioinformatics 25:2078-2079

Li W, Godzik A (2006) Cd-hit: a fast program for clustering and comparing large sets of protein or nucleotide sequences. Bioinformatics 22:1658-1659

Mészáros B, Erdős G, Dosztányi Z (2018) IUPred2A: context-dependent prediction of protein disorder as a function of redox state and protein binding. Nucleic Acids Research 46:W329-W337

Moss BL, Mao H, Guseman JM, Hinds TR, Hellmuth A, Kovenock M, Noorassa A, Lanctot A, Villalobos LIAC, Zheng N, Nemhauser JL (2015) Rate Motifs Tune Auxin/Indole-3-Acetic Acid Degradation Dynamics. Plant Physiology 169:803-813

Nagpal P, Walker LM, Young JC, Sonawala A, Timpte C, Estelle M, Reed JW (2000) AXR2 Encodes a Member of the Aux/IAA Protein Family. Plant Physiology 123:563-574

Niemeyer M, Moreno Castillo E, Ihling CH, Iacobucci C, Wilde V, Hellmuth A, Hoehenwarter W, Samodelov SL, Zurbriggen MD, Kastritis PL, Sinz A, Calderón Villalobos LIA (2020) Flexibility of intrinsically disordered degrons in AUX/IAA proteins reinforces auxin co-receptor assemblies. Nature Communications 11:2277

Ouellet F, Overvoorde PJ, Theologis A (2001) IAA17/AXR3: Biochemical Insight into an Auxin Mutant Phenotype. The Plant Cell 13:829-841

Overvoorde P, Okushima Y, Alonso J, Chan A, Chang C, Ecker J, Hughes B, Liu A, Onodera C, Quach H, Smith A, Yu G, Theologis A (2006) Functional genomic analysis of the AUXIN/INDOLE-3-ACETIC ACID gene family members in Arabidopsis thaliana. The Plant cell 17:3282-300

Preston C, Dolman FC, Boutsalis P (2013) Multiple Resistance to Acetohydroxyacid Synthase–Inhibiting and Auxinic Herbicides in a Population of Oriental Mustard (Sisymbrium orientale). Weed Science 61:185-192

Preston C, Malone JM (2015) Inheritance of resistance to 2,4-D and chlorsulfuron in a multiple-resistant population of Sisymbrium orientale. Pest Management Science 71:1523-1528

Ramans Harborough S, Kalverda AP, Thompson GS, Kieffer M, Kubes M, Quareshy M, Uzunova V, Prusinska JM, Hayashi K-i, Napier R, Manfield IW, Kepinski S (2019) A fuzzy encounter complex precedes formation of the fully-engaged TIR1-Aux/IAA auxin co-receptor system. bioRxiv:781922

Rinaldi MA, Liu J, Enders TA, Bartel B, Strader LC (2012) A gain-of-function mutation in IAA16 confers reduced responses to auxin and abscisic acid and impedes plant growth and fertility. Plant Molecular Biology 79:359-373

Robinson MD, McCarthy DJ, Smyth GK (2010) edgeR: a Bioconductor package for differential expression analysis of digital gene expression data. Bioinformatics 26:139-140

Rogg LE, Lasswell J, Bartel B (2001) A Gain-of-Function Mutation in IAA28 Suppresses Lateral Root Development. The Plant Cell 13:465-480

Tan X, Calderon-Villalobos LIA, Sharon M, Zheng C, Robinson CV, Estelle M, Zheng N (2007) Mechanism of auxin perception by the TIR1 ubiquitin ligase. Nature 446:640-645

Tao S, Estelle M (2018) Mutational studies of the Aux/IAA proteins in Physcomitrella reveal novel insights into their function. New Phytologist 218:1534-1542

Tatematsu K, Kumagai S, Muto H, Sato A, Watahiki MK, Harper RM, Liscum E, Yamamoto KT (2004) MASSUGU2 Encodes Aux/IAA19, an Auxin-Regulated Protein That Functions Together with the Transcriptional Activator NPH4/ARF7 to Regulate Differential Growth Responses of Hypocotyl and Formation of Lateral Roots in Arabidopsis thaliana. The Plant Cell 16:379-393

Team RC (2013) R: A language and environment for statistical computing.

Thorvaldsdóttir H, Robinson JT, Mesirov JP (2013) Integrative Genomics Viewer (IGV): high-performance genomics data visualization and exploration. Brief. Bioinform. 14:178-192

Tian Q, Reed JW (1999) Control of auxin-regulated root development by the Arabidopsis thaliana SHY2/IAA3 gene. Development 126:711-721

Ulmasov T, Liu ZB, Hagen G, Guilfoyle TJ (1995) Composite structure of auxin response elements. The Plant Cell 7:1611-1623

Walsh TA, Neal R, Merlo AO, Honma M, Hicks GR, Wolff K, Matsumura W, Davies JP (2006) Mutations in an Auxin Receptor Homolog AFB5 and in SGT1b Confer Resistance to Synthetic Picolinate Auxins and Not to 2,4-Dichlorophenoxyacetic Acid or Indole-3-Acetic Acid in Arabidopsis. Plant Physiology 142:542-552

Yang X, Lee S, So J-h, Dharmasiri S, Dharmasiri N, Ge L, Jensen C, Hangarter R, Hobbie L, Estelle M (2004) The IAA1 protein is encoded by AXR5 and is a substrate of SCFTIR1. The Plant Journal 40:772-782

Yang Y, Zhang X, Yu B (2015) O-Glycosylation methods in the total synthesis of complex natural glycosides. Natural Product Reports 32:1331-1355

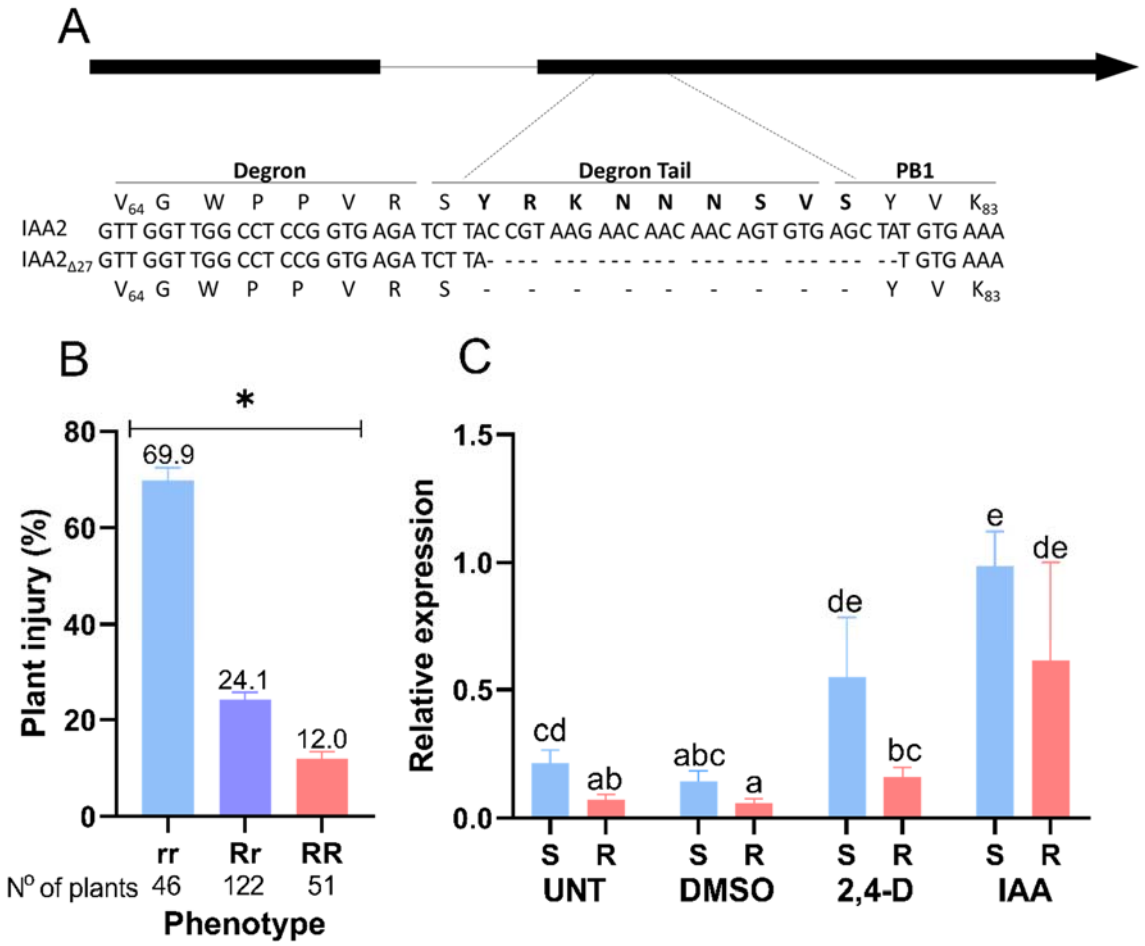

Figure 4.1. Deletion of 27 nucleotides from the *Sisymbrium orientale IAA2* gene results in a 9 amino acid deletion in the degron tail region of IAA2. A) *SoAUX/IAA2* schematic representation with two exons (black boxes) and one intron (line). Sequences showing differences between S (*IAA2*) and R (*IAA2*$_{\Delta 27}$) alleles, broken lines show the nucleotides and amino acids that were deleted in the R allele. B) The deletion allele co-segregates with 2,4-D resistance in an F2 population. plants were sprayed with 2,4-D and evaluated for plant injury 28 days after treatment and genotyped using KASP markers. C) 2,4-D treatment increases *IAA2* expression in S but not in R lines. Seedings were exposed to 100 µM of auxin or DMSO for one hour and *IAA2* expression was measured using cyclophilin and actin2 as normalization genes (n = 3 plants). Error bars correspond to standard deviation. Asterisk symbol or different letters correspond to statistical significance between different treatments (p-value ≤ 0.05).

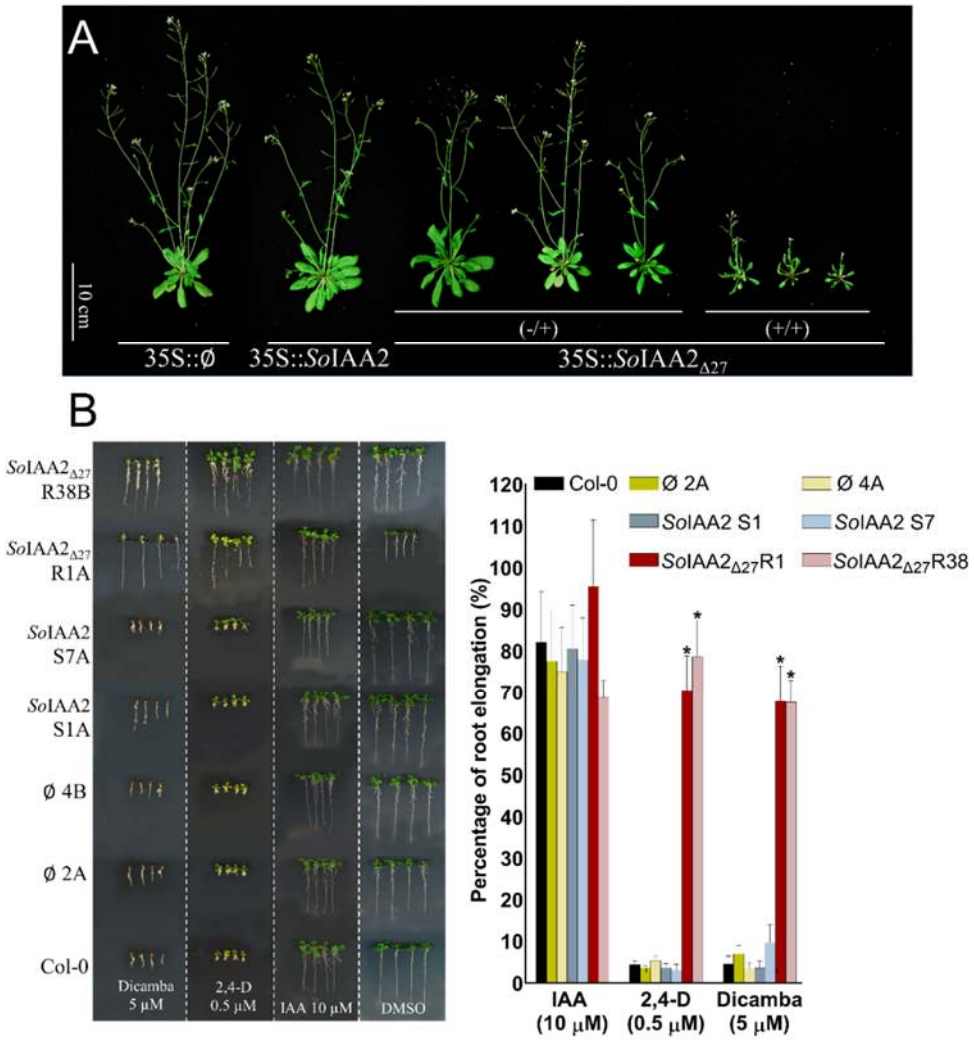

Figure 4.2. Transformation of *Arabidopsis thaliana* with *IAA2* wild-type allele and *IAA2*$_{\Delta 27}$ allele from *Sisymbrium orientale* results in different responses of root growth to auxin and herbicides. A) Pictures of transgenic lines 28 days after germination. Lines with vector control (35S::Ø), *IAA2* (35S::*So*IAA2) and *IAA2*$_{\Delta 27}$ (35S::*So* IAA$_{\Delta 27}$). +/- correspond to heterozygous and +/+ correspond to homozygous plants. Pictures are representative of at least three selected transformants for Basta resistance. B) Only *IAA2*$_{\Delta 27}$ allele can grow on media containing auxinic herbicides. Representative photos of seedlings of Col-0 (WT) and two independent lines for each (Ø), IAA2 and IAA$_{\Delta 27}$ constructs under DMSO and different auxins, 16 days after germination. On the left, a histogram representing the percentage of root elongation based on root growth on DMSO medium. Error bars correspond to standard deviation. Asterisks correspond to statistical significance between different treatments ($n \leq 12$ plants; p-value ≤ 0.05).

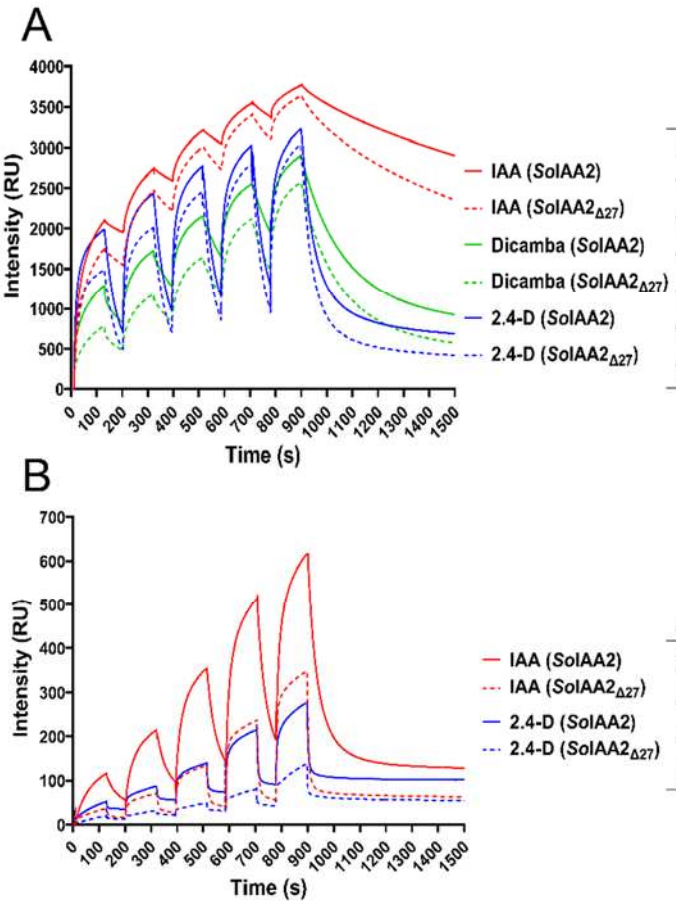

Auxin-binding activity	Auxin	KD (nM)
TIR1-*So*IAA2$_{\Delta 27}$	IAA	40.7
TIR1-*So*IAA2	IAA	11.4
TIR1-*So*IAA2$_{\Delta 27}$	2,4-D	296
TIR1-*So*IAA2	2,4-D	135
TIR1-*So*IAA2$_{\Delta 27}$	Dicamba	694
TIR1-*So*IAA2	Dicamba	250

Auxin-binding activity	Auxin	KD (nM)
AFB5-*So*IAA2$_{\Delta 27}$	IAA	354
AFB5-*So*IAA2	IAA	252
AFB5-*So*IAA2$_{\Delta 27}$	2,4-D	749
AFB5-*So*IAA2	2,4-D	550

Figure 4.3. IAA2$_{\Delta 27}$ has lower recognition and binding interactions and high instability of complex TIR1-auxin-IAA2 formation compared to WT IAA2. SPR analysis for TIR1-IAA2 or IAA2$_{\Delta 27}$ (A) peptides association and dissociation under natural (IAA) and synthetic auxins (dicamba, and 2,4-D). Same analysis was done on AFB5 (B). Auxins were mixtures of TIR1 in buffer solution before injection over the biotinylated IAA2 peptides. RU, resonance units. Tables show auxin K_D values for natural and synthetic auxin binding capacity to IAA2 WT and IAA2$_{\Delta 27}$. Those values were calculated based on nonlinear regressions, saturation binding experiments (Ka) and dissociation rates (Kd), generated by SPR experiments.

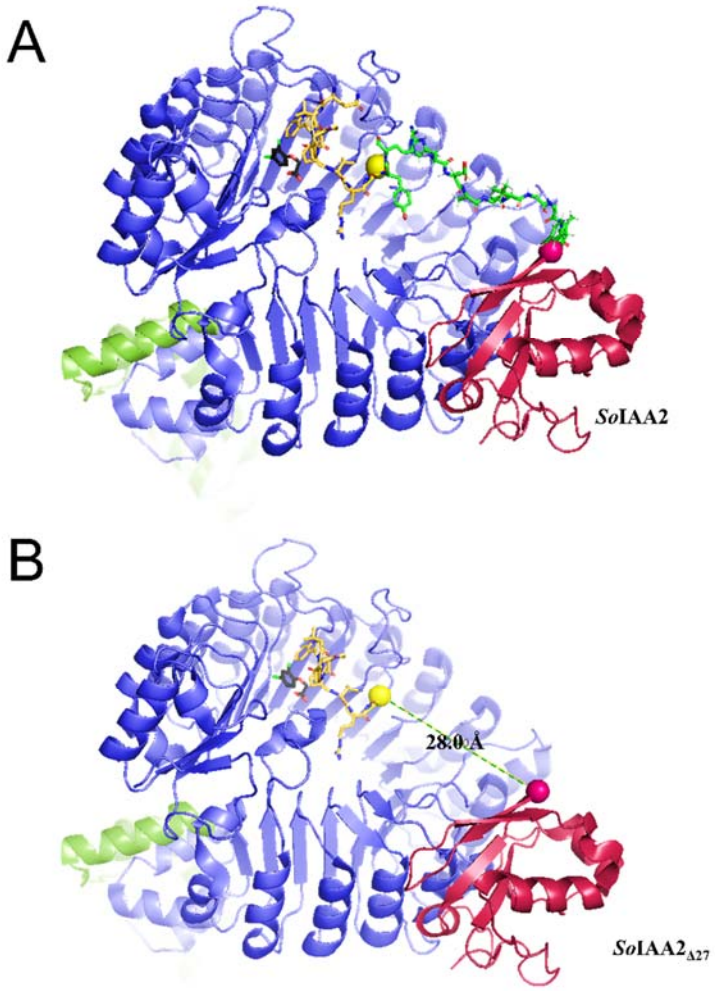

Figure 4.4. Predicted mechanistic effects of IAA2$_{\Delta 27}$ deletion on association with the TIR1/synthetic auxin/IAA protein complex. A) Crystallographic model shows ASK1 in light green, TIR1 in blue, 2,4-D in black, the components of *So*IAA2 protein are showed in three different colors, core degron in yellow, degron tail in green and PB1 domain in red. Spheres were used to define the limits of each region of the IAA2 protein as well to denominate the region that was lost on IAA2$_{\Delta 27}$. B) The loss of 9 amino acids reduces the distance of the domain III of IAA2 from domain II by 28 Angstroms, which is predicted to impair the ability of the IAA2 protein to interact with the TIR1/synthetic auxin complex.

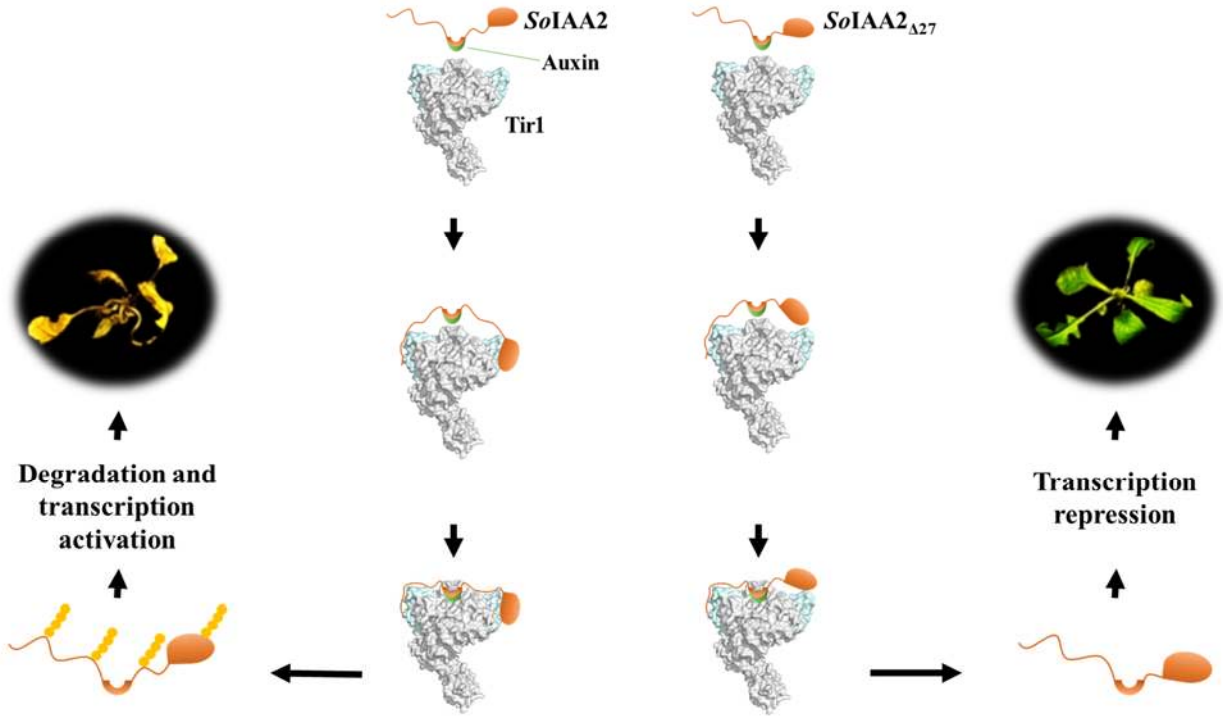

Figure 4.5. Predicted mechanistic effects of IAA2$_{\Delta 27}$ deletion on association with the TIR1/synthetic auxin/IAA protein complex based on (Niemeyer et al., 2020). SoIAA2 interacts with transient auxin independent binding sites at TIR1, helping the core degron in the presence of auxin to reach its binding site. Then the SCF-complex is assembled, *So*IAA2 is ubiquitinated and degraded by 26S proteasome, inducing auxin transcription activation, culminating in plant death. With the loss of the of degron tail, IAA2$_{\Delta 27}$ reduces its capacity to reach auxin independent biding site for the PB1 domain. Due to the higher proximity of the PB1 domain and core degron, the latter binding capacity in the presence of auxin becomes more unstable, leading to rapid dissociation to the SCF$^{TIR1/AFB5}$-complex. Thus, IAA2$_{\Delta 27}$ escapes ubiquitination and proteolysis, maintaining transcriptional repression of auxin-regulated genes, making resistant plants survive, even with very high doses of auxinic herbicides.

CONCLUDING REMARKS

Taken together, the present work contributes for a better understanding of the different aspects of auxinic herbicide resistance in weeds. In *Amaranthus tuberculatus*, we identified a non-target-site mechanism of herbicide resistance. A difference in herbicide metabolism was identified between resistant and susceptible populations, where 2,4-D was metabolized 5-6 times faster in resistant plants. Resistant and susceptible populations had distinct metabolic profiles, in which susceptible plants performed amino acid conjugation, turning 2,4-D into 2,4-D-Aspartic acid; in contrast, resistant plants were able to hydroxylate the herbicide into 5-OH-2,4-D. The pre-treatment with a cytochrome P450 inhibitor before 2,4-D treatment indicated that herbicide detoxification was governed by such enzymes. 5-OH-2,4-D was rapidly converted into 5-OH-2,4-D-Glucosyl and posteriorly into 5-OH-2,4-D-(6-O-Malonyl)-Glucoside. All plant organs were able to produce 2,4-D metabolites; however, hydroxylated compounds were exclusive for resistant phenotypes. Furthermore, toxicological studies showed that 2,4-D-Asp still has auxinic toxic effect or can be converted back to the parent herbicide, reducing plant root growth and promoting auxin transcriptional responses. Additionally, the gene families that may govern or contribute to the 2,4-D metabolism reactions described both in susceptible and resistant were proposed after a literature review. This certainly will help future researchers with the genetic functional validation of those genes, which will contribute to the understanding of the adaptation of the metabolic machinery of weed to overcome herbicide selection pressure in agriculture systems.

In another section of this work, the mechanism of adaptation related to change in 2,4-D targeted protein was discovered in *Sisymbrium orientale*. Transcriptome analysis in recombinant inbred lines comparing resistant and susceptible revealed a 27 bp deletion located at the degron

tail of Aux/IAA2 repressor protein that correlated to resistant phenotype, confirmed by further genotyping analysis. Gene function validation in *Arabidopsis thaliana* and SPR *in vitro* binding assays confirmed role of the Aux/IAA2$_{\Delta 27}$ in conferring resistance to 2,4-D due to its lower recognition and higher instability to TIR/AFB5-auxin-Aux/IAA2$_{\Delta 27}$ complex formation. Protein structure analysis did not show significant changes in protein folding or oligomerization, however, a crystallography model predicted that the loss of the degron tail leads to reduction of the molecular distance between the core degron and the PB1 domain in Aux/IAA2$_{\Delta 27}$, which may reduce the capacity of PB1 domain to reach its interacting site at TIR1 leucine reach repeat domain. Additionally, the loss of ubiquitin targeted amino acids at the degron tail (one lysine and two serines) may prevent proper protein ubiquitination for proteolysis. Those results prove the role of Aux/IAA mutations in weed resistance to auxinic herbicides, opening new perspectives on the importance of the degron tail vicinity regions in protein stability.

Overall, the novel findings of target site and metabolic changes presented in this work increases the current knowledge of auxinic herbicide resistance weed species and open new perspectives for capability of weed adaptation under herbicide selective pressure in agronomic systems. Those results imply an urgent need to adopt integrated management systems to reduce the probability of herbicide selection, especially now that new dicot transgenic crops resistant to auxinic herbicides are available in the market. The adoption in large scale of those crops may increase the use of this herbicide class in the field for the next years, increasing the chances of selection and the establishment of novel weed populations resistant to auxinic herbicides. In this way, herbicide molecules that have been used for decades will lose their efficacy, compromising food production yields.

APPENDIX

[^{14}C] 2,4-D Absorption and Translocation

In an first experiment at Kansas State University (KSU), 2,4-D-resistant and susceptible *A. tuberculatus* were grown in a greenhouse (25/20ºC day/night temperature, 15/9 h day/night photoperiod). When the seedlings reached 5-6 cm tall, they were transferred to growth chambers maintained at 32.5/22.5 ºC, 15/9 h photoperiod, and 60-70% relative humidity. Light in the growth chamber was provided by fluorescent bulbs delivering 550 µmol m^{-2} s^{-1} photon flux at plant canopy level. Plants were watered as needed both under greenhouse and growth chamber conditions. Ten to 12 cm tall plants were treated with four × 2.5 µl (3.33 kBq) droplets of [^{14}C] 2,4-D on the adaxial surface of a fourth or fifth youngest leaf, which was marked with a black permanent marker. Unlabeled 2,4-D was added to the radioactive solution to obtain the field labeled rate of 280 g ha^{-1} in a carrier volume of 187 L ha^{-1}. The adjuvants crop oil concentrate (COC, Agridex, Helena Holding Co., Wilmington, DE) and ammonium sulfate (AMS, Liquid N-PaK; Agriliance, LLC, Inver Grove Heights, MN) were added at 1% v/v and 0.85% v/v, respectively, to maximize adherence of herbicide solution to the leaf surface. The treated plants were returned to the same growth chamber. Plants were harvested at 6, 24, 48 and 72 h after treatment (HAT) and dissected into the tissue of treated leaf (TL), above the treated leaf (ATL), below the treated leaf (BTL), and roots (R). Treated leaves were rinsed for approximately 60 sec with 5 ml wash solution containing 10% methanol and 0.05% Tween™ to remove any herbicide that was not absorbed. Liquid scintillation spectrometry (LSS; Tricarb 2100 TR Liquid Scintillation Analyzer; Packard Instrument Co., Meriden, CT) measured the amount of radioactivity in the leaf rinsate. The harvested samples were wrapped in a single layer of tissue paper and dried at 60°C for 16 h. Subsequently, the plant samples were combusted using a

biological oxidizer (OX-501, RJ Harvey Instrument, Tappan, NY) and radioactivity was determined via LSS. Total 2,4-D absorption was determined by the following equation: % absorption = (total radioactivity applied – radioactivity recovered in wash solution) × 100 / total radioactivity applied. Herbicide translocation to each plant tissue was determined by the following equation: % absorbed = (radioactivity oxidized in plant tissue/total radioactivity absorbed) × 100. Total translocation was the sum of radioactivity recovered in ATL, BTL, and R.

[^{14}C] Metabolism

In an experiment at KSU, 2,4-D-resistant and –susceptible common plants were grown as described previously for [^{14}C] 2,4-D absorption and translocation experiments. Ten to 12 cm tall plants were treated with [^{14}C] 2,4-D (3.99 kBq) as ten by 1µL droplets on the adaxial surface of fully expanded fourth and fifth youngest leaves. To remove any unabsorbed herbicide, the treated leaf was harvested and subsequently rinsed with 5% Tween™ solution at 24, 48, and 72 HAT. All above ground plant tissue was immediately frozen in liquid nitrogen to prevent ongoing metabolism and then homogenized with mortar and pestle. [^{14}C] 2,4-D and its metabolites were extracted as described (Godar et al., 2015) with minor modifications. Samples were centrifuged at 5,000×g for 10 min. Supernatants were extracted and concentrated for 2-3 h at 45°C until reaching an approximate final volume of 500 µl (Centrivap, Labconoco, Kansas City, MO). The 500 µl extract samples were transferred to 1.5 ml microcentrifuge tubes and then centrifuged 10 min at 10,000×g. Total radioactivity per sample was measured via LSS. Samples were then normalized to 6,000 dpm using acetonitrile:water (50:50, v/v) prior to high-performance liquid chromatography (HPLC).

Total extractable radioactivity in 50 µL was resolved into parent [^{14}C] 2,4-D and its metabolites by reverse-phase HPLC (Beckman Coulter, System Gold, Brea, CA) following the protocol optimized previously in our laboratory (Godar et al., 2015). Reverse-phase HPLC was performed with a Zorbax SB-C18 column (4.6 × 250 mm, 5-µm particle size; Agilent Technologies) at a flow rate of 1 mL min^{-1}. The radioactivity in the sample was measured using radio flow detector LB 5009 (Berthold Technologies). The metabolism experiment had three replicates for each treatment and the experiment was repeated. As the parent [^{14}C] 2,4-D had a retention time of 11.6 min in the KSU experiment, the radioactivity measured at this retention time was considered to be non-metabolized [^{14}C] 2,4-D. The percent non-metabolized [^{14}C] 2,4-D was calculated as the radioactivity measured at 11.6 min compared to total amount recovered.

Data Analysis

The experiments conducted at KSU were in randomized complete blocks and a single plant represented an experimental unit. Absorption and translocation experiments included four replications and experiments were conducted twice. The metabolism studies included three replications and were conducted twice. All data were analyzed using the PROC GLIMMIX procedure of SAS (SAS Institute Inc., Cary, NC 27513) for generalized linear mixed model analysis to incorporate normally distributed random effects. Variances were homogenous among individual runs within each experiment and thus runs were combined for analysis and presentation. Treatment means were separated by Fisher's protected least significant difference at $P \leq 0.05$ level of significance.

Supplementary Table 1.1. Equation parameters for [^{14}C] 2,4-D absorption, translocation, and metabolism.

Figure	Population	Equation
1A, absorption	Susceptible	f(x) = (72.6907(x))/(0.11*43.2083+x)
	Resistant	f(x) = (72.9682 (x))/(0.11*33.4752+x)
1B, translocation	Susceptible	f(x) = (22.4823(x))/(0.11*61.3814+x)
	Resistant	f(x) = (81.0326 (x))/(0.11*614.8625+x)
2C, metabolism	Susceptible	f(x) = (100) exp(− exp(-0.618446 (log(x) – 58.015172)))
	Resistant	f(x) = (100) exp(− exp(-0.749272 (log(x) − 13.595200)))
3A, metabolism	Susceptible, - malathion	f(x) = ((3.05020)/ (1 + exp(1.13179(log(x) − log(21.74716))))
	Resistant, - malathion	f(x) = ((3.23644)/ (1 + exp(1.16502(log(x) − log(176.48644))))
	Susceptible, + malathion	f(x) = ((3.15715)/ (1 + exp(1.78556(log(x) − log(22.74036))))
	Resistant, + malathion	f(x) = ((3.18549)/ (1 + exp(0.69062(log(x) − log(24.42846))))

Supplementary Table 2.2. Absorption (percentage of radioactivity applied) and translocation (percentage of absorbed radioactivity) of [^{14}C]-2,4-D in 2,4-D-resistant (R) and –susceptible (S) *A. tuberculatus*.

Data are means with standard errors in parentheses from experiment conducted at Kansas State University. Means followed by different letters indicate significant differences.

		Time after treatment				
Plant part	**Biotype**	**6 h**	**24 h**	**48 h**	**72 h**	**96 h**
		^{14}C 2,4-D (as % applied)				
Leaf rinse	R	63.22 (2.73) a	47.65 (3.04) a	51.02 (2.59) a	49.39 (3.57) a	43.87 (2.21) a
	S	59.51 (0.84) a	45.59 (3.55) a	48.69 (2.89) a	49.17 (3.30) a	41.88 (2.95) a
Total absorbed	R	36.77 (2.73) a	52.34 (3.04) a	48.97 (2.59) a	50.61 (3.57) a	56.12 (2.21) a
	S	40.49 (2.44) a	54.40 (3.55) a	51.30 (2.89) a	50.82 (3.30) a	58.11 (2.95) a
		^{14}C 2,4-D recovered in plant (as % absorbed)				
Treated leaf (TL)	R	96.40 (1.19) a	89.96 (7.17) a	95.02 (1.07) a	93.28 (1.61) a	95.60 (0.66) a
	S	96.38 (0.11) a	87.98 (7.20) a	91.70 (2.60) a	90.11 (1.77) a	92.46 (2.35) a
Shoot above (ATL)	R	0.59 (0.19) a	0.85 (0.33) a	0.91 (0.22) a	0.67 (0.12) a	0.39 (0.06) a
	S	0.58 (0.71) a	0.81 (0.41) a	2.43 (1.95) a	1.15 (0.43) a	0.78 (0.26) a
Shoot below (BTL)	R	2.43 (0.93) a	3.64 (2.22) a	2.55 (0.63) a	4.54 (1.39) a	2.26 (0.45) a
	S	2.73 (0.07) a	9.78 (6.18) a	4.50 (0.88) a	6.50 (1.09) a	4.82 (1.86) a
Roots (BG)	R	0.55 (0.15) b	5.53 (4.68) a	1.51 (0.41) a	1.50 (0.37) b	1.73 (0.33) b
	S	0.41 (0.07) a	1.40 (0.64) b	1.35 (0.51) b	2.22 (0.73) a	1.93 (0.30) a
Total translocated	R	3.59 (1.20) a	10.03 (7.17) a	4.98 (1.07) a	6.72 (1.62) a	4.39 (0.67) a
(ATL+BTL+BG)	S	3.62 (0.84) a	12.01 (7.20) a	8.30 (2.60) a	9.89 (1.78) a	7.53 (2.36) a

Supplementary Table 2.3. Least square means and ANOVA of percent parent compound [^{14}C] 2,4-D remaining in resistant and susceptible *A. tuberculatus* populations (P) at three harvest (H) timings from experiment.
Conducted at Kansas State University.

	Parent Compound [^{14}C] 2,4-D* (%)	
Harvest	Resistant	Susceptible
24 HAT	47.8	84.3
48 HAT	29.4	57.2
72 HAT	33.6	53.3
ANOVA		
P	<0.0001	
H	0.0004	
P by H	0.3609	

*Analysis of variance using PROC GLIMMIX in SAS 2013 using Fisher's Protected LSD at $P \leq 0.05$ level of significance. Values reflect three replications and two runs. Each plant received 3.98 kBq of radiation.

Purified metabolite 2 (Met 2):

5-OH-2,4-D-(6-O-malonyl)-glucoside (3-([(3*S*,6*S*)-6-[5-(carboxymethoxy)-2,4-dichlorophenoxy]-3,4,5-trihydroxyoxan-2-yl]methoxy)-3-oxopropanoic acid)

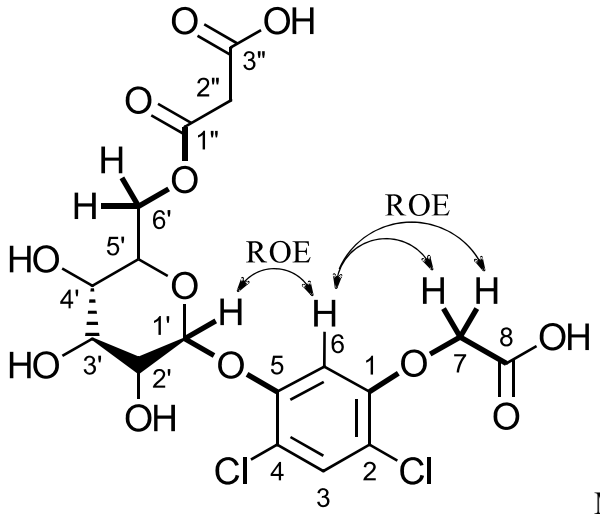

Molecular formula: $C_{17}H_{18}Cl_2O_{12}$

Position	δ (^{1}H)	δ (^{13}C)	Position	δ (^{1}H)	δ (^{13}C)
2,4-D			Glucosyl		
1		153.30	1’	5.01 (d, J = 7.4 Hz)	101.04
2		116.26	2’	3.55 – 3.50 (m)	72.48
3	7.47 (s)	130.75	3’	3.55 – 3.50 (m)	74.89
4		115.17	4’	3.55 – 3.50 (m)	68.62
5		150.82	5’	3.73 (d, J = 9.5 Hz)	73.66
6	6.69 (s)	104.63	6’	4.37 (s)	63.22
7	4.54 (s)	69.39	Malonyl		
8		175.21	1”		170.27

HRMS: (ESI–), $[M-H]^-$, MS: *m/z* 483.0100 ($C_{17}H_{17}Cl_2O_{12}$, Δ 2 ppm); 439.0192; 397.0094

MS/MS: *m/z* 380.0060; 234.9561; 176.9518.

Purified metabolite 3 (Met 3):

5-OH-2,4-D-glucoside ((2,4-dichloro-5-{[(2*S*,5*S*)-3,4,5-trihydroxy-6-(hydroxymethyl)oxan-2-yl]oxyphenoxy)acetic acid**)**

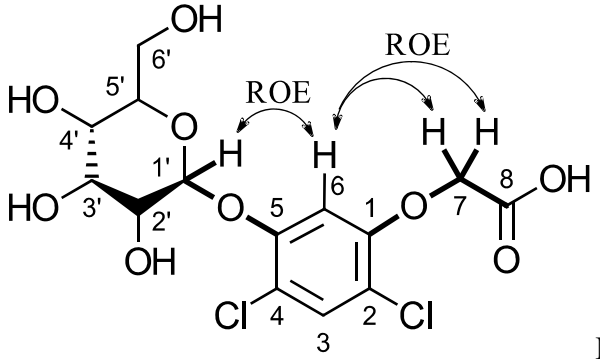

Molecular formula: $C_{14}H_{16}Cl_2O_9$

Position	δ (^{1}H)	δ (^{13}C)	Position	δ (^{1}H)	δ (^{13}C)
2,4-D			Glucosyl		
1		152.76	1’	4.97 (d, *J* = 7.3 Hz)	100.87
2		116.12	2’	3.46 – 3.39 (m)	75.62
3	7.47 (s)	130.35	3’	3.58 – 3.46 (m)	72.53
4		114.42	4’	3.58 – 3.46 (m)	75.62
5		151.47	5’	3.58 – 3.46 (m)	68.97
6	6.72 (s)	103.17	6’	3.67 (dd, *J* = 12.6, 5.2 Hz) 3.86 (dd, *J* = 12.6, 2.3 Hz)	60.65
7	4.51 (s)	67.55			
8		174.97			

HRMS: (ESI–), $[M-H]^-$, MS: *m/z* 397.0094 ($C_{14}H_{15}Cl_2O_9$, Δ 1.5 ppm);

MS/MS: *m/z* 339.0032; 234.9562; 176. 9518.

Parent herbicide

2,4-D (2,4-Dichlorophenoxyacetic acid)

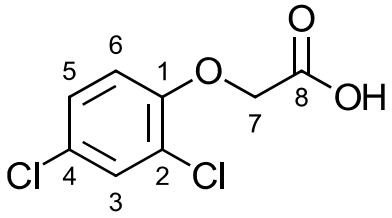

Molecular formula:$C_8H_5Cl_2O_3$

Position	δ (^{1}H)
3	7.48 (d, *J* = 2.6 Hz)
5	7.25 (dd, *J* = 8.9, 2.6 Hz)
6	6.93 (d, *J* = 9.0 Hz)
7	4.71 (s)
HRMS: (ESI–), [M-H]$^-$, MS: *m/z* 218.9618 ($C_8H_5Cl_2O_3$, Δ 2 ppm), MS/MS: *m/z* 160.9558	

Synthesized metabolite 1 (Met 1):

2,4-D-Asp ((2-(2,4-dichlorophenoxy)acetyl)-L-aspartic acid)

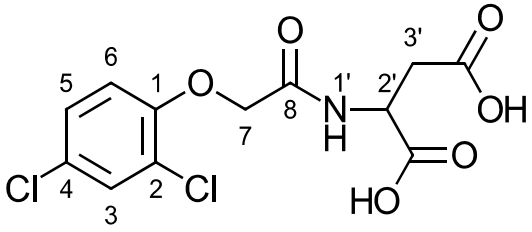

Molecular formula: $C_{12}H_{11}Cl_2NO_6$

Position	δ (^{1}H)	Position	δ (^{1}H)
2,4-D		Aspartic acid	
3	7.60 (d, J = 2.6 Hz)	1’	8.28 (d, J = 8.1 Hz)
5	7.34 (dd, J = 8.9, 2.6 Hz)	2’	4.61 (dt, J = 8.1, 5.8 Hz)
6	7.08 (d, J = 8.9 Hz)	3’	2.72 (m)
7	4.68 (s)		
HRMS: (ESI–), [M-H]$^-$, MS: *m/z* 333.9886 ($C_{12}H_{10}NO_6$, Δ 2 ppm) MS/MS: *m/z* 160.9558.			

Synthesized metabolite 2:

5-OH-2,4-D (2,4-dichloro-5-hydroxyphenoxyacetic acid)

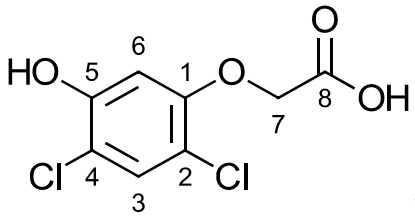

Molecular formula:$C_8H_6Cl_2O_4$

Position	δ (^{1}H)
3	7.42 (s)
6	6.58 (s)
7	4.73 (s)

HRMS: (ESI–), $[M-H]^-$, MS: *m/z* 234.9570 ($C_8H_5Cl_2O_4$, Δ 1.5 ppm), MS/MS: *m/z* 176. 9518.

Supplementary Table 3.1: Structure characterization of 2,4-D and its main metabolites found in *Amaranthus tuberculatus* in susceptible (Aspartyl) and resistant (Aspartyl and hydroxylated metabolites) populations. Tables contain the NMR spectra assignments in δ and High Resolution Mass Spectrometry, MS and MSMS results as *m/z* and it was obtained in negative ESI. Accurate masses were calculated in order to predict the chemical composition of the metabolites and synthesized products The ^{1}H-NMR, zTOCSY, ROESYAD, c2hsqcse, and HMBC spectra of all synthesized and purified metabolites using a BRUKER US400 system operating at 400 MHz at 25 ºC and the solvent used for 2,4-D and sugar metabolites was D_2O (residual H_2O peak was used as a internal standard, δ 4.68), while 2,4-D-Asp and 5-OH-2,4-D were in DMSO-d_6 and 0.03% (v/v) TMS (Tetramethylsilane – internal standard, δ 0). For the sugar metabolites, ROESYAD signals are represented by double-headed arrows in the drawn structure. Thick dark lines correspond to c2hsqcse relationships on metabolite 2 the 1”-C of the malonyl group (δ 170.27) and 6’-H_2 of the glucosyl moiety (δ 4.37). In both metabolites 2 and 3, c2hsqcse relationships are between 5-C phenoxy moiety (δ 150.82 on met 2 and δ 151.47 on met 3) to 1’-H glucosyl moiety (δ 5.01 on met 2 and 4.97 on met 3), between 1-C phenoxy moiety (δ 153.30 on met 2 and δ 152.76 on met 3) to 7-H_2 at the acetyl moiety (δ 4.54 on met 2 and δ 4.51 on met 3), and between 7-H_2 acetyl moiety (δ 4.54 on met 2 and δ 4.51 on met 3) to 8-C at the carboxyl group (δ 175.21 on met 2 and δ 174.97 on met 3).

Supplementary Table 3.2. Equation parameters for root growth of waterhemp populations and Arabidopsis in 2,4-D, 2,4-D-Asp and 5-OH-2,4-D (Figure 3.3).

Graph	Population	Equation
AI	Susceptible	$f(x) = -26.65 + ((3940 – (-26.65)) / (1 + \exp(0.0913(\log(x) - \log(0.003311))))^{4.162}$
	Resistant	$f(x) = -3.924 + ((104.02 – (-3.924)) / (1 + \exp(14.1(\log(x) - \log(2.854))))^{0.188}$
AII	Susceptible	$f(x) = 181.372 / (1 + \exp(0.732(\log(x) - \log(16.215))))$
	Resistant	$f(x) = 142.568 / (1 + \exp(1.856(\log(x) - \log(81.837))))$
AIII	Susceptible	$f(x) = (338.8 + (-0.335(x))) / (1 + \exp(-0.179(\log(x) - \log(4.158))))$
	Resistant	$f(x) = ((275.513 + (-0.267\ (x))) / (1 + \exp(-0.069(\log(x) - \log(15.276))))$
B	2,4-D	$f(x) = 0 + (99.532 - 0) \exp(- \exp(-0.967(\log(x) - 0.0034)))$.
	2,4-D-Asp	$f(x) = 0 + (112.415 - 0) \exp(- \exp(-1.446\ (\log(x) - 102.015)))$.
	5-OH-2,4-D	$f(x) = 0 + (81.61 - 0) \exp(- \exp(-1.515(\log(x) - 0.508)))$.

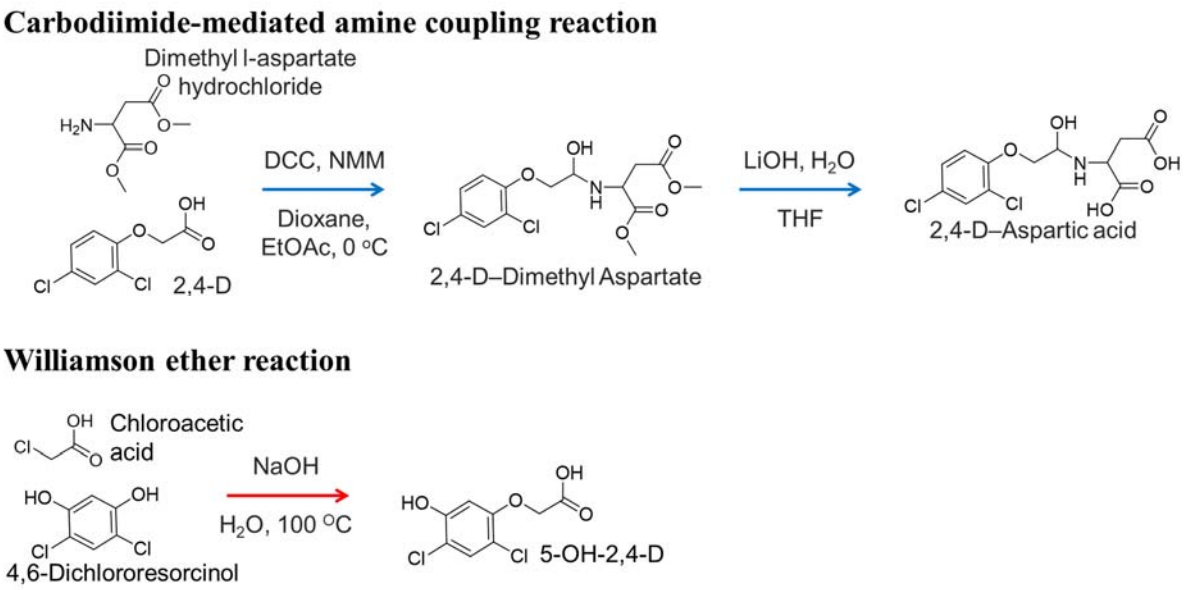

Supplementary figure 3.1. Schematic representation of waterhemp metabolite synthesis for 2,4-D aspartic acid and 5-OH-2,4-D. Synthesis of 2,4-D-Asp was done in two reactions (Eyer et al., 2016), 1 – Synthesis of 2,4-D-dimethyl aspartate (yield = 95%) using 2,4-D and dimethyl l-aspartate hydrochloride with N,N'-dicyclohexylcarbodiimide and N-methylmorfoline as catalysts in dioxane and Ethyl acetate at low temperature. 2 – Saponification reaction to eliminate dimethyl dicarboxylates at the aspartic acid moiety using lithium hydroxide, water, and THF as a solvent. 2,4-D-Asp was obtained in 30% yield. 5-OH-2,4-D was synthesized using 4,6-dichlororesorcinol and chloroacetic acid in water with sodium hydroxyde at pH 7. The final yields were 20%.

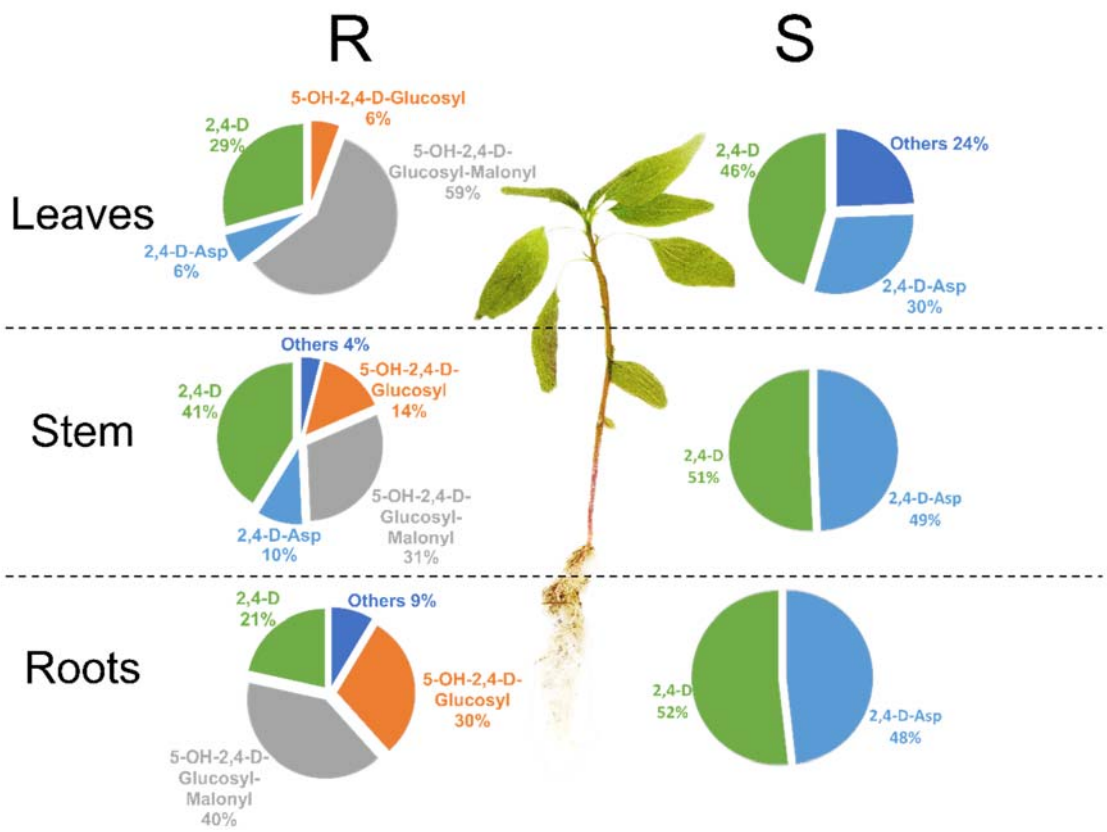

Supplementary Figure 3.2: Plant organ qualitative and quantitative characterization of 2,4-D metabolism in resistant (R) and susceptible (S) *A. tuberculatus*. Pie graphs show the percentage of each metabolite recovered in leaves, stems, and roots of R and S plants, 96 hr after [^{14}C] 2,4-D exposure. The colors correspond to: green: 2,4-D; light blue: 2,4-D-Aspartate; orange: 5-OH-2,4-D-Glucosyl; gray: 5-OH-2,4-D-(6-O-malonyl)-glucoside and dark blue: uncharacterized metabolites.

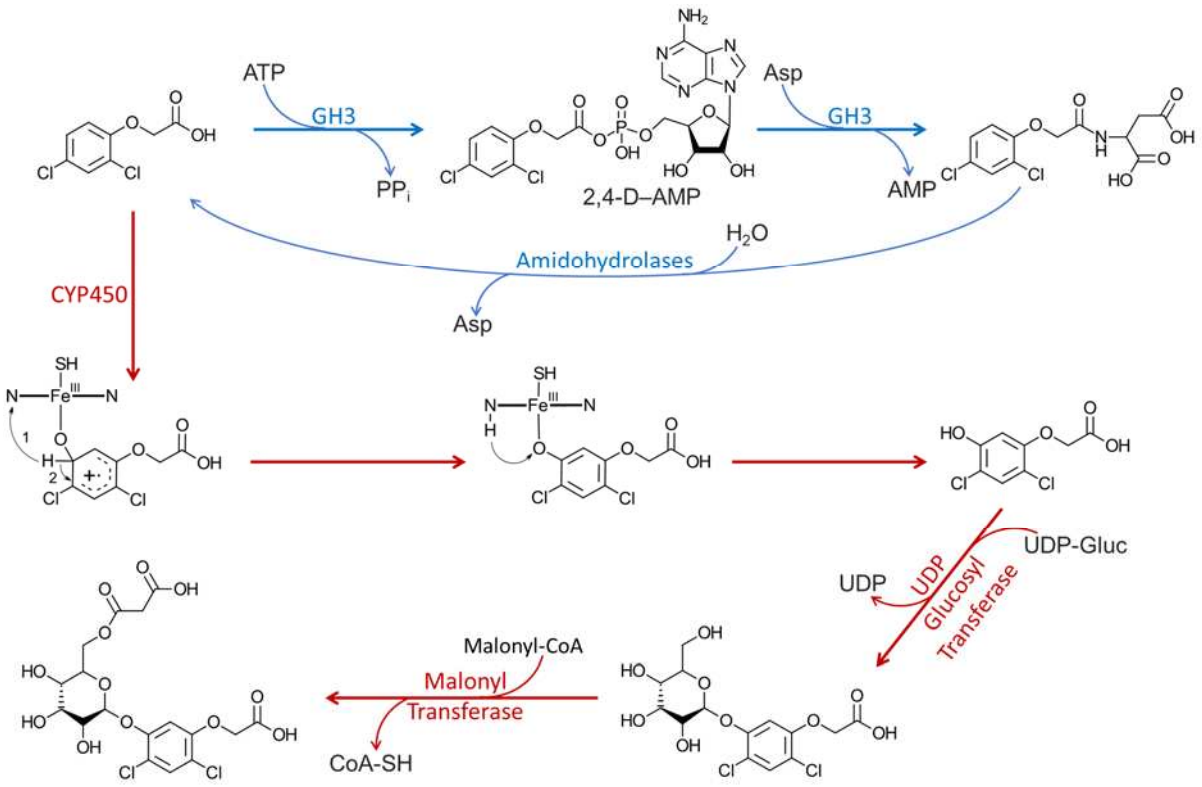

Supplementary Figure 3.3: Proposed mechanistic reactions of 2,4-D metabolism, catalyzed by GH3s and P450s. In the process of amino acid conjugation, 2,4-D-Asp, GH3 enzymes perform adenylation of the herbicide using ATP and releasing pyrophosphate. Then in another reaction facilitated by the same enzyme, an NH_3^+ nucleophilic group of an aspartic acid will attack the carbonyl group of 2,4-D-AMP, resulting in the final 2,4-D-Asp. The conjugate metabolite can be turned back to 2,4-D through a hydrolysis reaction mediated by amidohydrolase action. In detoxification reactions, the meta oxidation of 2,4-D phenoxy group undergoes an attack by the FeO heme complex in a cytochrome P450 enzyme. In this reaction FeO_3^+ oxygen will be added to C5 substrate at 2,4-D phenol to form a tetrahedral intermediate σ-complex, then a proton reaction mechanism, where the hydrogen is abstracted by one of the nitrogens at the P450 porphyrin, causing pi bond between C4 and C5 to be restored, regaining ring aromaticity. In the last step, abstracted hydrogen bounces back to the carbonyl oxygen at C5, releasing 5-OH-2,4-D. In the following glucosyl conjugation, a UDP-Glucosyltransferase rapidly transfers a glucosyl group from uridine 5'-diphospho-glucuronic acid (UDP-Gluc) to the hydroxyl nucleophilic group at 5-OH-2,4-D. As a secondary conjugation, 5-OH-2,4-D-glucosyl is esterified with a malonic acid at position 6’ of glucose by a malonyl-CoA, forming 5-OH-2,4-D-(6-O-malonyl)-Glucoside, via malonyl transferases.

Supplementary table 4.1. Primer list.

Experiment	Primer	Sequence
Candidate gene validation	PCR genotyping	Amplicon size testing primer FW 5'-AACTCAAATCGTTGGTTGGC-3' Resistant specific FW 5'- CGTAAGAACAACAACAGTGTGAGC -3' Susceptible specific FW 5'- CTCCGGTGAGATCTTATGTG -3' Universal reverse RV 5'-CTTTATCCTCGTACGTTGGTACG-3',
	KASP genotyping	HEX-FW 5'-GAAGGTCGGAGTCAACGGATT*CTCCGGTGAGATCTTATGTG*-3' FAM-FW 5'-GAAGGTGACCAAGTTCATGCT*CGTAAGAACAACAACAGTGTGAGC*-3' Universal RV 5'-ATTTTGCGGAGGTATGGTGC-3'
Arabidopsis transformation	PFGC5941 cloning using AscI and BamHI as restriction sites	1AA2 -AscI-FW 5'-TTGGCGCGCC ATGGCGTACGAGAAAGTCAATGAGCTTA-3' 1AA2- BamHI-RV 5'-CGGGATCCTCATAAGGAAGAGTCATCAGATCCT TTCATGATTC-3'
IAA2 expression in *Sisymbrium orientale*	*So*IAA2$_{WT}$	FW 5'- GAACAACAACAGTGTGAGCTATG -3' RV 5'- GCCTTGAGAAGCTCTGGATAG -3'
	*So*IAA2$_{\Delta 27}$	FW 5'- CTCCGGTGAGATCTTATGTG -3' RV 5'- CTCCGGTGAGATCTTATGTG-3'
	*So*Cyclophilin	FW 5'- CATGTGCCAAGGAGGAGATT-3' RV 5'-GTGTGCTTCCTCTCGAAGTT-3'
	SoActin2	FW 5'- GTGGAACCACTATGTTCTCTGG-3' RV 5'- GGAGGTGCAACGACCTTAAT-3'
IAA2 expression in *Arabidopsis thaliana*	*At*Cyclophilin	FW 5'- GTCTGATAGAGATCTCACGT -3' RV 5'- AATCGGCAACAACCACAGGC -3'
	*At*Actin2	FW 5'- GGCAAGTCATCACGATTGG -3' RV 5'- CAGCTTCCATTCCCACAAAC -3'
IAA2 expression in *E. coli*	pFN2A (GST) Flexi Vector SgfI and PmeI as restriction sites	GST-IAA2-SgfI-FW 5'-ttGCGATCGCGGCGTACGAGAAAGTCAATG-3' GST-IAA2-PmeI-RV 5'-ttGTTTAAACTCATAAGGAAGAGTCATCAGATCCT TTCATGATTC-3'

Supplementary table 4.2. Biotinylated IAA2 degron peptides used on SPR analysis

Biot-TKT	Degron	Degron tail	Fraction of PB1
IAA2	QIVGWPPVR	SSRKNNNSV	SYVKVS
$IAA2_{\Delta 27}$	QIVGWPPVR		SYVKVS

Supplementary table 4.2. Biotinylated IAA2 degron peptides were designed to SPR analysis. The peptides contained the core degron, degron tail (on WT IAA2), and a fraction of 6 amino acids correspondent to PB1 domain.

Supplementary table 4.3. Detection of *IAA2*$_{\Delta 27}$ in multiple *Sisymbrium orientale* populations from South Australia with resistance to 2,4-D and lack of detection in susceptible populations.

Population	No. of individuals tested	Banding pattern		
		$IAA2_{WT}$	$IAA2_{\Delta 27}$	$IAA2_{WT}/IAA2_{\Delta 27}$
PB-R (R)	20		20	
PB-R2 (R)	20		20	
P15 (S)	15	15		
P17 (R)	20		14	6
P28 (R)	20	20		
P31 (S)	5	5		
P49 (S)	5	5		
P50 (S)	5	5		

Supplementary table 4.3. *IAA2*$_{\Delta 27}$ genotype correlates with 2,4-D resistant genotype in several field populations of *Sisymbrium orientale* from South Australia. All plants of the four susceptible populations tested were genotyped as WT *SoIAA2* allele (P15, P31, P49, P50). In resistant populations, all the plants tested for PB-R, PB-R2 and P17 were homozygous for R or heterozygous. Resistant population P28 was homozygous for the WT *IAA2*, evidently showing that this population evolved differently for auxin herbicide resistance.

Protein alignment

```
Arab_IAA_Col-0                  MAYEKVNELNLKDTELCLGLPGRTEKIKEEQEVSCVKSNNKRLF---EETRDEEESTPPT   57
Mustard_IAA2_deletion_protein   MAYEKVNELNLKDTELRLGLPGT-EQVKEEQEVSCVRSNKRQFQIDNEENREEEESTPPT   59
Mustard_IAA2_full_protein       MAYEKVNELNLKDTELRLGLPGT-EQVKEEQEVSCVRSNKRQFQIDNEENREEEESTPPT   59
                                *************** *****  *::*********:**::::    **.*:********

Arab_IAA_Col-0                  KTQIVGWPPVRSSRKNNNSVSYVKVSMDGAPYLRKIDLKTYKNYPELLKALENMFKVMIG   117
Mustard_IAA2_deletion_protein   KTQIVGWPPVRS---------YVKVSMDGAPYLRKIDLKTYKNYPELLKALENMFKFTVG   110
Mustard_IAA2_full_protein       KTQIVGWPPVRSYRKNNNSVSYVKVSMDGAPYLRKIDLKTYKNYPELLKALENMFKFTVG   119
                                ************         **********************************. :*

Arab_IAA_Col-0                  EYCEREGYKGSGFVPTYEDKDGDWMLVGDVPWDMFSSSCKRLRIMKGSDAPALDSSL     174
Arab_IAA2_120A3                 EYCEREGYKGSGFVPTYEDKDGDWMLVGDVPWDMFSSSCKRLRIMKGSDAPALDSSL     174
Mustard_IAA2_deletion_protein   EYCEREGYKGSEVVPTYEDKDGDWMLVGDVPWDMFSSSCKRLRIMKGSDDSSL----     163
Mustard_IAA2_full_protein       EYCEREGYKGSEVVPTYEDKDGDWMLVGDVPWDMFSSSCKRLRIMKGSDDSSL----     172
                                *********** .**********************************  :*
```

Supplementary Figure 4.1. Amino acid alignment between *At*IAA2, *So*IAA2$_{\Delta 27}$ and *So*IAA2. The protein alignment shows 87.1% of aa identity and 89.9% similarity, comparing *At*IAA2 to *So*IAA2.The colored amino-acid regions refer to the conserved elements in all functional domains at Aux/IAA proteins. In green there is the ethylene response factor associated amphiphilic repression (EAR) motifs (amino acid sequence LxLxL) that binds to TOPLESS (TPL), a transcriptional corepressor. The sequence highlighted in red corresponds to the Degron motif, which binds to auxin and the co-receptors TIR/AFB proteins. In blue there are the K and DxD and ExD sequences (OPCA) motifs in the PB1 domain. Those two domains form complementary interaction centers, where K makes one portion of the protein basic and OPCA makes the other portion acidic, leading the formation of complex oligomer between Auxin Response Factors (ARF) and other Aux/IAA proteins that have the same highly conserved PB1 domain (Tao and Estelle, 2018). The 9 aa (positions 72-80) deletion in the herbicide resistant population of *Sisymbrium orientale* occurs between the Degron and PB1 motifs, a region denominated degron tail (Niemeyer et al., 2020).

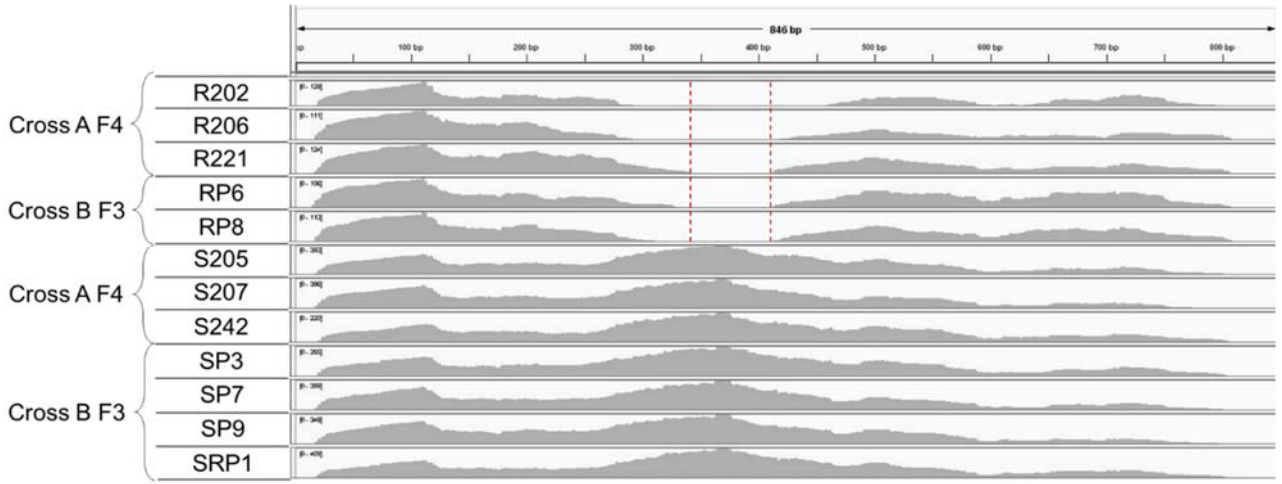

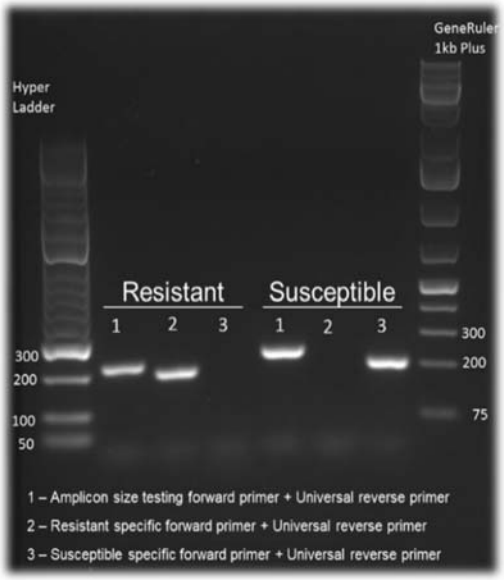

Supplementary Figure 4.2. Read depth and PCR assay 27 bp deletion confirmation in *So*IAA2. Read depth of *So*IAA2 transcripts in resistant Recombinant Inbred Lines (RILs), 3 plants from F4 cross A (R 202, 206 and 221) and 2 plants from F3 cross B (RP6 and 8). Followed by susceptible RILs, 3 plants from F4 cross A (S 205, 207 and 242) and 4 plants from F3 cross B (SP3, 7, 9 and SRP1). The identified region with red dotted lines in the resistant RILs graphs shows the 27bp deletion at the Degron tail (DT) region of *So*IAA2. The electrophoresis gel confirms the absence of 27bp in resistant plants. The bands named 1 shows the different sizes between resistant (212 bp) and susceptible (239 bp) *So*IAA2 alleles. The set of primers that generated band 2, corresponds to specific nucleotides flanking the DT deleted region, which just amplify in the resistant allele (band present on resistant but not in susceptible sample). The set of primers 3, just anneal in the nucleotides in the DT that are just present in the original wild type *So*IAA2 allele, but it does not amplify in resistant plants (band present in resistant but absent in susceptible sample). The PCR reactions were performed using cDNA synthesized from RNA of R221 and S205 F4 RILs.

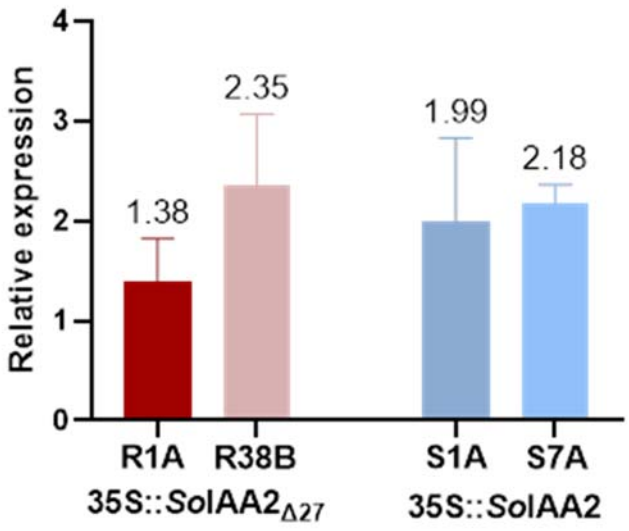

Supplementary Figure 4.3. RT-PCR data for Arabidopsis *So*IAA2$_{\Delta 27}$ and *So*IAA2 transgenic lines. Relative expression of *So*IAA2 comparing to the reference genes *At*Cyclophilin and *At*Actin2 in T3 homozygous Arabidopsis lines with a single copy of T-DNA vector. Histograms correspond to the average of three plants of each lines with standard error bars.

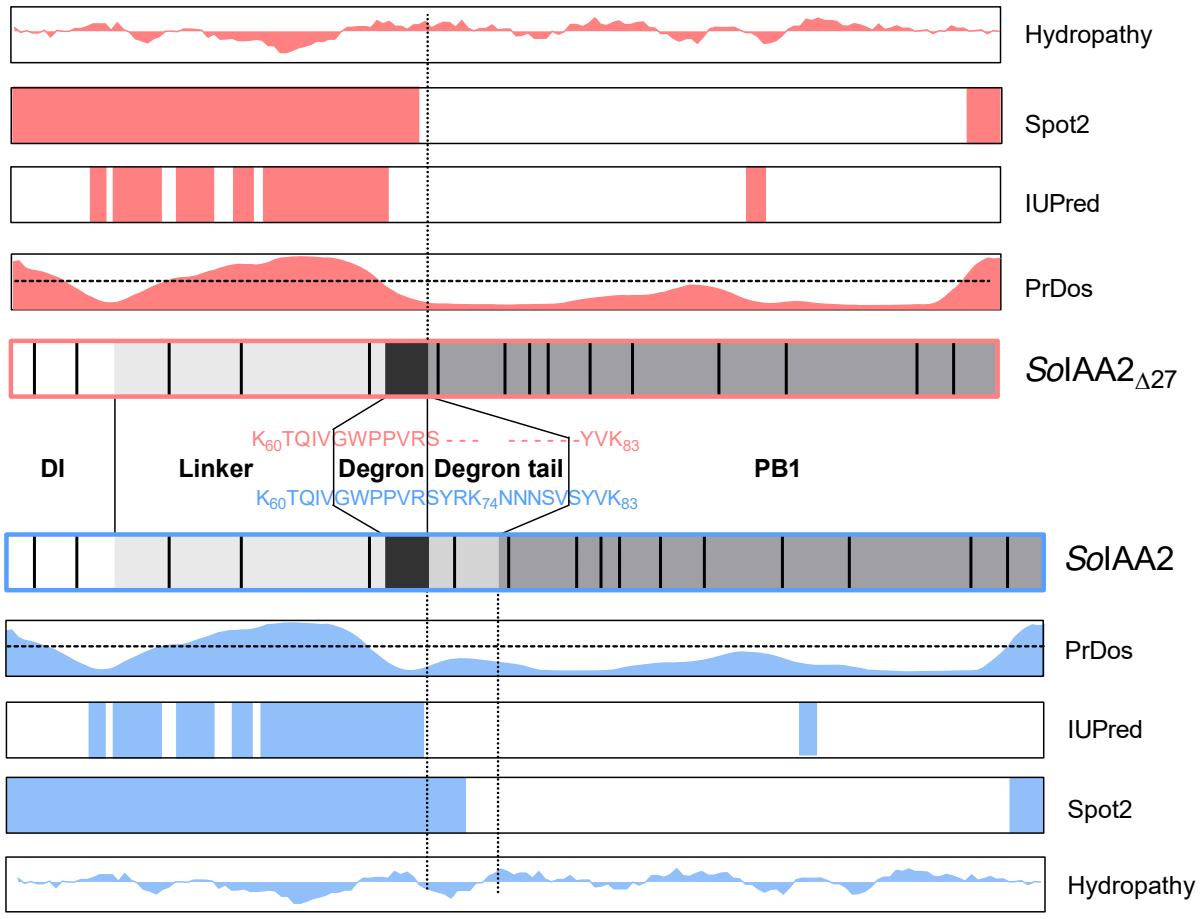

Supplementary Figure 4.4. Intrinsic disordered regions (IDR) and hydropathy predictions of the *SoIAA2* (Blue) and *SoIAA2*$_{\Delta 27}$ (Red). *In silico* analysis of IDR using PrDos, IUPred and Spot2. PrDos shows different levels of disorder predictions (disordered: > 0.6; intermediate disordered: 0.4-0.6; ordered: < 0.4), the dotted line corresponds to 0.5 score of IDR. IUPred and Spot2 maps show colored regions correspondent to high scores for IDR. Kyte-Doolittle hydropathy maps scaled from -4 to +4, negative values correspond to hydrophilic protein segments and positive to hydrophobic.

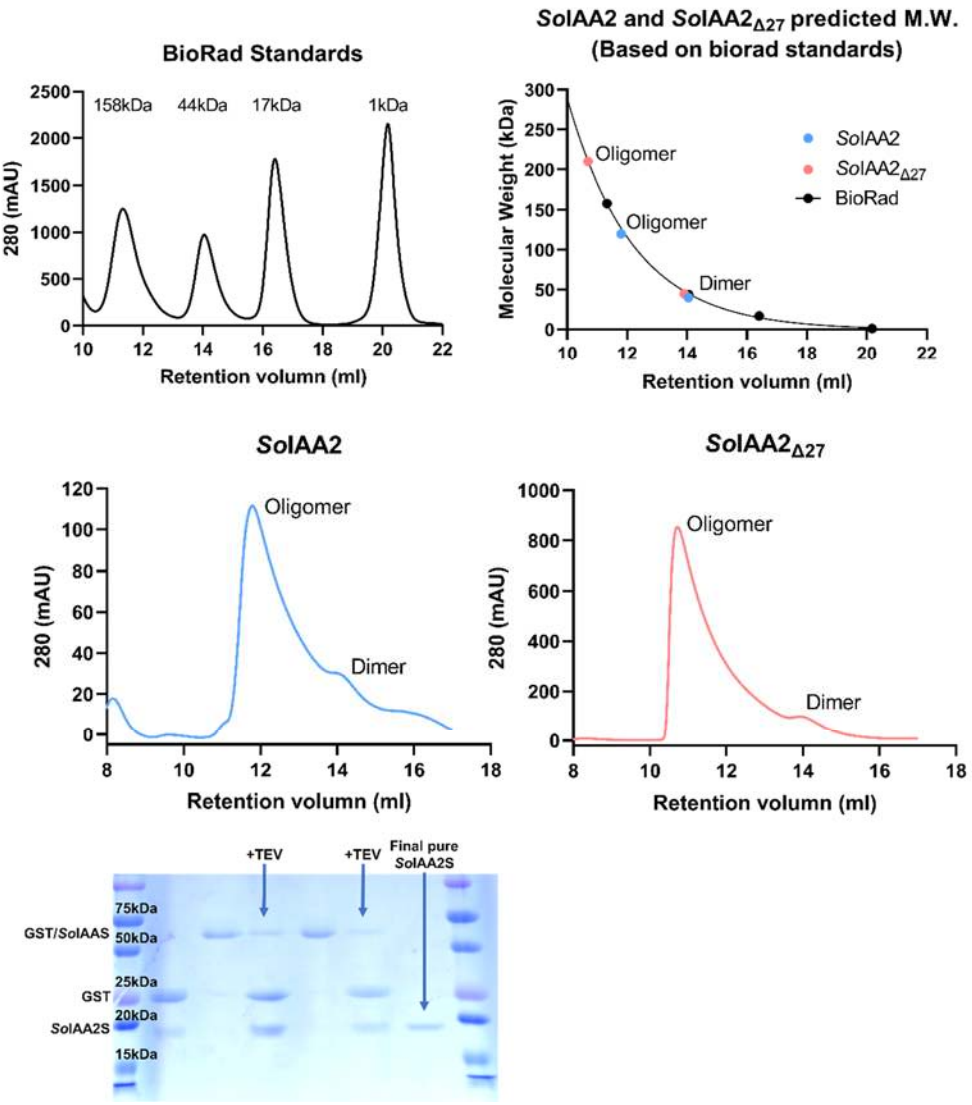

Supplementary Figure 4.5. Size exclusion chromatography using a SuperDex 200 on untagged purified AUX/IAA2 WT and Δ27 alleles from *Sisymbrium orientale* heterologous expressed in *Escherichia coli*. Size exclusion chromatograms for the Biorad standards as well as *So*IAA2 and *So*IAA2$_{\Delta 27}$ proteins. Each of the retention volume peaks are plotted on the standard curve to give approximate molecular weights (Top panels). The smaller peaks at ~14mls are close to a dimer, and the larger oligomer peaks are between 6 to 12 molecules (*So*IAA2 closer to 6 and *So*IAA2$_{\Delta 27}$ closer to 12 – middle panels). An SDS-PAGE on the bottom shows the different sizes of the entire GST-*So*IAA2 protein (~47 KDa), before and after TEV cleavage and size exclusion chromatography purification. GST ~27 KDa and final pure *So*IAA2 ~20 KDa. Due to higher stability during the purification process *So*IAA2$_{\Delta 27}$, injections for that protein had higher amounts of protein, which probably induced bigger groups of oligomers.

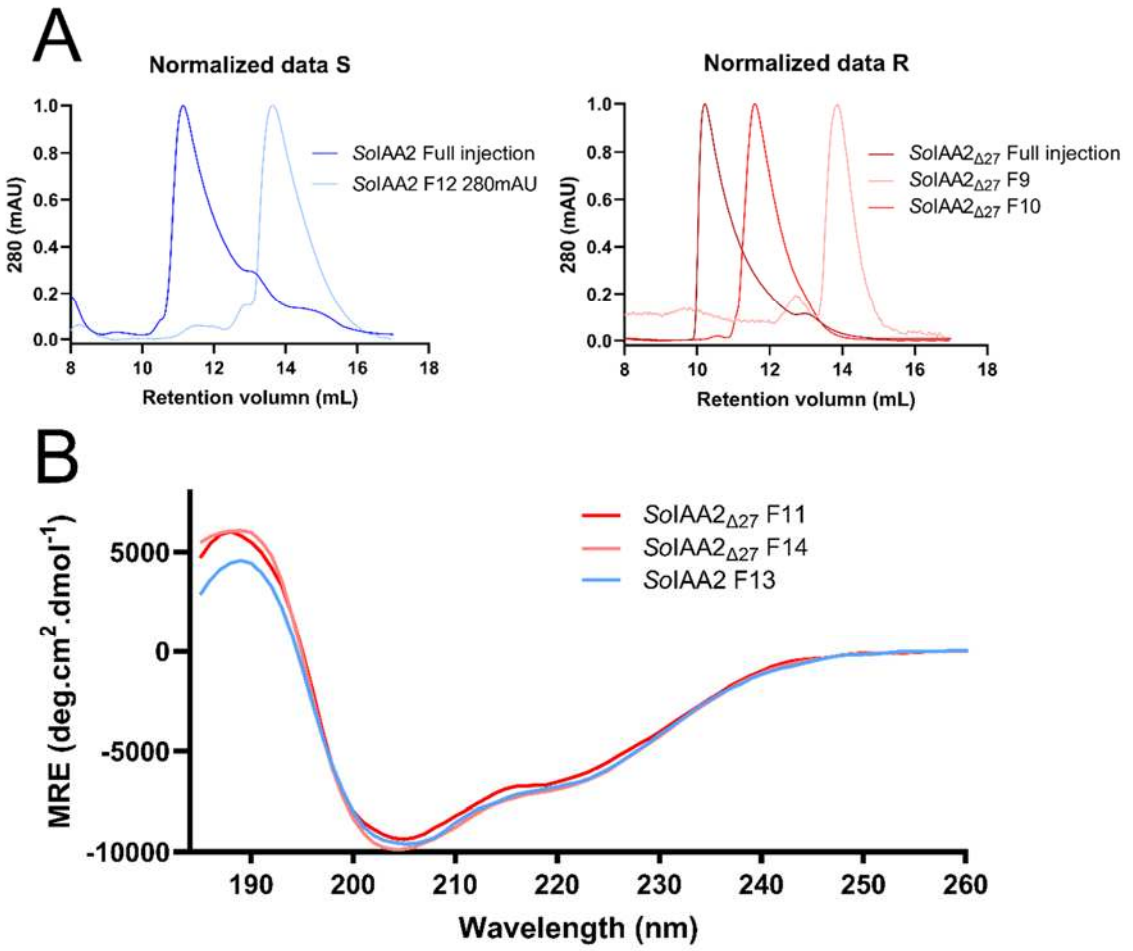

Supplementary Figure 4.6. Oligomerization of purified SoAUX/IAA2 (*So*IAA2) WT and Δ27 show a concentration dependence for oligomerization. Both versions of *So*IAA2 fractions analyzed on CD have near identical spectra, number of molecules or the Δ27 deletion do not seem to significantly alter the protein fold. A) Chromatograms from sequential runs for SoIAA2 WT (Blue) and Δ27 (Red) normalized to 1 mA.U. The dark colored curves are the original SuperDex 200 gel filtration runs, while the light-colored curves (light blue is the F12 of the *So*IAA2 full injection and the light red colors are F9 and F10 of *So*IAA2$_{\Delta 27}$ full injection) are diluted fractions from the original dark colored run peak, reinjected for another run. As in, if the sample is diluted, then the number of molecules in the oligomer decreases. B) CD data for SoIAA2 WT (Blue) and Δ27 (Red colors) from the primary peak (fractions 13 from *So*IAA2 and 11 *So*IAA2$_{\Delta 27}$ respectively), as well as *So*IAA2 $_{\Delta 27}$ fraction 14 which is off peak at 12.7mls (~4 molecules). The IAAS CD spectra shows an alpha, beta, other content of 12.9%: 38.4%: 48.7%, which is in agreement with a partial structure from the PB1 domain but about half of the protein being disordered or "other".